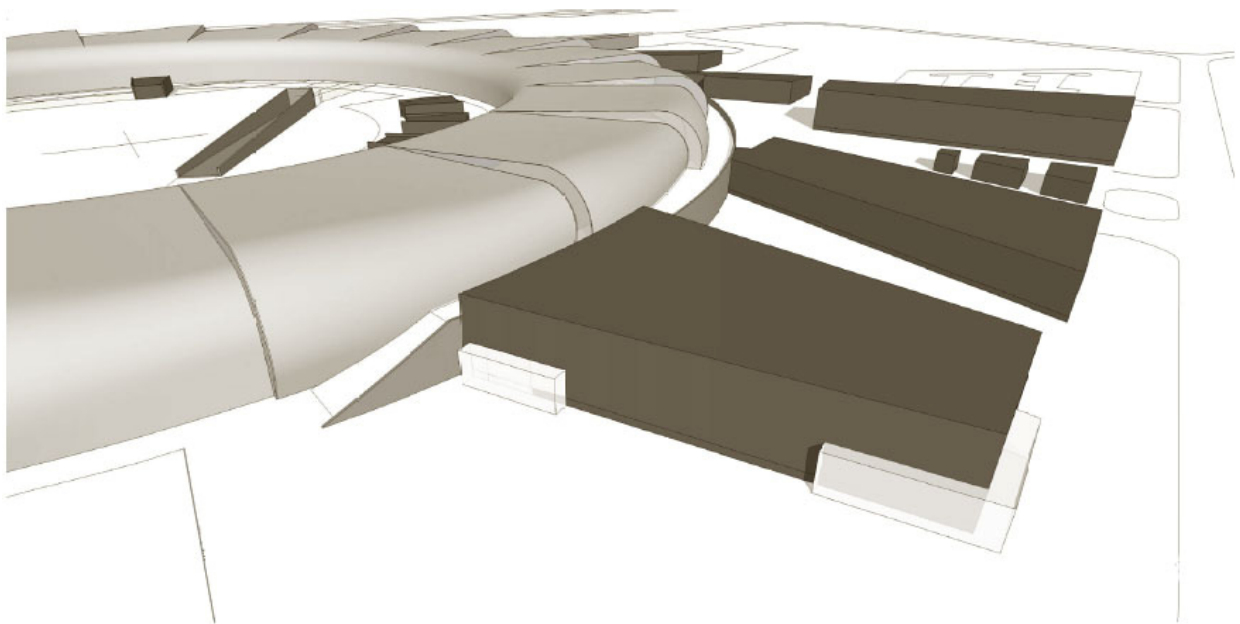




Revised design of the MAX IV facility

Background material for the VR evaluation
September 2009



1. INTRODUCTION	2
2. THE STORAGE RINGS	3
The revised 3 GeV ring.....	3
The revised 1.5 GeV ring.....	5
Fig. 5. The magnet structure of a lattice cell is machined into one solid block of iron. The lower half of such a structure is shown here. MAX III	10
MAX III	11
3. CONSEQUENCES FOR THE HARD X-RAY ACTIVITIES	12
Beamlines at the 3.0 GeV ring in the CDR report.....	12
Suggested beamlines/ experimental techniques at the 3 GeV ring that are not present or only partly covered in the CDR:	12
A dedicated SAXS beamline, a solution SAXS beamline.....	12
Powder diffraction	13
Tomography/Imaging.....	13
Other beamlines for the exploitations of the coherent properties of the radiation.....	14
High kinetic energy photoemission (HIKE)	14
Relocation of MAX II hard X-ray beamlines.....	14
4. CONSEQUENCES FOR THE SOFT X-RAY ACTIVITIES.....	14
General considerations	14
Specific beamlines	16
Suggested beamlines/experimental techniques at the 1.5 GeV ring that are not present or only partly covered in the CDR:	17
5. BUDGET	17
6. CONCLUSIONS.....	18

1. INTRODUCTION

The Conceptual Design Report (CDR) from 2006 describes the MAX IV facility as two 12-cell rings with a circumference of 287 m placed upon each other. One ring would be operating at 1.5 GeV mainly serving the soft X-ray user community and the other ring would be operating at 3 GeV for hard X-ray applications. In addition, the existing 700 MeV MAX III storage ring was planned to be transferred to the new facility. This design was evaluated by the Swedish Research Council (VR). A first evaluation panel was going through the technical design of the accelerators and a second one was evaluating the scientific case and the general project plan. Both evaluations came to very positive conclusions and led to the recommendation that the project should be funded.

The design work has continued after the completion of the CDR with funding from VR. One important part was to continue the planning of the scientific program and the layout of the beamlines. In 2007 and 2008 the MAX IV workshops "Science at MAX IV" and "New Directions for MAX IV" were arranged in order to get continued input from the user community. A major outcome of this work was that the number of straight sections at the 3 GeV ring was considered to be too small. This limitation would affect both the hard and soft X-ray regimes. There was a demand for more beamlines in the hard X-ray regime. Furthermore several soft X-ray beamlines would benefit from being placed at the suggested 3.0 GeV ring instead of the 1.5 GeV one. Hence, the relationship on the demand of beamlines on the suggested two rings was unbalanced.

The design of the MAX IV facility has therefore been revised. The unique properties of the storage rings in the CDR have been kept or even improved (especially for the new 3 GeV ring) but the relationship between the different rings has been changed. In the revised design a larger, 528 m circumference, 3 GeV ring with 20 cells is combined with a new 96 m circumference 12 cell storage ring. The smaller ring will be operated at 1.5 GeV. This storage ring will serve the IR & UV user communities as well as hosting most of the soft X-ray beamlines. Thus it will replace the 1.5 GeV ring from the CDR as well as the MAX III storage ring. The revised MAX IV design reflects better the demand of beamlines and offers improved performances over almost the entire energy range and for the vast majority of the planned beamlines.

In chapter 2 of this report we describe the new accelerator design. We compare the accelerator parameters to those of the initial design. We also give a brief status report of the continued work to investigate all aspects of the accelerator performance. In the following two chapters we discuss the consequences for the beamline plans. The scientific case presented in the CDR is still the basis for the MAX IV project. In this document we summarize how the beamlines in the different energy regimes are affected by the revised proposal and we make a summary of new experimental techniques/beamlines that has been discussed after the publication of the CDR in 2006. In chapter 3 we discuss the hard X-ray beamlines and in chapter 4 we discuss the consequences for the soft X-ray regime and the proposed soft X-ray beamlines. The proposed short pulse facility (SPF) has not been influenced by the revision and is therefore not discussed in this report. In chapter 5 we discuss the economical consequences of the modified design.

2. THE STORAGE RINGS

The revised 3 GeV ring

The revised proposal entails building a larger 3.0 GeV ring with 20 cells in the lattice and with an even lower horizontal emittance than for the original design. The circumference has increased from 287 to 528 m. The design principle of scaling down the size of the accelerator components and the larger ring allows the use of a larger number of magnets or magnetic structures resulting in a further reduction in the emittance.

Description of the MAX IV 20-fold 7- bend lattice

The expansion of the 3 GeV MAX IV ring from 12 to 20 achromats was motivated mainly by the demand of additional straight sections for Insertion Devices (IDs). Below the consequences associated with this expansion. Since the MAX IV 12-fold lattice has been evaluated earlier, we concentrate on the differences between the 12-fold and 20-fold lattices.

The reduction of the electron beam emittance is generally prevented by the reduction of the Dynamic Aperture (DA) and Energy Acceptance (EA) of the lattice to unacceptable limits. The reason for this decrement is the need to bring the natural negative chromaticity to positive values. This is done by using sextupole magnets, progressive lenses, which are preferably placed at large dispersion positions in the magnet lattice. The focusing of off-momentum particles can be compensated at these positions. These non-linear devices can, however, have a severe effect on the DA and EA. As the number of magnet cells is increased, the dispersion decreases so the strengths of these sextupoles must be increased. When doing so, the Hamiltonian driving terms for higher resonances are increased and both the DA and AE are decreased. This Hamiltonian formalism has been refined by Johan Bengtsson (NSLS II) and a computer optimizer (OPA) was developed by Andreas Streun (SLS).

In a conventional Double Bend Achromat (DBA) or Triple Bend Achromat (TBA) the cancellation of the higher order driving terms takes place between the achromats, which makes the lattice sensitive to the introduction of IDs which breaks this cancellation. By increasing the number of magnets within the achromat, this cancellation of the driving terms can take place within the achromats and the lattice becomes quite insensitive to disturbances of the lattice symmetry when IDs are introduced. The robustness of the lattice is further increased by a high periodicity. This was further studied in [1] where both the 12-fold and 20-fold seven bend achromats were examined.

Once the need to expand the MAX IV lattice became clear, the 20-fold 7-bend achromat was investigated in detail [2] and found to be surprisingly stable. The DA is quite sufficient for injection as well as for Touschek scattered particles and the EA is huge which, in combination with a 100 MHz RF system gives a comfortable Touschek life-time. The smaller emittance has a positive effect on the Touschek lifetime. The opposite could be envisaged, since the higher electron density will increase the collision rate. This is, however, counteracted by the fact that the transverse oscillation energy is decreased so most collisions yield a smaller energy transfer in the horizontal direction. This effect, plus a large EA and a large bucket height result in an increased Touschek lifetime [2].

The impact from IDs on the electron beam emittance is larger for the 20-fold lattice than for the 12-fold case. The reason is that the synchrotron radiation losses are almost halved in the former case, while the losses due to IDs remain constant or are increased since we can house a larger number of them. Damping wigglers are introduced to reduce the emittance defined by the lattice. These wigglers will also serve as radiation sources and can thus either be regarded as "damping wigglers" or regular IDs for synchrotron radiation generation. Their eigen-emittance

is, however, only a factor of two smaller than the lattice emittance, so the reduction in total emittance is limited.

The in-vacuum undulators have smaller, but still rather high synchrotron radiation losses and their eigen-emittance is orders of magnitudes smaller than those for the wigglers. These IDs are thus very effective for emittance reduction. Another positive impact of the strong IDs is the reduction of the Intra Beam Scattering (IBS) effect. The relatively long damping time of the naked lattice is shortened by the synchrotron radiation losses caused by the IDs. The IBS effect is strongly reduced due to this effect.

The positive effect of choosing a low frequency RF system to achieve a large RF bucket height was noticed already in the studies of the 12-fold lattice. This effect is even more pronounced for the 20-fold lattice since the momentum compaction factor is further reduced. This high RF bucket height in combination with the large EA and the small emittance result, as noted above, in a long Touschek life-time.

The capacity-loaded design of the cavities pushes up the frequencies of the Higher Order Modes (HOMs). The ratio between the lowest HOM and the fundamental mode is now higher than four, while the ratio for a classical pill-box design is around 1.5.

The emittance

The horizontal emittance of the revised 3.0 GeV ring has decreased to 0.336 nrad for the naked lattice. The total emittance will depend on the effects of the chosen insertion devices but it is expected to further decrease to about 0.24 nrad. Already in the previous design, the emittance (0.86 nrad) was outstanding compared to most other existing or planned sources. The vertical emittance is chosen by the coupling to match the diffraction limit at 1 Ångström, 0.009 nrad. This was also the case with the previous design. With the revised design, the goals for the X-ray spot sizes reported in the CDR could be obtained with shorter beamlines, thus reducing the sensitivity for vibrations. The decreased emittance could also be used to even further decrease the spot size where that would be an advantage, i.e. the nanofocus beamlines. It must, however, be noted that to fully exploit the lower emittance, more severe demands must be implemented on the beamline optics (surface roughness and other errors). With the lowered emittance, also the coherent properties of the X-ray radiation are increased.

The straight sections

The length of the 20 (long) straight sections on the 3 GeV ring will be 5 meters. Out of these, 19 can be used for insertion devices. Compared to the previous design, 8 more beamlines could be placed on the 3 GeV ring. The straight sections will have the same type of insertion devices as discussed in the CDR, although the increase in length (from 4.6 m) will permit adding a few more magnetic periods. It also improves the possibility to put two insertion devices in one straight section. Most of the straight sections will be used for small gap in-vacuum undulators with relatively short period lengths. On the 3 GeV ring these will offer an outstanding brilliance in energies up to about 30 keV. In addition, it is foreseen that two 2.2 T permanent magnet wigglers will be installed in opposing straight sections to act as damping wigglers. These will offer a possibility to reach photon energies up to 100 keV. Elliptically polarized undulators (EPU)'s covering energies between 150 eV and 1.5 keV by the fundamental harmonic are the preferred insertion devices for some of the soft X-ray spectroscopy beamlines to be placed on the 3.0 GeV ring.

The short straight sections

There are two short (1.5 m) straight sections per cell in the 20-cell lattice 3 GeV ring, which gives a total of 40 short straight sections in the ring. However, especially high magnetic field

insertion devices on these sections will have a somewhat negative effect on the total emittance of the storage ring but utilizing at least some of these straight sections could be considered in future expansions.

The dipoles

The majority of the bending magnets will have a flat magnetic field of 0.55 T. The relatively long critical wavelength of 4.14 Ångström for the emitted radiation from these dipoles indicates that they will mainly be used for diagnostic purposes.

Technical development

Vacuum system - The need of small apertures is further stressed by the introduction of stronger sextupole magnets. The NEG-coated copper tube vacuum system has been further examined and cost estimated [3]. Two NEG-coated copper tube dipole vacuum chambers have been installed in the MAX II storage ring and tested for more than one year [4]. The photon beam extraction from the ring has also been investigated [3].

Magnets - The magnet design has been slightly changed [3] and new prototype magnets are underway.

Girders - The vertical beam size in the long straight sections is calculated to be 2.6 μm and the beam movements have to be restricted to 260 nm. This calls for a girder construction which pushes all vibrational eigenfrequencies up above 100 Hz. This is extremely difficult when using steel constructions. A concrete girder prototype has been developed and tested. All eigenfrequencies are above 100 Hz and the accelerator cave is now modeled to find a proper design for this.

RF system - The need for RF power is smaller in the 20-achromat case since the dipole magnet fields are lower. The power needed is now more dependent on the type and number of IDs chosen. A flexible, expandable and modular system is being designed [3]. Four HOMs remain to be damped for a circulating current of 0.5 A.

Dipole correction scheme - The vertical electron beam emittance should be reduced to the diffraction limit at 1 Å corresponding to a coupling of 2%. This is not an extremely small coupling, but the strong sextupole magnets will call for a precise steering of the electron beam in the sextupole magnets. A solution satisfying these demands has been designed and will be presented in ref 3.

References:

[1] M. Eriksson, L. J. Lindgren, M. Sjöström, E. Wallén, L. Rivkin, and A. Streun, Nucl. Instr. and Meth. A 587, 221 (2008).

[2] S. C. Leeman et al, Beam Dynamics for the MAX IV 3 GeV Storage Ring, submitted to N. I. M. and appended here as Appendix 1

[3] MAX IV Detailed Design Report, work in progress (User name: Electron, Password: Photon)
http://www.maxlab.lu.se/local/maxiv_ddr/index.html

[4] A. Hansson et al, Experiences from nonevaporable getter-coated vacuum chambers at the MAX II synchrotron light source, to be submitted and appended here as Appendix 2

The revised 1.5 GeV ring

The 1.5 GeV ring of the CDR will be replaced by a smaller ring with almost the same circumference (96 m) as the present MAX II ring (90 m). An overview of the ring is seen in fig. 1. The magnet cells are more compact than those in MAX II, so 12-cells could be used instead of 10. The energy on this ring will be 1.5 GeV. Since the ring will be significantly smaller compared to the one from the CDR report (96 m circumference instead of 287 m) it will be placed in a separate experimental hall next to the main building. The advantage with the CDR design with

two storage rings placed upon each other was mainly reducing the experimental hall area and sharing some of the infrastructure (such as radiation shielding) between the rings. It must, however, be concluded that the new design with separate rings will make the whole facility less vulnerable since a malfunction of one ring will not affect the possibility to use the other. The amount of available floor space per beamline has also increased.

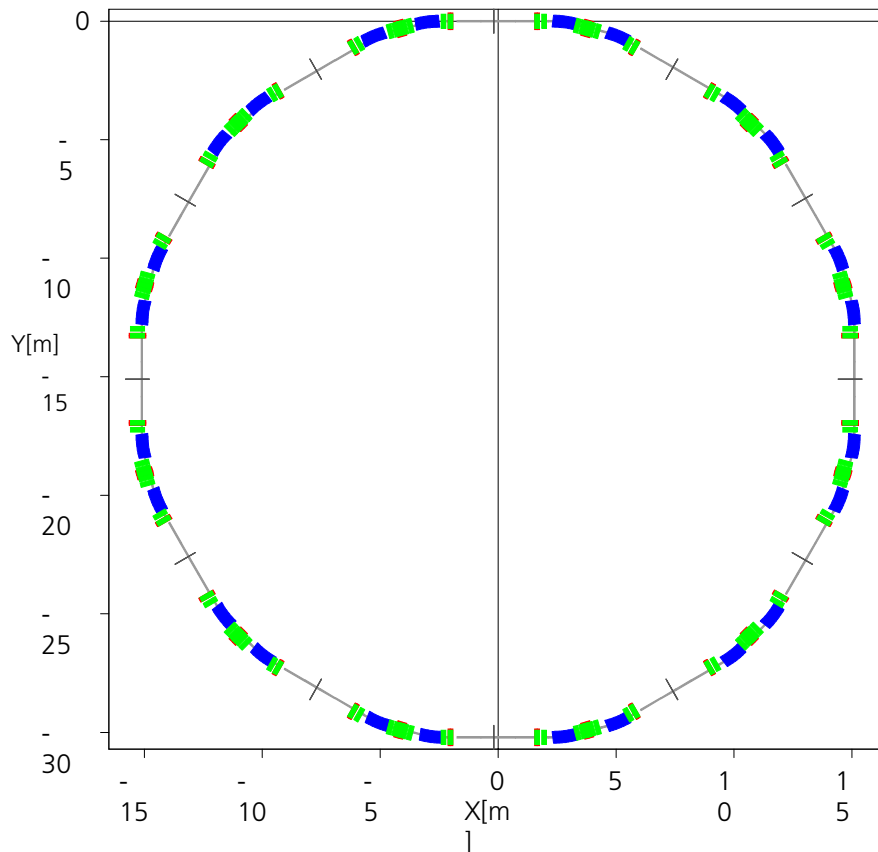


Fig. 1. The revised MAX IV 1.5 GeV ring

The photon energy range

The 1.5 GeV ring will host the present IR & UV beamlines on the MAX III ring. There will be no need to cover the hard X-ray range with this ring and the energy can therefore be optimized so that the ring will cover the range from IR, UV up to soft X-rays (6 meV - 1.2 keV). We find that this optimum corresponds to an electron energy of 1.5 GeV.

The emittance

The horizontal emittance of 5.6 nrad on the new 1.5 GeV ring will be a significant improvement compared to the present MAX II and MAX III ring that have 9 and 13 nrad respectively. The coupling between the horizontal and vertical emittance is yet to be decided but in the table below 2% coupling has been used which could be considered to be rather conservative. The 1.5 GeV ring presented in the CDR had, however, an emittance of only 0.34 nrad. The implication of this increase on the proposed beamlines will be described in the following chapter.

The straight sections

The number of straight sections that could be utilized for insertion devices will then be the same (11) as in the previous (CDR) design, but they will be slightly shorter, 3.48 instead of 4.6 m.

Machine layout

The revised MAX IV 1.5 GeV ring is rather similar to the MAX II ring. It can, however, be constructed according to the MAX III technology, which lowers the price and increases the magnet stability. The vacuum system could favorably be based totally on the NEG technology. This lowers the prize and increases the vacuum quality.

A 100 MHz RF system with 3rd harmonic Landau cavities is foreseen. This avoids the resistive wall instability, which otherwise could be of a problem due to the small vacuum chamber aperture.

The horizontal beta function in the long straight section is smaller than that in the MAX II ring. This, together with a factor of two smaller beam emittance, reduces the horizontal beam size by almost a factor of two.

The magnet cells are more compact than those in MAX II, so 12 cells could be used instead of 10. The long straight sections are a bit longer to house BPMs and valves. The circumference is 6 m larger for the new ring.

The machine design is summarized in Figs. 2-5 and Tables 1-3.

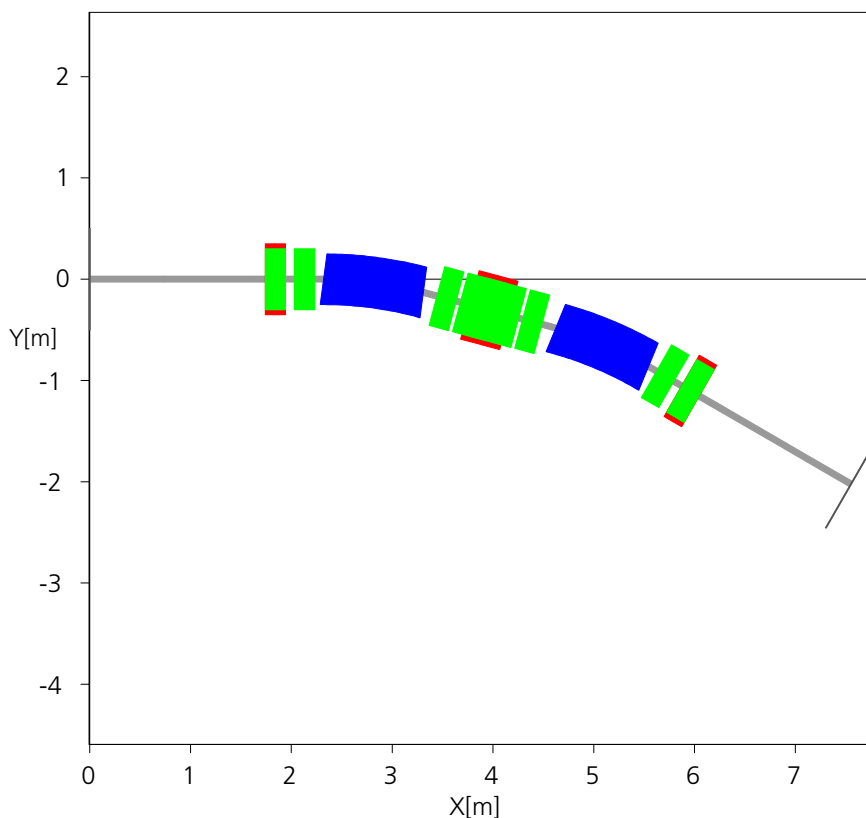


Fig. 2. One cell in the revised 1.5 GeV ring

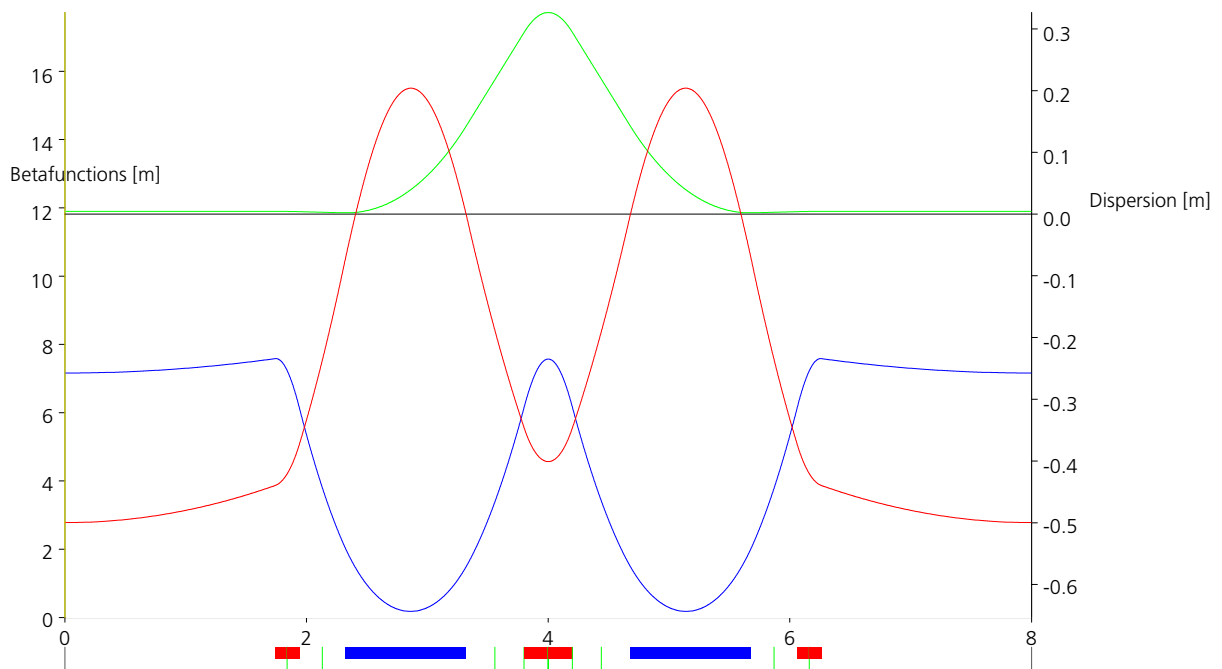


Fig. 3. The revised MAX IV 1.5 GeV machine functions

Table 1. Machine parameters

Circumference	96.0 m
Q _x	11,22
Q _y	3.17
Straight section length	3.48 m
Hor. Chrom (nat/corrected)	-26.5/1
Vert. Chrom (nat/corrected)	-16.4/1
Mom comp factor	0.00304
Energy	1.5 GeV
Hor emittans	5.6 nm rad
Energy loss/turn	117 keV
Energyspread (RMS)	0.074 %
τ_x	5.7 ms
τ_y	8.2 ms
τ_E	5.2 ms

Table 2. Magnet parameters

	Length (m)	Field (T)	Gradient (T/m)	S (T/m ²)
QFend	0.200	0	27.07	159.6
DIP	1	1.309	-6.23	0
QFmid	0.4	0	25.075	147.8
SD	0.1	0	0	-375
SDH	0.1	0	0	-399.7

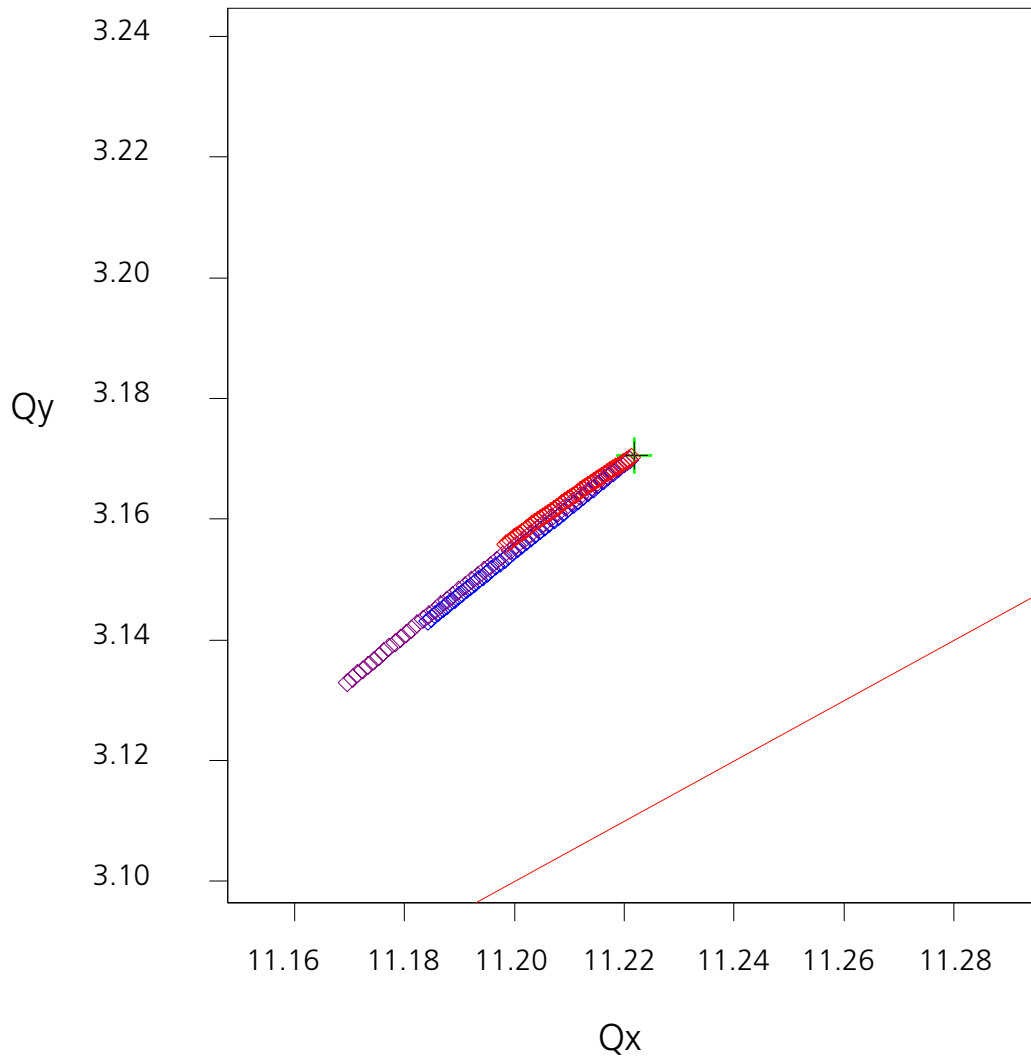


Fig. 4. Tune variation for 15 mm horizontal and 8 mm vertical displacements

Table 3. Lattice half-cell

½ straight	1.740 m
QFend	0.200 m
Straight	0.190 m
SDH	0.100 m
Straight	0.190 m
Dip	1.000 m
Straight	0.240 m
SD	0.100 m
Straight	0.240 m
QFmid (1/2)	0.200 m

23/enr/2009.09.25.42

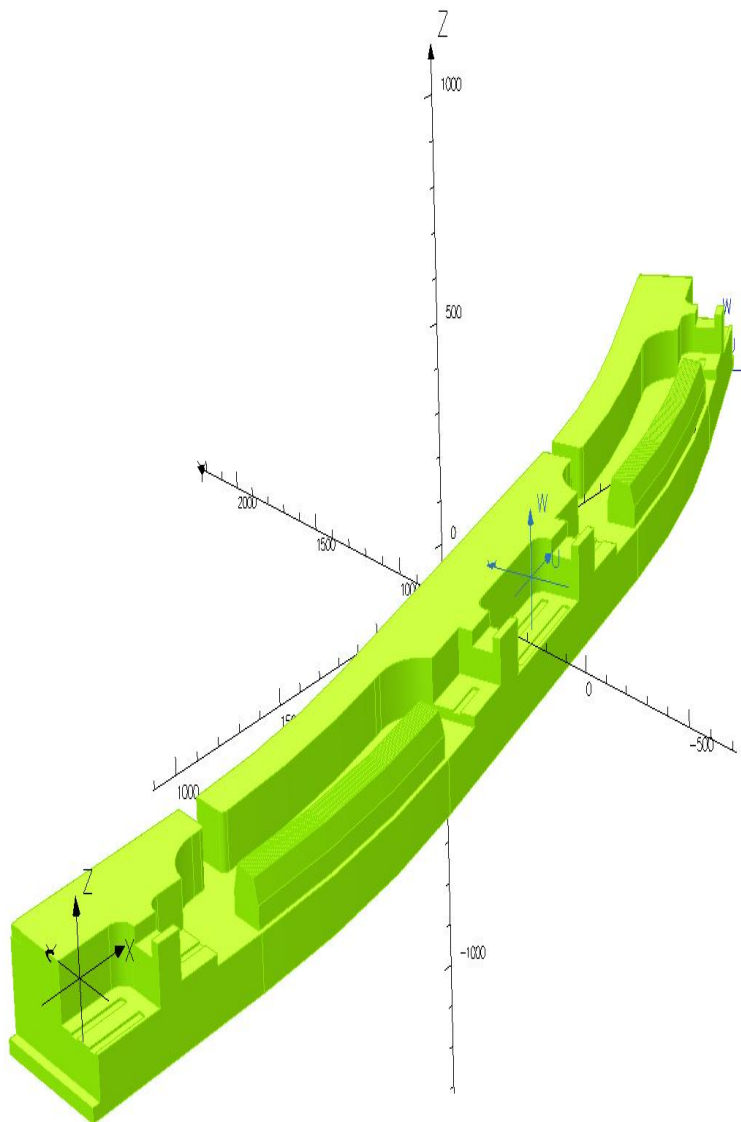


Fig. 5. The magnet structure of a lattice cell is machined into one solid block of iron. The lower half of such a structure is shown here.

MAX III

In the new revised design the MAX III storage ring is not expected to be transferred to the MAX IV facility. The beamlines from MAX III be moved the revised 1.5 GeV ring, where the electron energy will be optimized to cover also these lower photon energies. As long as this can be done without degrading performance of the beamlines there are several advantages with this scenario. The most obvious is that the linac does not need to be designed to inject electrons also at 700 MeV. There will also be less need for floor space. It could also be expected that the transfer of only the beamlines and not the storage ring will reduce the downtime when moving to the new facility. Finally, it is expected that the number of available straight sections on the revised 1.5 GeV ring is enough to host also the beamlines from the MAX III ring.

This performance of the IR & UV beamlines will be discussed more thoroughly in chapter 4 but the basic conclusion is that the improved emittance and current on the revised 1.5 GeV ring compared to the MAX III ring will more than enough compensate for the effect of the higher electron energy.

The table below summarizes the properties of all the storage rings in the revised as well as the original design.

	Energy [GeV]	Circumference [m]	Stored current [A]	Horizontal emittance [nmrad]	Vertical emittance [nmrad]	Horizontal size (σ) [μm]	Vertical size (σ) [μm]
Original Design (CDR)							
MAX IV 12-lattice	3.0	287	0.5	0.86	0.0086	83	4
MAX IV 12-lattice	1.5	287	0.5	0.34	0.034	52	8
MAX III	0.70	36	0.3	13	1.3	400	34
Revised Design							
MAX IV 20-lattice	3.0	528	0.5	0.24	0.009	44	2.6
MAX IV 12-lattice	1.5	96	0.5	5.6	~ 0.12 (assuming 2% coupling)	200	19

Table I. Parameters of the storage rings

3. CONSEQUENCES FOR THE HARD X-RAY ACTIVITIES

Beamlines at the 3.0 GeV ring in the CDR report

In the *MAX IV Conceptual Design Report* from 2006, the number of possible beamlines on the 3.0 GeV ring was limited to eleven; nine very high performance undulators and two high energy/high flux wiggler beamlines. The design did not permit using the bending magnets as radiation sources for the hard X-ray beamlines. In the report the following beamlines were suggested to be housed at the 3.0 GeV ring:

- Nanofocussing: Microscopy and Spectroscopy (NANO-1)
- Nanofocussing: Diffraction, Imaging and μ -tomography (NANO-2)
- Macromolecular Crystallography: High-throughput and Phasing (MX-1)
- Macromolecular Crystallography: Microfocus (MX-2)
- High Resolution Powder Diffraction and Small/Wide Angle X-ray Scattering
- Microfocus X-ray Spectroscopy
- Very High Resolution Soft X-ray Spectroscopy
- Magnetism: Spectroscopy and Spectromicroscopy
- Materials Science and Extreme Sample Conditions (wiggler)

With this suggestion, nine out of eleven possible straight sections would be occupied already from the beginning, and only one of the remaining straight sections could be used for an optimized undulator, as one of them would have to house the second wiggler. This would be a serious limitation for the possibility of future expansions to other experimental techniques, not presented in the proposal. It would also limit the possibility to relocate existing beamlines on the MAX II ring to the 3.0 GeV ring where they would serve an important purpose, e.g. I811 and I911. The limitation in the number of possible beamlines did also put some pressure on sharing different experimental techniques on the same beamline in ways that could be suboptimal. Thus the revised design offers not only generally better conditions for all above beamlines by lowering the emittance and source size but equally important it offers the possibility to host at least eight more high performance beamlines on the ring.

Suggested beamlines/ experimental techniques at the 3 GeV ring that are not present or only partly covered in the CDR:

The beamlines presented in the CDR are still the base when the decision will be made on what beamlines to be built on the MAX IV facility, but after the publication of the CDR report in 2006 there have been several suggestions for new beamlines or new experimental stations that were either missing or only partly covered in the CDR. These suggestions, mainly on the 3 GeV ring, were for instance manifested at the well attended *Science at MAX IV* and *New Directions for MAX IV* workshops held in 2007 and 2008, respectively.

A dedicated SAXS beamline, a solution SAXS beamline

Small Angle X-ray Scattering (SAXS) is, especially at MAX-lab, a rapidly expanding experimental technique where the number of allocated days has increased from 15 to 124 in only three years. There has been a concern that sharing the two experimental techniques of powder diffraction and SAXS, as suggested in the original CDR report, is not an optimal solution. Even though the suggested design did not result in sacrificing the performance, the fact that two separate techniques are implemented on the same beamline inevitably will result in a loss of beamtime when changing between the techniques. The expanding activity within this field may also suggest that a dedicated SAXS beamline may better reflect the need within this user community. This type of beamline would also utilize the outstanding emittance of the MAX IV ring. The possibility to keep a very low divergence and simultaneously a small spot size without sacrificing intensity will permit measuring with a spatial resolution of a few micrometers, reaching very low

scattering angles and still being able to study reactions with a time resolution that is determined more by the experimental set-up than the flux.

Another very attractive possibility would be to have a dedicated set-up for solution SAXS as a compliment. In this type of experiments extreme precautions must be made to ensure stable experimental conditions required due to the very low signal to background ratio. A permanent set-up instead of hosting these on a multipurpose SAXS station would be very beneficial especially if it would be combined with a strong involvement by the groups at University of Copenhagen, which are very successful in this field. Such collaboration has already started around the existing SAXS set-ups at MAX-lab with the ultimate goal to implement micro fluidic cells for macromolecular solution scattering (bioSAXS). At present considerable work is put into this technique within the user community interested in bioSAXS. Micro fluidic studies permits using very small volumes, thus for instance enabling scanning over a wide range of different sample environments, in terms of e.g. salt concentration or pH, to find the optimal crystallization conditions or to study reactions involving macromolecules in physical relevant conditions. The technique has proved to be very promising, and this collaboration has already resulted in successful measurements at the rather restricted set-up on beamline I711. A dedicated high performance station on MAX IV equipped with this type of equipment that is fully incorporated both hard and software wise with the beamline would both in terms of hardware and software be a world unique facility.

Powder diffraction

Since the start of MAX II there has been a strong Nordic interest in performing powder diffraction experiments at MAX-lab. Due to limitations in the experimental set-ups these have been focused more on in-situ measurements than on high resolution structure determinations. At MAX IV it would be an advantage if these in-situ experiments could be done at higher energies than those that are obtainable at an undulator beamline (< 30 keV). Therefore such an experimental beamline/ station should be placed on one of the wiggler stations. This would permit experiments with energies up towards 100 keV. The increased flux at a wiggler source in combination with a fast position sensitive detector will also make it very suitable for kinetic studies down towards the millisecond regime. However, the superior collimation of an undulator beam will make it the preferred choice for the most demanding experiments in terms of resolution. Experiments, like structural refinement of more complex substances, where an instrumental resolution of < 0.01° is required, suggest a high resolution scanning powder diffractometer to be placed on a minimal (vertical) divergence X-ray beamline. Suggestions of combining the technique with different types of spectroscopy (i.e. XAFS and Raman) methods are also of interest.

Tomography/Imaging

The uniquely low emittance of the 3 GeV ring will make it an ideal X-ray source for phase contrast enhanced imaging or tomography. Imaging in two or three dimensions with the high acquisition speed possible at synchrotron sources has found countless applications in fields as diverse as materials research, life science, archaeology and paleontology. Recent advances in beam properties (flux and coherence), hardware (detectors, optics and computers) as well as mathematical methods have made especially three dimensional imaging a very rapidly growing field. Although these techniques were at least partly covered in the CDR on one of the nano-focus beamlines a dedicated and somewhat less experimentally demanding beamline would clearly be advantageous and better reflect the user demands.

Other beamlines for the exploitations of the coherent properties of the radiation

The coherence of the radiation will increase from the lowered emittance of the redesigned 3 GeV ring and this will be beneficial for as mentioned imaging and tomography applications but also for some other activities, such as spectroscopy and spectromicroscopy of magnetic samples (e.g. speckle spectroscopy). Additionally, the exceptionally small emittance of the 3.0 GeV ring makes it an ideal source for X-ray photon correlation spectroscopy (XPCS). This possibility was not pointed out in the CDR, but a session at the *Science at MAX IV* workshop demonstrated the growing interest in the XPCS technique. The prospect of offering such capabilities at MAX IV should therefore be kept in mind.

High kinetic energy photoemission (HIKE)

In the CDR, the idea of building a high kinetic energy photoemission endstation at the Materials Science wiggler beamline was mentioned. However, the increasing involvement and interest from Swedish and Nordic groups in this technique motivate a more dedicated solution. At the session concerned with high kinetic energy photoemission at the *Science at MAX IV* workshop it was made clear that an undulator source would be much superior to a wiggler for this purpose, and that the combination of photoemission with scanning techniques such as EXAFS on the same beamline is impractical. Instead, a combination with inelastic X-ray scattering, a spectroscopic technique with similar demands, would be much more suitable.

Relocation of MAX II hard X-ray beamlines

The relocation of beamline I811 and the central SAD/ MAD station on I911 was mentioned as a possibility in the CDR. If these beamlines could be moved to the new facility without any major modifications they would offer a very cost effective possibility to do bulk experiments with EXAFS and protein crystallography. The limited number of straight sections and the limited possibility of using the bending magnets due to their inadequate spectral range would, however, make this unlikely. The revised 20-cell ring design with an increased number of straight sections and further possibility for an upgrade to use some of the short straight sections has again highlighted this option.

4. CONSEQUENCES FOR THE SOFT X-RAY ACTIVITIES

General considerations

The change from the conceptual design of the MAX IV facility will affect the soft X-ray research. Below, some specifics for the beamlines and activities presented in the CDR will be discussed, but some general observations can be made. The revised smaller 1.5 GeV storage ring will cover the needs for the soft X-ray communities, but there are a couple of differences with this solution. First of all the emittance and source size on the revised 1.5 GeV ring is somewhat larger compared to the original design. This will reduce the brilliance somewhat. Secondly the length of the straight sections are shorter than those originally planned for MAX IV (3.48 m vs. 4.6 m). However, the reduction in terms of photon flux, as will be discussed below, is not a major issue and the vertical beam size is still small enough to give an ultimate energy resolution (limited mainly by the available quality of optics) for typical monochromators like SX-700 type PGMs and collimated PGMs.

In Appendix 3 we have collected a number of calculations relevant to soft X-ray beamlines.

In chapter 1 of this appendix the performance of collimated PGMs is investigated and the statement above that the electron beam size has a negligible influence on the energy resolution is confirmed.

The following four chapters in the appendix deal with the photon flux from IDs under different source conditions. The results are given in terms of photon flux in the energy range below 2 keV calculated for emission angles that match the acceptance angles of a typical soft X-ray monochromator.

Chapter 2 compares the revised 1.5 GeV ring with the MAX II ring. In this scenario the MAX II ring has been upgraded with new vacuum chambers to allow for 300 mA constant stored current (using top-up) and running at a lower coupling than today (i.e. smaller vertical beam size). This comparison was done since moving MAX II to the new MAX IV site has been one possible option after abandoning the original 1.5 GeV ring presented in the CDR. From the flux curves it is obvious that the (almost cost-neutral) choice of a revised 1.5 GeV ring is the best choice.

Chapter 3 deals with the UV/VUV beamlines presently running at MAX III (700 MeV). These are beamlines covering the photon energy range 5-50 eV and 13-200 eV, respectively. As seen from the flux curves the revised 1.5 GeV ring gives higher flux over the whole energy range from 5 to 50 eV. This is even more accentuated at photon energies above 50 eV (not shown). The IR spectromicroscopy beamline on MAX III (presently under construction) will also be possible to install on the revised 1.5 GeV ring. Thus, the revised 1.5 GeV ring can host the present MAX III beamlines, and even improve their performance, and the original plan to move MAX III to the new MAX IV site can be canceled.

In chapter 4 the issue of running the revised 1.5 GeV ring at lower energies is addressed. The reason for looking into this is simply that lowering the electron energy also lowers the horizontal emittance and leads to a smaller beam size. However, comparing the flux for a 1.0 GeV operation with 1.5 GeV it is clear that 1.0 GeV is not a good choice for photon energies above 100 eV. Below this photon energy the gain for 1.0 GeV operation is only about 20% (a more detailed comparison is seen in figure 3.1, chapter 3).

These flux curves are calculated for a typical soft X-ray monochromator and do not apply for microscopy/imaging beamlines with exceptionally small acceptance angles (e.g. focusing with Fresnel zone plates or holographic imaging using micrometer sized pin-holes). However, since the main applications for such beamlines are in the water window (300-500 eV) or even higher photon energies, e.g. for the 3d magnetic materials, the difference in flux still favors operation at 1.5 GeV.

Chapter 5 shows a few examples of soft X-ray undulators placed on the revised 1.5 GeV and 3 GeV rings, respectively. Undulators that cover the photon energy range from 38 eV and upwards (black and red curves in figure 5.1) give higher flux at the 3 GeV ring over the whole photon energy range. This might suggest that soft X-ray beamlines should be placed at the 3 GeV ring and not on the 1.5 GeV ring. However, the gain in flux comes with a high price in emitted power which will not be easy to handle together with the demand of very high precision optics. The output power from undulators on the 1.5 GeV ring is in the range 1-2 kW, which we know we can handle, while the power from the 3 GeV ring is ten times higher. These high power loads (10-20 kW) will be a technical challenge, especially when combined with requirements on high energy resolution, beam stability and easy operation. Nevertheless, some soft X-ray beamlines with special demands on flux and/or beam size will be built on the 3 GeV ring, and the new 20 cell design allows for this without intruding on space for hard X-ray beamlines. These soft X-ray beamlines are e.g. the "Very High Resolution Soft X-ray Spectroscopy" beamline and the "Magnetism: Spectroscopy and Spectromicroscopy" beamline. In the latter case the reason for choosing the 3 GeV ring is that with this electron energy a

polarizing undulator (EPU) can deliver 100% circular polarized light up to and above 1 keV from the fundamental harmonic.

Finally chapter 6 compares the radiation from bending magnets from the present MAX II ring with the revised 1.5 GeV ring. A substantial improvement over today's situation is seen.

Specific beamlines

In the CDR, four beamlines intended to be built at the 1.5 GeV ring were presented:

- Ultra high resolution VUV scattering
- Soft X-ray nanoscience and spectromicroscopy
- Soft X-ray spectroscopy and surface reactions
- Soft X-ray gas phase spectroscopy

Additionally, the possibility of relocating the beamlines I311, I411, I511 and D1011 to the new ring was considered.

Added to this list should be the three beamlines from the present MAX III ring:

- Infrared high-resolution spectroscopy and spectromicroscopy.
- Angular- and spin- resolved photoemission, atomic and molecular spectroscopy, luminescence 5 - 50 eV.
- Angular resolved photoemission 13 - 200 eV.

Some of the more salient points for each beamline with regards to the situation at MAX IV are discussed below.

Ultra high resolution VUV scattering (30-600 eV)

VUV scattering is a very flux demanding experiment. The achievable resolution depends very much on the spot size at the sample position, and the design goal for the spot size in the CDR was $1 \times 1 \mu\text{m}$. This beamline is a complement to the one suggested for the 3.0 GeV ring (the *Very High Resolution Soft X-ray Spectroscopy* beamline), but working at a lower energy.

Soft X-ray nanoscience and spectromicroscopy (90 -1500 eV)

Similar considerations apply to this beamline as to the *Ultra high resolution VUV scattering* beamline: A small spot size is needed on the sample, for both the XPEEM and the STXM end stations. Further investigations are needed to determine if this beamline should be placed at the 1.5 GeV ring or the 3 GeV ring.

Soft X-ray spectroscopy and surface reactions (60-1500 eV) and Soft X-ray gas phase spectroscopy (90-1500 eV)

These beamlines have more moderate demands on the beam size at the sample than the two previous beamlines. Since the full energy range can be covered by optimized undulators on a 1.5 GeV ring, and the low vertical emittance will allow very high photon energy resolution, the new design will mean if any only minor drawbacks.

Relocated beamlines from MAX II

The relocation of MAX II beamlines will provide a cost effective way of achieving several high quality standard spectroscopy beamlines. They will give users easy access to XAS and XPS experiments. Another important aspect is that they can be used for training of new unexperienced users and for educational purposes.

Suggested beamlines/experimental techniques at the 1.5 GeV ring that are not present or only partly covered in the CDR:

The above listed beamlines still form the basis of soft X-ray beamlines in the MAX IV project but during the workshops *Science at MAX IV* and *New Directions for MAX IV* workshops held in 2007 and 2008, respectively some further ideas have emerged.

An Environmental Science beamline in the energy range of 1 – 3 keV

The energy range of 1-3 keV is of special interest for the environmental science community as the absorption edges for aluminum, silicon, phosphorus and sulphur are in this region, elements of utmost importance in many environmental research areas. This energy regime is considered to be difficult since it is in the intermediate range between grating and crystal optics. It puts special demands on optics, detectors and sample manipulations and it is difficult to cover this energy regime at more standard high energy EXAFS beamlines without sacrificing performance. This beamline is actually planned to be put into operation already now on D811 (a bending magnet on the MAX II ring) but designed already from the start with the intention of an ultimate placing on either of the MAX IV 1.5 or 3 GeV ring.

A coherent imaging beamline

In recent years a tremendous development has taken place in the field of soft X-ray imaging. Utilizing the partial coherence of the undulator radiation, lens-less holographic imaging has proved feasible. Images of nanostructured surfaces show that a lateral resolution in the 40-50 nm range can be achieved at today's storage rings. Using polarized radiation and the magnetic dichroism effect, images of nano-sized magnetic domains have been demonstrated. These, and related, techniques should of course be exploited within the MAX IV project. If these experiments will require a dedicated beamline or if they could be performed on a branch line on one of the spectroscopy beamlines is still to be decided. These soft X-ray experiments might be set-up at the 3 GeV ring since, due to its lower emittance, it has a higher degree of coherence.

5. BUDGET

The first cost estimate of the MAX IV facility was presented in 2005. At that time a large number of the details in the design were unknown. Since then the cost estimates have been continuously refined and updated. During the detailed design phase of the project it was realized that a new layout of the accelerator complex would better correspond to the user needs. We have therefore investigated if these modifications can be made without increasing the total cost of the project. We find that this is possible.

First of all we find that the total accelerator costs have not increased due to the redesign. Even if the 3 GeV ring is considerably larger in the new design there are cost reductions that compensate for this. The cost of increasing the circumference of the 3 GeV ring from 287 to 528 m is to a large extent compensated by the decreased size of the 1.5 GeV ring (96 m vs 287 m). We can also accommodate all MAX III beamlines at the revised 1.5 GeV ring. This removes the relocation and installation costs for MAX III. This also simplifies the injector design since electrons need only be extracted from the linac at two energies instead of at three energies.

If we compare the costs for the old design calculated in 2005 and the present estimated cost there is an increase from 690 MSEK (value 2005) to 840 MSEK (value 2009). This corresponds rather well to the increase in cost for an identical system during these four years. A substantial part of this is due to the change in exchange rate for the SEK.

Also for the beamlines the costs remain constant in real values. All proposed changes in beamline layout have been made in such a way that the total cost remains the same. Furthermore, the program for beamline build-up contains a lot of flexibility. The proposed build-up incorporates a number of new beamlines as well as several beamlines that are relocated from the present MAX-lab. There is of course the possibility of a staged build-up of beamlines, although it is important to incorporate all major scientific disciplines already from the beginning.

Our main concern when looking at the possibility to modify the accelerator design was the cost of the building. The radius of the building increases significantly but it is mainly the area that is of importance. It is found that the modified design does not automatically lead to an increased size of the building. The estimated area of the original design was 32 400 m². The present area is instead 32 000 m². In fact, this corresponds to a substantial reduction of the size of the ring, laboratory and office buildings. During the design work it was realized that the original layout of the linac tunnel had to be modified. A second tunnel is needed for safety reasons and for securing an efficient operation. This adds 2500 m² to the total area. This modification would have been necessary also for the original layout of the accelerators. This implies that we have managed to reduce the size of the remainder of the building. With the larger storage ring circumference it is possible to place office space above the ring and between the beamlines on the floor of the ring building. The larger circumference of the ring building also makes it possible to make the building less wide for the same length of the beamlines.

There is an increased cost of the building but these are then mainly due to the following parts:

- Upgrade of the linac building: 180 MSEK
- Building index: 50 MSEK
- Originally the City of Lund had allocated a minimal area around the MAX IV building. They have now changed their plans and increased this area: 70 MSEK
- The development of the scientific plans have also identified the need for a few long beamlines that were not identified in the very initial design. This is connected to the identified potential to produce beamlines with extreme nanofocussing capabilities. The required length for these beamlines is in fact smaller for the new design which implies that this additional cost is reduced by the redesign: 25 MSEK

For some of the parts of the building we have rather managed to reduce the costs. In total the estimated cost of the building has increased by about 300 MSEK. All of this is independent of the redesign of the accelerator layout. The redesign itself has rather led to a small reduction of the investment cost.

Also the operational budget is independent of the redesign since it has not modified the number of planned beamlines.

6. CONCLUSIONS

We present a modified layout of the MAX IV accelerators. For the 3 GeV ring we go from a 12-cell to a 20-cell ring. This corresponds better to the user requirements for beamlines at the 3 GeV ring. It relaxes the need for combining different techniques at the same beamline and it allows putting those soft X-ray beamlines that benefit from a higher ring energy at the 3 GeV ring. Furthermore, there will be several unoccupied straight sections that can be used at a later stage. The beamlines at the 3 GeV ring will also benefit from the smaller electron beam emittance of the 20-cell ring compared to the original 12-cell ring.

A large part of the soft X-ray beamlines will be placed at the 1.5 GeV ring. There is a slight reduction of performance of some of these due to the larger electron beam emittance compared to the original 1.5 GeV ring. This is, however, more than compensated by the increased performance of those soft X-ray beamlines that fit better on the 3 GeV ring. All MAX III beamlines can be accommodated at the 1.5 GeV ring which removes the need to move the MAX III ring.

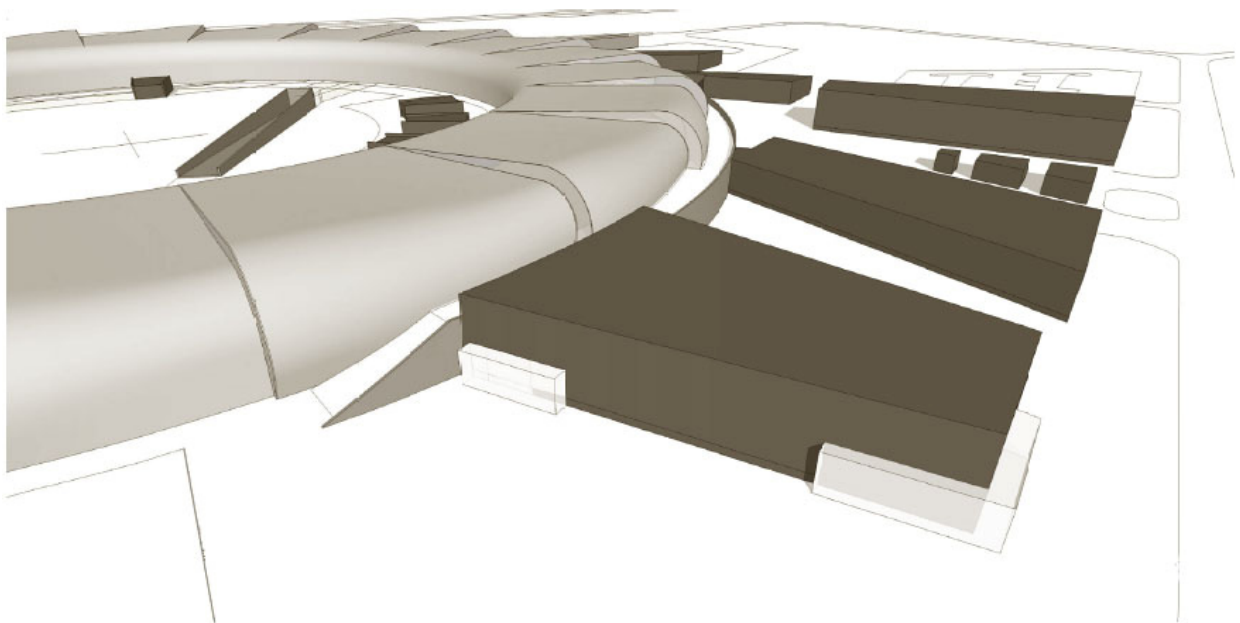
We conclude that the redesign can be made without increasing the accelerator costs. Also the building costs have been found to be essentially unaffected by the redesign.



Appendix 1

Revised design of the MAX IV facility

Background material for the VR evaluation September 2009



Beam dynamics for the MAX IV 3 GeV storage ring

S. C. Leemann,* Å. Andersson, M. Eriksson, L.-J. Lindgren, and E. Wallén
MAX-lab, Lund University, S-22363 Lund, Sweden

J. Bengtsson
NSLS-II, Brookhaven National Laboratory, Upton, NY 11973, USA

A. Streun
SLS, Paul Scherrer Institute, CH-5232 Villigen, Switzerland
(Dated: August 4, 2009)

MAX IV will be Sweden's next-generation high-performance synchrotron radiation source. The project has recently been granted funding and construction is scheduled to begin in 2010. User operation for a broad and international user community should commence in 2015. The facility is comprised of two storage rings optimized for different wavelength ranges, a linac-based short-pulse facility and a free-electron laser for the production of coherent radiation. The main radiation source of MAX IV will be a 528 m ultra-low emittance storage ring operated at 3 GeV for the generation of high-brightness hard X-rays. This storage ring was designed to meet the requirements of state-of-the-art insertion devices which will be installed in nineteen 5 m long dispersion-free straight sections. The storage ring is based on a novel multi-bend achromat design delivering an unprecedented horizontal bare lattice emittance of 0.33 nm rad and a vertical emittance below the 8 pm rad diffraction limit for 1 Å radiation. In this paper we present the beam dynamics considerations behind this storage ring design and detail its expected unique performance.

PACS numbers: 29.20.db, 29.27.Bd, 29.27.Eg, 41.60.Ap

I. INTRODUCTION

Several high-performance third generation synchrotron radiation sources like SLS [1], SOLEIL [2], and Diamond Light Source [3] have gone into operation in the last decade. As the technology of insertion devices (IDs) develops, requirements for synchrotron sources increase. This has sparked the design of advanced third-generation sources which push even higher brightness, sub-micron stability, and high constant stored current. Several such sources are presently under construction around the world: NSLS-II in the USA [4, 5], PETRA III in Germany [6], and MAX IV in Sweden [7].

The MAX IV approach accounts for the fact that the different requirements of advanced synchrotron radiation sources cannot be equally fulfilled by a single machine. The required spectral range stretches from infrared to hard X-rays while the time structure is required to satisfy both intense pulses in the fs domain as well as high average brightness in long pulses. In addition to spontaneous radiation, there is also an increasing demand for both temporally and spatially coherent radiation. A global optimization of the MAX IV facility based on this wide range of challenging demands has resulted in a solution with two separate storage rings and a linac-driven short-pulse facility which in a second stage will be upgraded with a free-electron laser. The two storage rings are operated at different energies to provide radiation of high

brightness over a broad spectral range. The 3 GeV linac serves as a full-energy injector for the storage rings as well as the driver of the short-pulse facility delivering intense X-ray pulses below 100 fs at 100 Hz [8]. In the first stage this will be spontaneous radiation with an upgrade to a coherent free-electron laser source based on seeding and/or cascading expected in a second stage.

The UV and soft X-ray storage ring will be a new 1.5 GeV storage ring. It is similar to the existing MAX II storage ring [9] in size, but will feature a new vacuum system, an upgraded lattice, and new magnets to provide better performance for modern IDs, but also in order to extend to lower energy beamlines. Thus present-day beamlines at the 700 MeV MAX III storage ring [10] can be moved to the new 1.5 GeV ring. By building a new 1.5 GeV ring rather than relocating MAX II and MAX III to the new MAX IV site, a "dark period" for UV users at MAX-lab can be avoided.

An entirely new 3 GeV storage ring which has been optimized for hard X-rays will complete the MAX IV facility. The lattice is based on the 20-fold 7-bend achromat described in [11]. With its unprecedented horizontal bare lattice emittance of 0.33 nm rad and a vertical emittance adjusted to the diffraction limit of its IDs it is the most demanding storage ring at MAX-lab. Initial design studies [7, 11–15] have been heavily revised and a detailed design is presently being completed [16]. Construction of the facility is scheduled to begin in 2010. User operation should commence in 2015.

This paper will highlight the MAX IV 3 GeV storage ring lattice and the beam dynamics considerations of the detailed design study. The following section presents the

*Electronic address: simon.leemann@maxlab.lu.se

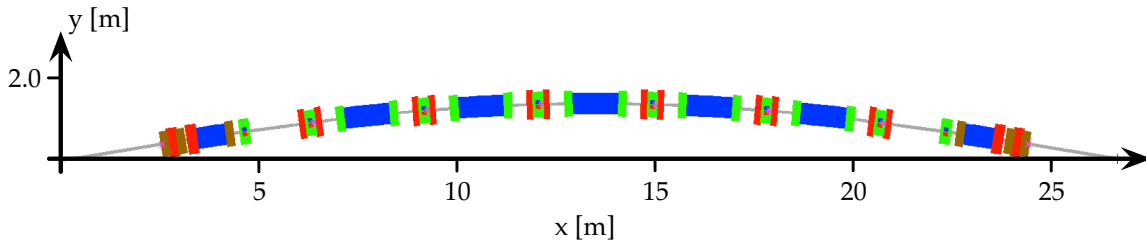


FIG. 1: (Color online) Schematic of one of the 20 achromats in the 3 GeV storage ring. Magnets indicated are gradient dipoles (blue), focusing quadrupoles (red), sextupoles (green), and octupoles (brown).

lattice, nonlinear optimizations and damping wigglers. Section III touches on related magnet, vacuum, and RF technology issues. Finally, Section IV demonstrates the expected dynamic performance of the lattice but also of the entire machine as a high-brightness source of synchrotron radiation. A summary and conclusions are given in Section V.

II. LATTICE

A. Multi-bend Achromat

The figure of merit of a modern synchrotron radiation facility is a small emittance of the electron beam. The magnet lattice defines the emittance as $\varepsilon = C E^2 / N_d^3$ where E is the beam energy, N_d is the number of dipole magnets, and C is a constant given by the lattice. The bare lattice emittance is then further reduced by strong IDs. Minimizing C by appropriate choice of the lattice functions is the Theoretical Minimum Emittance (TME) design approach [17]. This approach however is hampered by problems of nonlinear optics design and high sensitivity to lattice imperfections resulting from overstrained optical functions. Instead, the MAX IV 3 GeV storage ring is based on a very simple but robust design approach: ultra-low emittance is achieved by increasing the number of dipoles N_d . In order to prevent the ring from becoming large and costly, the number of magnets is increased by shortening the magnet cells. However, shorter magnet cells require stronger focusing gradients to keep the electron optics optimized. The strong gradients required for the MAX IV 3 GeV storage ring are achieved by a reduction of the transverse dimensions of the magnet elements (see Section III B for associated vacuum issues).

The storage ring is composed of 20 achromats (super-cells) which each contain seven magnet cells: five unit cells plus two matching cells. The matching cells are separated from the unit cells by a 1.3 m long short straight where RF cavities can be installed [47]. The achromats are connected by 5 m long straight sections. The matching cells closely resemble the unit cell, but with only half a dipole (similar to a missing magnet dispersion sup-

pressor). A schematic of one MAX IV 3 GeV achromat is given in Fig. 1. The unit cells contain 3° bending magnets with a gradient for vertical focusing. Focusing quadrupoles are interleaved between the dipoles [48]. The matching cells contain short 1.5° gradient bends with a soft-end (that is, a longitudinally varying dipole field with field strength reducing towards the long straight) to reduce synchrotron radiation heat load on the downstream ID [49]. A quadrupole doublet in the matching section allows matching of the achromat optics to the ID in the long straight section.

TABLE I: Parameters for the MAX IV 3 GeV storage ring. Permanent-magnet damping wigglers (PMDWs) are used to further reduce the storage ring emittance (see Section II C).

Energy [GeV]	3.0
Main radio frequency [MHz]	99.931
Harmonic number	176
Circulating current [mA]	500
Circumference [m]	528
Number of achromats	20
No. of long straight sections available for IDs	19
Betatron tunes (horizontal / vertical)	42.20 / 14.28
Natural chromaticities (horizontal / vertical)	-49.8 / -43.9
Corrected chromaticities (horizontal / vertical)	+1.0 / +1.0
Momentum compaction factor	3.07×10^{-4}
Horizontal damping partition J_x	1.86
Horizontal emittance (bare lattice) [nm rad]	0.326
Horizontal emittance (with 4 PMDWs) [nm rad]	0.263
Radiation losses per turn (bare lattice) [keV]	360.0
Radiation losses per turn (with 4 PMDWs) [keV]	572.1
Natural energy spread	0.077%
Energy spread (with 4 PMDWs)	0.096%
Required dyn. acceptance (hor. / ver.) [mm mrad]	7.1 / 1.3
Required lattice momentum acceptance	$\pm 4.5\%$

The optical functions for one achromat are displayed in Fig. 2 and the main parameters of the 3 GeV storage ring are given in Table I. The strong gradient in the bending magnets yields a very compact lattice (12.5 m horizontal betatron wavelength). A summary of the dipole and quadrupole strengths is given in Table II. The optics in

TABLE II: Dipole field and quadrupole gradients for different magnet families in the MAX IV 3 GeV storage ring (bare lattice). For the dipoles, the length given corresponds to the iron length; for the quadrupoles the hard-edge magnet length is specified. The quadrupole gradient of the matching cell dipole specified here corresponds to the peak strength; the dipole gradient in the soft-end dipole varies longitudinally in the same way as the dipole field.

	Length [m]	Dipole Peak Field [T]	Quadrupole Gradient [T/m]
Dipole (unit cell)	0.974	0.524	-8.69
Soft-end dipole (matching cell)	0.554	0.524	-8.69
Focusing quadrupole (unit cell)	2×0.15	—	40.39
Focusing quadrupole (facing matching cell)	2×0.15	—	37.80
Final focusing quadrupole (matching cell)	0.25	—	35.34
Final defocusing quadrupole (matching cell)	0.25	—	-22.40

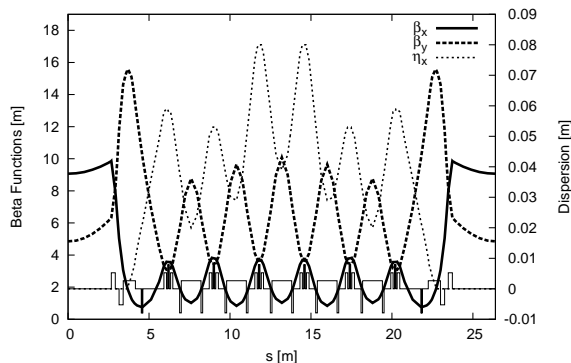


FIG. 2: Beta functions β_x , β_y and dispersion η_x for one achromat of the 3 GeV storage ring. The position of the dipoles, quadrupoles, and sextupoles are indicated at the bottom.

the achromat have been tuned in such a way that the vertical beam size in the straight section is below the diffraction limit even for modest values of coupling. At a radiated wavelength of $\lambda_{\text{rad}} = 1 \text{ \AA}$ the photon diffraction limit is $\varepsilon_{\text{rad}} = \lambda_{\text{rad}}/4\pi = 8 \text{ pm rad}$. This is 2.4% of the horizontal bare lattice emittance and corresponds to a vertical beam size of $6 \text{ }\mu\text{m}$ at the center of the straight section. However, for longer wavelength beamlines, a larger vertical beam size would be sufficient to meet the diffraction limit. Because of intrabeam scattering and lifetime concerns (see Section IV E), it is not advisable to chose a vertical beam size below the diffraction limit. Therefore it is foreseen to include a set of geometric and chromatic skew quadrupoles in the lattice in order to gain tight vertical beam size control. Betatron coupling leading to spurious vertical dispersion will be suppressed so the vertical beam size meets the diffraction limit in the IDs delivering the hardest radiation. The vertical beam size in the achromats can then be increased in order to retain good lifetime by local control of the vertical dispersion (h_{00101}) without driving global linear coupling (h_{10100} and h_{10010}) [18].

B. Nonlinear Optics and Higher-order Correction

Although the overall optics are relaxed (considering the ratio $\xi_x/\nu_x \approx -1.2$), the compact lattice is of strong focusing nature leading to a large negative natural chromaticity. Chromatic sextupoles are required in order to reduce this high natural chromaticity. The nonlinearities of the lattice then have to be corrected to retain sufficient dynamic aperture. Because of the modest dispersion in the achromat, the chromatic sextupoles are strong. It was originally foreseen to integrate the focusing sextupole into the focusing quadrupoles between the unit cell dipoles. This idea was later dropped in order to retain full tuning capability and reduce nonlinearities arising from the long sextupole magnets. Instead, the focusing quadrupoles between the unit cell dipoles were split up and a short sextupole inserted in the center (see Section III A). This puts the sextupoles at local dispersion maxima which relaxes magnet requirements.

In addition to these focusing sextupoles, defocusing sextupoles have been installed in pairs flanking the unit cell dipoles and on the high-field end of the matching cell dipole. Because of the large number of installed sextupoles and the small magnet apertures (25 mm diameter) the sextupoles can be kept short. The OPA code [19] was used to optimize the sextupole settings: in addition to correcting the linear chromaticity to $\xi_{x,y} = +1.0$ [50] in both planes (driven by terms h_{11001} and h_{00111}), two first-order chromatic (h_{20001} and h_{00201}) and five first-order geometric terms (h_{21000} , h_{10110} , h_{30000} , h_{10020} , h_{10200}) of the sextupole Hamiltonian were minimized along with the quadratic chromaticities ($\xi_x^{(2)}$, $\xi_y^{(2)}$) and amplitude-dependent tune shifts ($\partial\nu_x/\partial J_x$, $\partial\nu_y/\partial J_y$, $\partial\nu_x/\partial J_y = \partial\nu_y/\partial J_x$) [20, 21]. Resulting amplitude-dependent tune shifts and chromatic behavior were verified with Tracy-3 [22] for the bare lattice and the lattice with IDs.

The high periodicity of the lattice reduces the number of allowed resonances. And although the choice of working point keeps the tunes clear of potentially limiting resonances, the number of sextupole families used to minimize the above-mentioned terms was insufficient. Amplitude-dependent tune shifts remained too

TABLE III: Sextupole and octupole gradients for different magnet families in the MAX IV 3 GeV storage ring (bare lattice). The specified length corresponds to the hard-edge field length.

	Length [m]	Sextupole Gradient [T/m ²]	Octupole Gradient [T/m ³]
Focusing sextupoles (unit cell)	0.1	2148 / 1700 / 1600	—
Defocusing sextupole (unit cell)	0.1	-1179	—
Defocusing sextupole (matching cell)	0.1	-1340	—
Focusing octupole (matching cell)	0.1	—	21814
Defocusing octupoles (matching cell)	0.1	—	-13143 / -6886

large leading to reduced dynamic aperture. However, since amplitude-dependent tune shifts are a second-order effect from the sextupole Hamiltonian, it is clear that sextupoles are inefficient at fighting them. Instead, three dedicated harmonic octupole families were added to the matching cell at positions with optimum beta function ratios [23, 24].

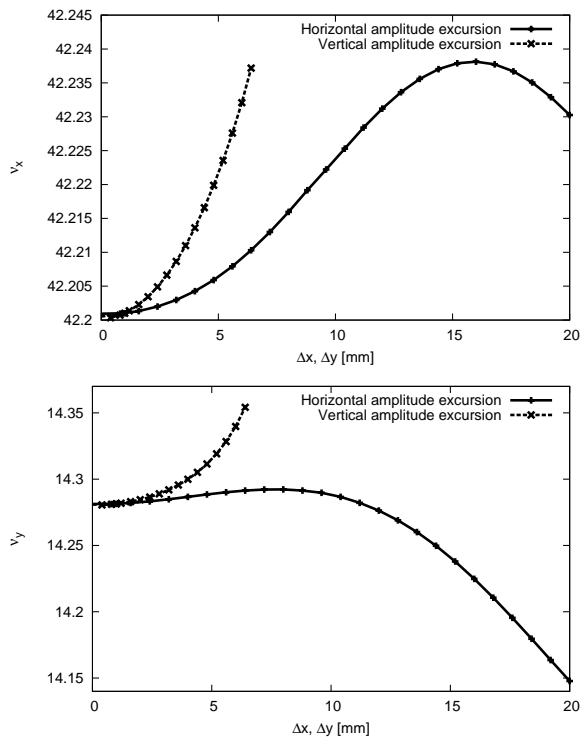


FIG. 3: Amplitude-dependent tune shifts for the 3 GeV storage ring bare lattice. Sextupoles and octupoles have been included in this calculation.

These three octupole families were then used to effectively fight the three Hamiltonian driving terms for amplitude-dependent tune shift: $h_{22000} \rightarrow \partial\nu_x/\partial J_x$, $h_{00220} \rightarrow \partial\nu_y/\partial J_y$, $h_{11110} \rightarrow \partial\nu_x/\partial J_y = \partial\nu_y/\partial J_x$. Accordingly, the sextupoles could then be re-optimized to fight only first-order sextupole terms and adjust chromatic tune shifts. By properly tuning the cubic chromaticities ($\xi_x^{(3)}, \xi_y^{(3)}$) and minimizing the quadratic chromaticities ($h_{11002} \rightarrow \xi_x^{(2)}, h_{00112} \rightarrow \xi_y^{(2)}$) the chromatic tune shift can be “wrapped up” around the working point keeping the chromatic tune footprint very compact (cf. Fig. 13). A summary of the sextupole and octupole parameters is given in Table. III. An in-depth comparison of the MAX IV 3 GeV storage ring lattice and its performance with and without higher-order octupole correction is given in [24].

maticities ($\xi_x^{(3)}, \xi_y^{(3)}$) and minimizing the quadratic chromaticities ($h_{11002} \rightarrow \xi_x^{(2)}, h_{00112} \rightarrow \xi_y^{(2)}$) the chromatic tune shift can be “wrapped up” around the working point keeping the chromatic tune footprint very compact (cf. Fig. 13). A summary of the sextupole and octupole parameters is given in Table. III. An in-depth comparison of the MAX IV 3 GeV storage ring lattice and its performance with and without higher-order octupole correction is given in [24].

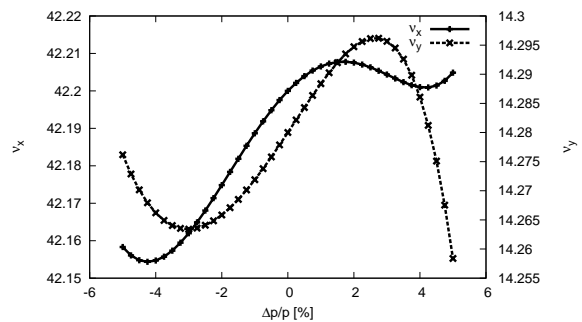


FIG. 4: Chromaticity for the 3 GeV storage ring bare lattice. Sextupoles and octupoles have been included in this calculation. The linear chromaticity has been corrected to +1.0 in both planes.

Because of the large beta function ratios at the chosen octupole locations, the required octupole strengths are low and the magnets can be kept short and simple. With the proper octupole tuning the amplitude-dependent tune shifts can be reduced to very small values (see Fig. 3). As a result of the sextupole re-optimization the chromatic tune footprint has been minimized and the overall sextupole strength reduced (see Fig. 4).

The resulting nonlinear optics settings also ensure that the two synchro-betatron terms h_{20001} and h_{00201} are kept as small as possible. This is crucial for good longitudinal acceptance (see Section IV B) because these terms drive the momentum-dependent beat of the beta functions ($d\beta_x/d\delta, d\beta_y/d\delta$). Dependence of the beta functions (at the center of the long straight section) on momentum deviation is shown in Fig. 5.

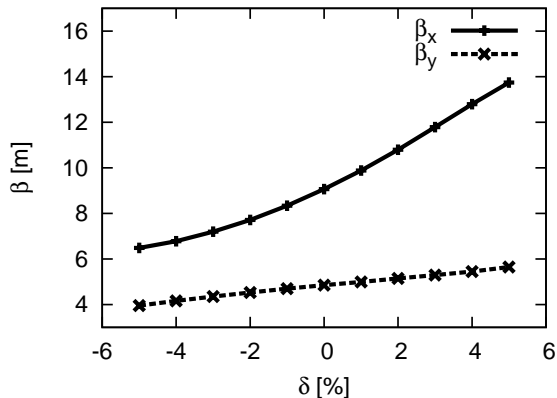


FIG. 5: Dependence of the beta functions (at the center of the long straight section) on momentum deviation for the bare lattice. Sextupoles and octupoles have been included in this calculation.

C. Damping Wigglers

Damping wigglers will be used to further reduce the bare lattice emittance and damping time. Two cases were studied so far. The first option makes use of two superconducting damping wigglers installed in opposite straight sections. Each of these devices is 1.5 m long and has a peak magnetic field of 3.5 T. An alternative option foresees the installation of two or four normal-conducting permanent magnet damping wigglers (PMDWs) in several straight sections. These devices will be 2 m long and have a peak magnetic field of 2.22 T (see Table IV). If four of these devices are installed in the MAX IV 3 GeV storage ring the horizontal emittance can be reduced from 0.33 nm rad to 0.26 nm rad. The radiated energy per turn is increased from 360 keV to 572 keV while the damping time is reduced by 24%.

TABLE IV: Parameters of the permanent magnet damping wigglers.

Length [m]	2.0
Period length [mm]	80
Peak magnetic field strength [T]	2.22
Full gap height [mm]	4
Radiated energy per turn [keV]	53

Due to their strong vertical focusing effect the damping wigglers have to be compensated in order to ensure optimum dynamic performance. This will be done in two steps. First, the final quadrupoles in the matching sections flanking the damping wigglers are adjusted to reduce the vertical beta function in the straight section making the beam less sensitive to the vertical focusing of the wiggler. In principle this local compensation could

be achieved in the opposite manner by reducing the vertical focusing at the entry to the straight to compensate for the additional vertical focusing of the wiggler. This however has the drawback of increasing the vertical beam size within the IDs. We therefore chose to compensate by increasing the vertical focusing in the straight even though this comes at the cost of a larger overall phase advance. In a second step, the main focusing quadrupole family and the defocussing pole strips in the dipoles are adjusted to restore the global working point. Studies have shown that this procedure does not necessarily require retuning the sextupole and octupole optics [16].

It is currently under investigation if such compensation should also be implemented in a feed-forward scheme for strong in-vacuum undulators with variable gap settings. The great advantage of such a combined local/global compensation for IDs is that the optical functions and tunes in the entire machine are kept as close as possible to their bare lattice design values for which the nonlinear optics have been optimized. The result is that dynamic performance should remain high regardless of ID gap settings since the working point is always restored and tune shifts away from it are kept small.

III. TECHNOLOGY

A. Magnets

The magnets for the MAX IV 3 GeV storage ring are required to be very compact. Together with the very low emittance of the beam this calls for very strong multipole magnets. The foreseen solution is to use magnets with very small apertures and a narrow vacuum chamber. The dipoles are C-type with a gradient; the gap therefore varies around the center value of 28 mm. The quadrupole, sextupole, and octupole magnets have full apertures of 25 mm. The good field region (defined as the area where the main field component is within $\pm 0.02\%$ of the design field strength) of these magnets extends to no less than ± 10 mm in the horizontal plane.

As already successfully demonstrated in MAX III [10], several magnets will be machined into a common iron block resulting in an integrated girder-magnet design. This inexpensive design approach has the advantage that alignment errors can be reduced to the level of machining accuracy (on the order of 10 μm). For the MAX IV 3 GeV storage ring it is foreseen to integrate the defocusing sextupoles together with the unit cell dipoles (displayed in Fig. 6), the focusing quadrupoles with the focusing sextupoles between the unit cells (displayed in Fig. 7), as well as the matching cell consisting of a defocusing sextupole, the soft-end dipole, the final focusing quadrupole doublet, and the octupoles.

The dipole magnet blocks will be installed on massive concrete supports at low height. In between these structures, quadrupole magnet blocks are installed on rigid bridge girders attached on both sides to the massive

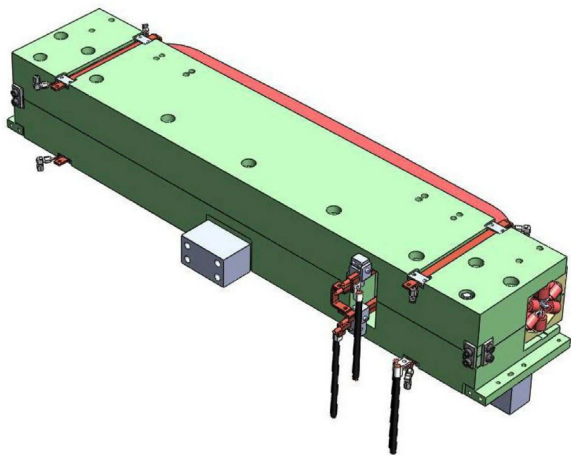


FIG. 6: (Color online) Illustration of the unit cell dipole magnet block. The common iron block integrates the unit cell dipole and the two flanking defocusing sextupoles.

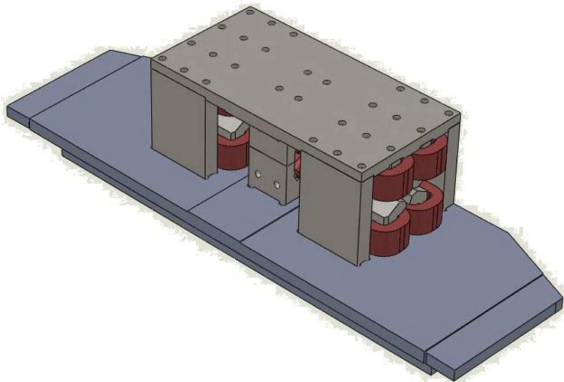


FIG. 7: (Color online) Illustration of the quadrupole magnet block. The common block integrates two focusing quadrupoles and a focusing sextupole between the unit cells. The block itself contains the supporting bridge girder which is attached on both sides to the massive concrete blocks supporting the dipole magnet blocks.

concrete supports. Alignment of the integrated magnet blocks on the concrete support will be done with adjustment screws similar to MAX III; beam-based alignment of the magnet cells will be performed using an established scheme based on corrector magnet strengths for the corrected orbit [10, 25]. The benefit of using small and therefore light magnets on massive but low support blocks is that the eigenfrequencies of the magnets are pushed beyond 100 Hz [16]. This is very important for the MAX IV 3 GeV storage ring since the tolerances for beam vibrations are very tight given the ultra-low beam size (a vertical beam size on the order of $3 \mu\text{m}$ at the ID center calls for a vertical beam stability of $\approx 300 \text{ nm}$ in the straight sections).

Pole face strips will be included in the dipoles to allow

for adjustments of the defocusing quadrupole strength. The focusing sextupoles as well as the final defocusing sextupole family are foreseen to carry additional windings so that horizontal and vertical orbit correction can be integrated (as done at SLS). In addition, there will be additional extra windings on the defocusing sextupoles for use as either auxiliary sextupoles (since all regular sextupoles are powered in families) or as skew quadrupoles. Additional windings on the two octupole families installed closest to the ID could be used as nondispersive skew quads.

B. Vacuum System

The small magnet apertures require a narrow vacuum chamber. Such vacuum systems are usually plagued by poor vacuum conductance. This problem has been solved for narrow-gap ID vacuum chambers by the introduction of NEG coating [26]. For the MAX IV 3 GeV storage ring it is foreseen to extend this technique to the entire storage ring vacuum chamber. First tests using NEG-coated copper tubes as dipole vacuum chambers in MAX II have shown promising results [27, 28].

It has therefore been decided to use a circular NEG-coated copper tube with an outer diameter of 24 mm within the storage ring achromats. In this way lumped absorbers can be avoided as synchrotron radiation is distributed along the tube yielding a lower power density. Small discrete ion pumps will be installed to pump rest gas along with dedicated roughing pumps. Short tapering sections in the straights will make the transition from the circular beam pipe to either the narrow-gap chamber or the ID chamber in case of in-vacuum devices. Heating for bake-out and reactivation of the NEG can take place in situ if baking tape is applied around the outside of the chamber as has been successfully demonstrated at SOLEIL [29].

C. RF System

Since the MAX IV facility has its own dedicated short-pulse facility the storage rings can be operated at low radio frequencies with long bunches. Long electron bunches have the advantage of a narrow power spectrum which counteracts the resistive wall instability and thus reduces the need to run at large positive chromaticities restricting the energy acceptance.

It is therefore foreseen to use 100 MHz RF cavities in the MAX IV 3 GeV storage ring. There is a lot of experience at MAX-lab with this cavity type [30]. Higher-order modes are pushed to relatively high frequencies, where their influence is diminished due to a poor form-factor. Six such cavities operated at 250 kV gap voltage will ensure 5.3% RF momentum acceptance for a machine with four PMDWs and 4.0% RF momentum acceptance for a

machine with four PMDWs and ten in-vacuum undulators (IVUs) [51].

The cavities are installed in the short straight sections keeping all but one long straight section (injection straight) free for IDs. Cavities are joined in pairs with 3 dB hybrids and connected to four 50 kW tetrode amplifiers. This scheme has the advantage that it reduces reflected power to the amplifier without the need for expensive circulators. At the same time power regulation can be achieved by phasing rather than by changing the power level of the amplifier.

In addition to the main RF cavities, three passive third-harmonic Landau cavities will be installed to further lengthen the bunches and improve lifetime. With such a double RF system the bunch length can be increased from 10 mm for the bare lattice (or 12 mm in the case of the machine with four PMDWs and ten IVUs) by a factor 4–5 [16].

IV. LATTICE AND MACHINE PERFORMANCE

A. Dynamic Aperture

Achieving sufficient dynamic aperture is crucial for good Touschek lifetime and injection efficiency. We foresee injection with a localized four-kicker bump in the 5 m long straight section (8 mm bump amplitude) moving both the injected and the stored beam to within 3.5 mm and 2.5 mm respectively to the 2.5 mm thick Lambertson septum [16]. From this we gather a horizontal dynamic aperture requirement of ± 8 mm in the straight section corresponding to a horizontal acceptance requirement of 7.1 mrad. In the vertical plane dynamic aperture requirements of a modern synchrotron radiation source are modest due to successful operation of mini-gap in-vacuum IDs. With such half-gaps on the order of 2 mm and typically $\beta_y = 3$ m at the end of the IDs, a vertical acceptance requirement of 1.3 mm mrad should be sufficient.

Dynamic aperture for the MAX IV 3 GeV storage ring has been calculated with both OPA and Tracy-3. The PMDWs have been modeled in Tracy-3 with both the wiggler model as well as with kick maps generated by RADIA [31]. Very good agreement was observed between results obtained with the OPA undulator model, the Tracy-3 wiggler model, and kick maps inserted in Tracy-3. Results for the center of the 5 m straight section indicate sufficient dynamic aperture in both planes for on and off-momentum particles as shown in Fig. 8. If the physical boundaries are included in the lattice file, the dynamic aperture extends to these boundaries confirming that nonlinearities are very small within the physical aperture.

Dynamic aperture was also calculated for a machine with imperfections. In a first study, ignoring girder correlations, quadrupole and sextupole magnets were assumed misaligned by 50 μm in both horizontal and vertical di-

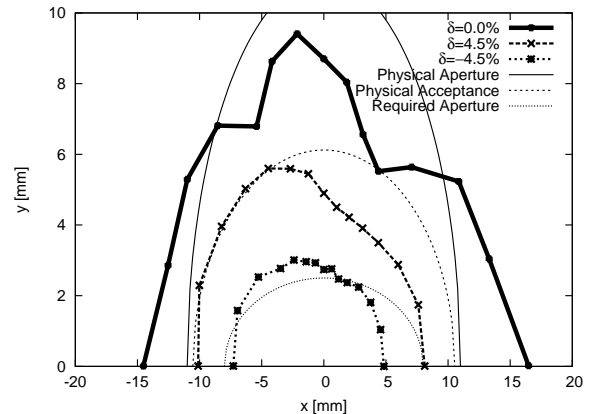


FIG. 8: Dynamic aperture at the center of the 5 m long straight section for the 3 GeV storage ring with four PMDWs installed. The data results from 6D tracking in Tracy-3 for one synchrotron period (≈ 500 turns).

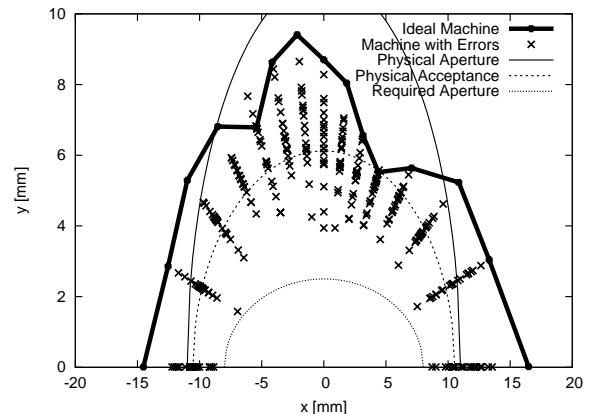


FIG. 9: On-momentum dynamic aperture at the center of the 5 m long straight section for the 3 GeV storage ring with four PMDWs installed. The crosses show dynamic aperture results for 20 seeds with random error distributions and applied orbit correction. While the dynamic aperture is reduced when the errors are included, it still substantially exceeds the requirements.

rection as well as rolled by 0.2 mrad (these are rms misalignments with a cut-off at 2σ). In addition, higher-order multipole errors were added to all quadrupoles and sextupoles. A tentative BPM/corrector layout with 10 BPMs and corrector pairs in each achromat was then used to simulate orbit correction with Tracy-3 and to obtain statistics (different random seeds). The resulting maximum required corrector strength was below 0.2 mrad and maximum offsets for the closed orbit remained below 70 μm in both planes. For each error seed the dynamic aperture was calculated. An example showing the result for 20 error seeds is given in Fig. 9; the applied errors were again 50 μm (horizontal and vertical

rms misalignment, 2-sigma cut-off) and 0.2 mrad (rms roll error, 2-sigma cut-off). The reduction of dynamic aperture is clearly visible, however the requirements are still fulfilled. It is known that the tolerances for the girder alignments can be relaxed, if they are tight for the magnets on the girder [21], so in a more realistic study it is expected that 100 μm misalignments to girders and 30 μm misalignments of the magnets with respect to the girder will suffice. For magnets that are machined into a common solid block of iron (see Section III A) we expect the alignment of the individual magnets within the same block to be on the order of only 10 μm .

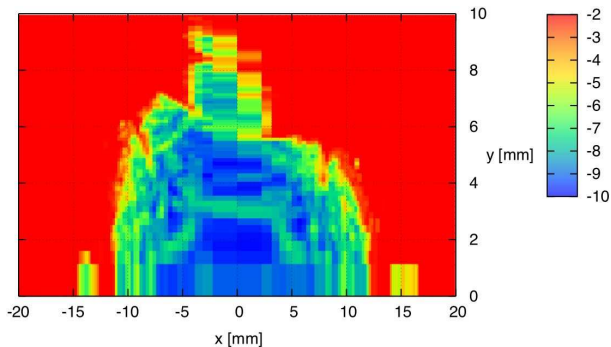


FIG. 10: (Color online) Diffusion map (2000 turns) at the center of the 5 m long straight section for the 3 GeV storage ring with four PMDWs installed. The scale is logarithmic in tune shift from low (blue) to high (red).

The dynamic aperture results are confirmed by diffusion maps calculated in Tracy-3. Particles are tracked for a certain number of turns (2048 here) and the final tunes compared with the initial tunes. Diffusion can then be defined as $D = \log \sqrt{(\Delta\nu_x)^2 + (\Delta\nu_y)^2}$ and plotted [52] for various initial transverse coordinates [32]. An example for on-momentum particles taken at the center of the 5 m long straight section is shown in Fig. 10. The dynamic aperture is essentially the same as in Fig. 8. A stop band (for $\Delta x = \pm 12$ mm caused by the octupolar coupling resonance $2\nu_x - 2\nu_y = 56$) is noticed.

In addition to the diffusion map, frequency map analysis also gives a tune footprint. An example is shown in Fig. 11 where the area within the required dynamic aperture has been inspected for resonant particle loss. Tracking data was gathered by sampling the transverse plane as shown in the diffusion map in the top of Fig. 11. The same data was plotted again in fractional tune space which is shown in the bottom plot. The amplitude-dependent tune shift away from the fractional working point 0.20/0.28 can be clearly recognized. Highest diffusion (roughly 10^{-6}) is encountered as the tune is shifted onto $5\nu_x = 211$; this corresponds to the bands seen in the top of Fig. 11 for $|\Delta x| \geq 4$ mm, $|\Delta y| > 1$ mm. Frequency map analysis demonstrates nicely how the amplitude-dependent tune shifts have been adjusted to “wrap around” the working point; tune shifts for betatron motion lead back to the working point thus reducing

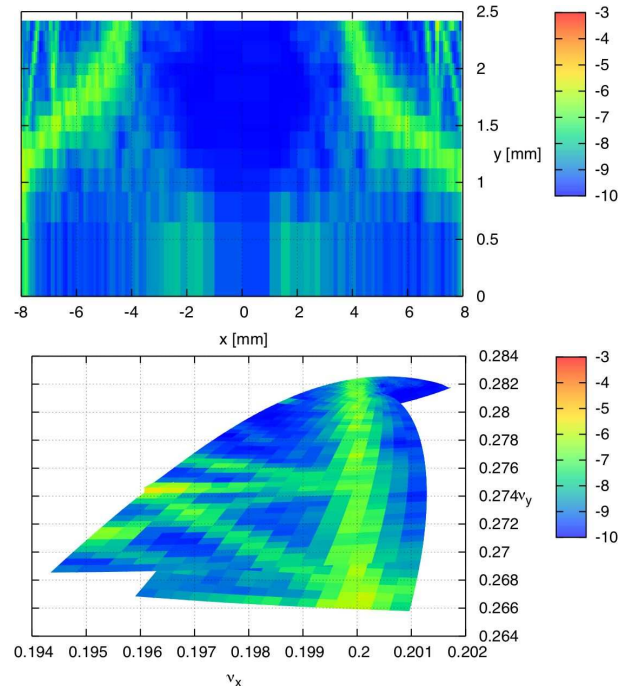


FIG. 11: (Color online) Diffusion map (top) and corresponding frequency map (bottom) for on-momentum particles in the 3 GeV storage ring with four PMDWs installed (2000 turns). The scale is logarithmic in tune shift from low (blue) to high (red). Note that compared to the diffusion map given in Fig. 10 the scale here has been shifted to lower diffusion rates by an order of magnitude.

the overall tune footprint and staying clear of potentially limiting resonances. The tune footprint confirms that the amplitude-dependent tune shifts in the MAX IV 3 GeV storage ring are very small for on-energy particles (cf. the extremely small area occupied in tune space in Fig. 11) and that there is no resonant particle loss for particles within the dynamic aperture required for injection and the stay-clear area in the straights.

B. Energy Acceptance

In order to achieve the required Touschek lifetime on the order of 10 h it is crucial to confirm a momentum acceptance of $\pm 4.5\%$. The overall momentum acceptance is given by the RF momentum acceptance and the lattice momentum acceptance. While choosing a total cavity gap voltage of 1.5 MV or greater is sufficient to achieve $\pm 4.5\%$ RF momentum acceptance in the storage ring with IDs, it has to be verified that the lattice itself has a momentum acceptance no less than $\pm 4.5\%$. The small dispersion within the MAX IV 3 GeV achromat ensures that dispersive orbits remain well within the limits of the physical aperture.

Tracking of off-momentum particles was done with

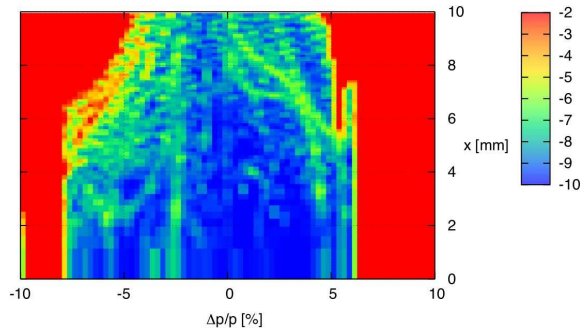


FIG. 12: (Color online) Diffusion map taken at the center of the long straight section for off-momentum particles in the 3 GeV storage ring with four PMDWs installed. The scale is logarithmic in tune shift from low (blue) to high (red).

Tracy-3. Particles with a constant vertical offset of $\Delta y = +1$ mm were given different momentum offsets and transverse amplitudes. After tracking for 2000 turns (corresponding to roughly a third of damping time) diffusion was calculated. A first example is shown in Fig. 12 where the lattice momentum acceptance can be clearly recognized at $+6\%$ and -8% . Particles with energy deviations beyond those limits will be lost regardless of the RF acceptance. Frequency map analysis shows that particle loss is caused by the integer resonance $\nu_y = 14$ for $\delta > +6\%$ and by the half-integer resonance $2\nu_y = 29$ for $\delta < -8\%$.

A more detailed view is given in Fig. 13 where horizontal excursions have been limited to low values. This is of interest because the Touschek scattering events leading to large energy deviations take place at the core of the bunch where particle density is greatest. The plot at the top of Fig. 13 is a diffusion map for energy deviations of $\pm 7\%$ at the bunch core and the bottom plot shows the corresponding frequency map in fractional tune space. Again the “wrap-up” of tune shifts around the working point can be recognized: two tune shifts lead away from the fractional working point at $0.20/0.28$. Energies above design ultimately lead to lower vertical tunes (covering less than 0.2 in vertical tune); their overall horizontal tune shift is less than 0.03 . The other branch in tune space, leading to larger vertical and lower horizontal tunes is for particles below design energy; their overall tune variation is however less than 0.1×0.1 . A stop band is recognized for $\delta > +6\%$ which stems from tune shifts onto the integer resonance $\nu_y = 14$. Particles with energy above design encounter increased diffusion for $\delta \approx +4.75\%$ ($4\nu_y = 57$) and $\delta \approx +5.5\%$ ($5\nu_y = 71$). For energies below design the main diffusion encountered is due to $6\nu_x = 253$ which is seen in the area around $\delta \approx -2.75\%$ as well as $\delta \approx -6\%$ for $|\Delta x| \geq 2$ mm. In the latter case diffusion is further increased by $3\nu_y = 43$.

Frequency map analysis demonstrates that the chromatic tune shifts in the MAX IV 3 GeV storage ring are very small. Horizontal tune excursions remain well

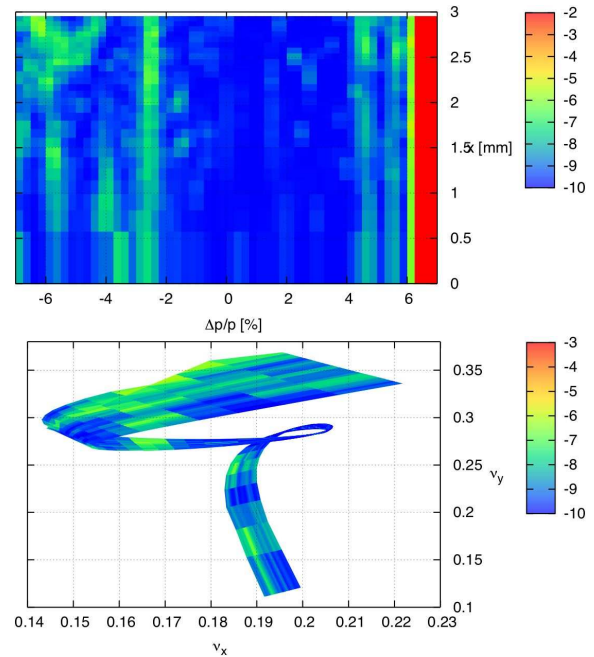


FIG. 13: (Color online) Diffusion map (top) and frequency map (bottom) for off-momentum particles in the 3 GeV storage ring with four PMDWs installed. The scale is logarithmic in tune shift from low (blue) to high (red). The “wrap up” of the chromatic tune shift around the working point is clearly recognized.

below 0.1 for all energies within the RF momentum acceptance; overall vertical excursions are no larger than 0.3 . This shows that even for extreme Touschek events no dangerous low-order resonances will be encountered ensuring good Touschek lifetime and large momentum acceptance.

Since all these considerations have been made for the ideal lattice, the importance of a sophisticated correction scheme has to be emphasized. As has been first demonstrated at the ALS [33, 34] and later at several other storage rings, it is indeed possible to meet the design momentum acceptance in the real machine and hence achieve the theoretically predicted Touschek lifetime by careful measurement and correction of the linear [35] and non-linear [36] optics. For example, meeting the design specifications of the SLS storage ring required the following measures: first, the orbit was corrected, including beam-based BPM calibrations, and the beta functions were restored. Then, small skew quadrupoles located in dispersive and non-dispersive sections were employed for precise vertical beam size control, control of vertical dispersion, and suppression of betatron coupling [37, 38]. Finally, the sextupole pattern was symmetrized by means of small auxiliary sextupoles [39].

C. Intrabeam Scattering

Because the transverse emittance of the MAX IV 3 GeV storage ring lattice is so small, intrabeam scattering (IBS) is expected to have a significant influence on the overall equilibrium emittance. Emittance values given so far take into account synchrotron radiation damping and quantum emission fluctuations, but not IBS. In order to quantify the effect of IBS on the equilibrium emittance, calculations have been performed in ZAP [40] and compared with Tracy-3 [41, 42]. The ZAP results calculated for a total stored current of 500 mA and a vertical emittance adjusted to the 1 Å diffraction limit $\varepsilon_y = 8$ pm rad are summarized in Table V.

TABLE V: Equilibrium values for the horizontal emittance of the MAX IV 3 GeV storage ring calculated with (right) and without (left) IBS using ZAP. The influence of the third-harmonic Landau cavities (LC) is also shown (with bunch lengthening to $\sigma_s = 50$ mm assumed).

	ε_x [nm rad]	
Bare Lattice	0.326	0.453
Bare Lattice with LC	0.326	0.372
Lattice with 4 PMDWs and LC	0.263	0.297
Lattice with 4 PMDWs, 10 IVUs, and LC	0.201	0.231

For very small lattice emittance values the influence of IBS on equilibrium emittance is very strong. Hence, for the MAX IV 3 GeV bare lattice, the total emittance is significantly underestimated when IBS is not taken into account (the inclusion of IBS leads to a 39% increase of the equilibrium emittance). However, once the third-harmonic Landau cavities and IDs are added, the additional radiation damping and bunch lengthening strongly reduce the influence of IBS on equilibrium emittance ($< 15\%$).

D. Touschek Lifetime

The lattice momentum acceptance has been calculated by tracking with Tracy-3 in 6D including effects of the nonlinear lattice. An error-free machine with realistic vacuum chamber dimensions (horizontal half-aperture $a_x = 11$ mm) was used for these calculations. The results for three different configurations of the MAX IV 3 GeV storage ring are displayed in Table VI. As required by the design specifications, the lattice momentum acceptance is always 4.5% or higher. For the following considerations on Touschek lifetime we therefore assume an RF momentum acceptance set to $\delta_{rf} = 4.5\%$ which should then dominate overall momentum acceptance.

The Touschek lifetime was then calculated with Tracy-3 [43]. We assumed 500 mA stored beam current in 176 bunches with a limiting RF acceptance set to 4.5% as detailed above. A Touschek lifetime of 9.85 h is obtained

TABLE VI: Minimum lattice momentum acceptance for different configurations of the error-free MAX IV 3 GeV storage ring calculated with Tracy-3 in 6D.

	δ_{acc}^{min}
Bare Lattice	5.2%
Lattice with 4 PMDWs	4.5%
Lattice with 4 PMDWs and 10 IVUs	4.8%

with four PMDWs installed and coupling adjusted to the 1 Å diffraction limit ($\varepsilon_y = 8$ pm rad). For the case where four PMDWs and ten IVUs are installed a Touschek lifetime of 9.31 h is determined. In addition to the main cavity, we also foresee installation of Landau cavities operating at the third harmonic. The bunch lengthening from the Landau cavities leads to an increase of Touschek lifetime by a factor 4–5. Touschek lifetime for various configurations of the MAX IV 3 GeV storage ring as well as the influence of IBS is shown in Table VII.

TABLE VII: Touschek lifetime for the MAX IV 3 GeV storage ring calculated with (right) and without (left) IBS using ZAP. The vertical emittance $\varepsilon_y = 8$ pm rad and RF acceptance $\delta_{rf} = 4.5\%$ were kept constant. The influence of the Landau cavities (LC) is also shown (with bunch lengthening to $\sigma_s = 50$ mm assumed).

	$\tau_{Touschek}$ [h]	
Bare Lattice	6.96	8.61
Bare Lattice with LC	28.98	29.02
Lattice with 4 PMDWs and LC	35.57	34.52
Lattice with 4 PMDWs, 10 IVUs, and LC	41.54	39.49

It should be pointed out that concerning Touschek lifetime the MAX IV 3 GeV storage ring operates in an atypical regime. As the emittance of the storage ring is further reduced by adding additional IDs, the Touschek lifetime actually improves. This is a unique property among third-generation synchrotron radiation sources and is ultimately a consequence of the ultra-low emittance of the MAX IV 3 GeV storage ring. An evaluation of the Touschek function shows that there is a sharp change in behavior once the transverse momenta in the bunch become small compared to the momentum acceptance. The physical explanation is that the transverse momenta in an ultra-low emittance bunch are insufficient to generate scattering events which result in momentum deviations that can no longer be contained by the longitudinal acceptance of the machine. This leads to overall fewer Touschek losses and hence increased lifetime at lower emittances. A plot showing Touschek lifetime vs. horizontal emittance for the MAX IV 3 GeV storage ring is displayed in Fig. 14. Clearly, further reducing the lattice emittance with additional damping wigglers and insertion devices has a beneficial effect on Touschek lifetime.

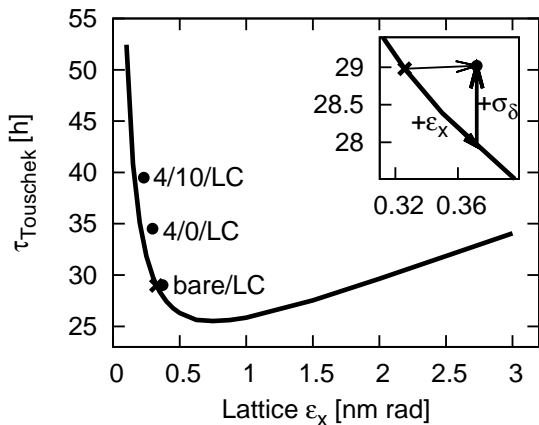


FIG. 14: The trend line shows Tauschek lifetime for the bare lattice (IBS neglected) if it were possible to vary the lattice emittance while keeping the energy spread constant. Specific configurations (bare lattice, 4 PMDWs, and 4 PMDWs plus 10 IVUs; all including LCs) are indicated by crosses and dots. Crosses indicate IBS neglected, dots indicate IBS included. The enlarged segment illustrates the effect of IBS for the bare lattice configuration: while the IBS emittance growth ($+\epsilon_x$) leads to a decrease of Tauschek lifetime, the IBS energy spread growth ($+\sigma_\delta$) leads to an increase of Tauschek lifetime.

With IBS taken into account, one cannot emphasize the benefits of Landau cavities enough. By increasing the bunch length and hence reducing the charge density in the bunch, the Landau cavities not only increase Tauschek lifetime, they also reduce the horizontal emittance blow-up from IBS, which in the case of the MAX IV 3 GeV storage ring increases the Tauschek lifetime even further. Figures 14 and 15 illustrate this situation.

E. Overall Lifetime and Top-up Injection

For lifetime and injection considerations we define a “worst-case” scenario. Firstly, the configuration with 4 PMDWs and 10 IVUs ensures large radiated energy losses. Secondly, we assume no extra RF stations are added; six cavities will give a maximum total cavity voltage of 1.5 MV. This results in a low RF acceptance of $\delta_{rf} = 4.0\%$. The Tauschek lifetime including Landau cavities is then 25.5 h.

The elastic gas scattering lifetime is given by the rest gas composition and the physical acceptance of the machine. A rest gas equivalent of 2 pbar of CO has been assumed. The vertical acceptance limitation comes from in-vacuum IDs (± 2 mm gap, $\beta_y = 3$ m at the end of the ID), whereas the horizontal acceptance is given by the maximum of the horizontal beta function ($\beta_{x,max} = 10$ m, chamber inner radius ± 11 mm). This gives an elastic scattering lifetime of 25.4 h. The inelastic gas scattering

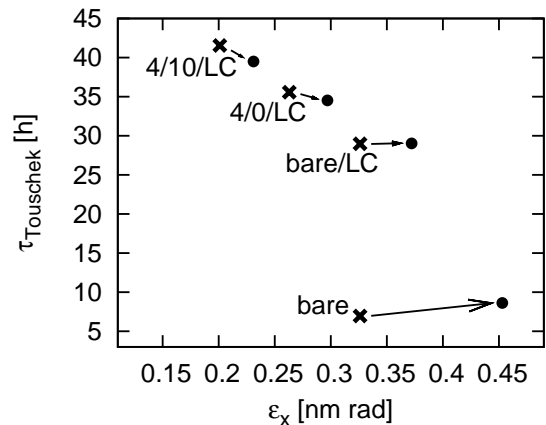


FIG. 15: Tauschek lifetime vs. horizontal emittance for different configurations of the MAX IV 3 GeV storage ring: bare lattice, lattice with 4 PMDWs, lattice with 4 PMDWs and 10 IVUs. Where indicated, the effect of the Landau cavities (LC) has been included (with bunch lengthening to $\sigma_s = 50$ mm assumed). The vertical emittance $\epsilon_y = 8$ pm rad and RF acceptance $\delta_{rf} = 4.5\%$ were kept constant. The effect of IBS is indicated by arrows. Crosses indicate IBS neglected, dots indicate IBS included.

lifetime also depends weakly on momentum acceptance. Assuming the same rest gas pressure, the inelastic gas scattering lifetime is calculated as 53.1 h for an energy acceptance of 4.0%.

These lifetime contributions are summarized for the “worst-case” scenario in Table VIII. When the MAX IV 3 GeV storage ring is operated with IDs and Landau cavities, as a consequence of the long Tauschek lifetime, overall beam lifetime will no longer be Tauschek dominated.

TABLE VIII: Contributions to the total MAX IV 3 GeV storage ring lifetime τ . The results have been calculated for a “worst-case scenario”: four PMDWs and ten IVUs are installed in the storage ring while the total applied RF voltage is 1.5 MV which corresponds to an RF acceptance of only $\delta_{rf} = 4.0\%$.

	τ [h]
Elastic gas scattering	25.4
Inelastic gas scattering	53.1
Tauschek scattering (with Landau cavities)	25.5
Total	10.3

It is foreseen to have top-up injection into the MAX IV 3 GeV storage ring. Assuming a maximum current variation of 0.2% is tolerated and taking into account the calculated “worst-case” total lifetime of 10.3 h, an injection of 1.8 nC will be required every 74 sec. The MAX IV 3 GeV injector linac will be capable of delivering up

to 10 nC in a 100 ns shot. Therefore the required top-up injection into the storage ring can be performed with a single shot. If we require five damping times for the residual kicker bump excitation of the stored beam to damp down, this yields a user dead time of 0.06%. A variable multi-shot injection at reduced charge is presently being considered in order to implement a filling pattern feedback. This would however come at the expense of more frequent top-up injections or a longer injection dead time (dominated by the repetition rate of the injector rather than the damping time) [16].

F. Brightness

The IDs for the MAX IV 3 GeV storage ring will be tailored to the specific needs of the beam lines. Conventional planar undulators as well as elliptically polarizing undulators will be installed in addition to the previously mentioned damping wigglers. The most demanding undulators are the flat field undulators for the production of undulator radiation at the highest possible photon energy, where the undulators combine shortest possible period length with highest possible magnetic peak field. The combination of short period length and high magnetic peak field points towards narrow gap in-vacuum undulators of hybrid type, where blocks of permanent magnet material are combined with soft magnetic materials. The peak field of an in-vacuum undulator can be increased by lowering the temperature of the magnetic material and recently cryogenically cooled in-vacuum undulators have been developed [44, 45].

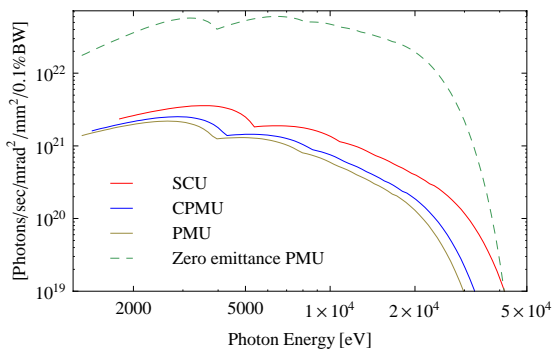


FIG. 16: (Color online) Brilliance limit for the 3 GeV MAX IV for in-vacuum permanent magnet undulators (PMU), cryogenically cooled in-vacuum undulators (CPMU), and superconducting undulators (SCU). The undulator parameters are given in Table IX.

Superconducting undulators would, provided that the technical problems of building superconducting undulators can be overcome, outperform undulators based on permanent magnet technology. The MAX IV 3 GeV

storage ring is well suited for the installation of superconducting undulators because of the long bunch length and soft ends of the dipoles flanking the straight section, which give a moderate heat load to the cryostat of a superconducting undulator. Table IX shows different types of IDs under consideration for the MAX IV 3 GeV storage ring. The undulators have been optimized for short period length while retaining overlap between first and third harmonic and have a maximum K -value of ≈ 2.2 .

Figure 16 shows the expected brilliance at peak energy of the undulators in Table IX installed at the MAX IV 3 GeV storage ring. The brilliance has been calculated with the code SPECTRA [46] using a horizontal emittance of 0.26 nm rad, a vertical emittance of 8 pm rad, and an rms energy spread of 0.1%. As a comparison, the brilliance of the PMU installed in the “ultimate source” (zero horizontal and vertical emittance, but with the same energy spread) has been included in Fig. 16. The plotted values are brilliance at peak energy and not maximum brilliance, which is found at slightly lower photon energy.

V. CONCLUSIONS AND OUTLOOK

The MAX IV 3 GeV storage ring has been shown to be a feasible concept to generate high-brightness X-ray radiation. The unprecedented ultra-low emittance is made possible by a novel lattice design approach using compact multi-bend achromats with gradient dipole magnets. This low emittance is then further reduced by the introduction of strong damping wigglers and in-vacuum undulators. The required strong focusing however, puts high demands on magnet design and vacuum system. Problems associated with vacuum pressure and transverse instability are mitigated by the use of NEG coating and a 100 MHz main RF system. If construction proceeds as expected, the MAX IV 3 GeV storage ring should go into operation in 2015. With a constant stored current of 500 mA and a horizontal emittance below 0.3 nm rad it will become the brightest storage ring-based synchrotron radiation source worldwide.

The focus is now being put on several remaining issues. Full 6D tracking for a lattice with realistic multipole field errors and magnet misalignments should give a better understanding of the dynamic behavior in the real machine. The orbit correction scheme is also under investigation: it is foreseen to implement correctors as additional windings in the sextupole magnets and install the BPMs between these sextupoles and the adjacent quadrupoles. We plan to verify that a fast orbit correction scheme with this corrector/BPM layout fulfills the tight beam stability requirements (due to the ultra-low beam emittance an RMS beam stability in the long straight on the order of 300 nm is required). Vibration studies with the foreseen low-height massive concrete support system are under way. Finally, the design of IDs and tailoring of IDs to specific beamline requirements is an ongoing activity.

TABLE IX: Insertion devices for the MAX IV 3 GeV storage ring. The peak magnetic field \hat{B} , device length L , and period length λ are given.

	\hat{B} [T]	λ [mm]	L [m]
Permanent magnet damping wiggler (PMDW)	2.22	80	2.0
In-vac. permanent magnet undulator (PMU)	1.28	19.0	3.0
Cryogenically cooled in-vac. undulator (CPMU)	1.38	17.5	3.0
Superconducting undulator (SCU)	1.70	14.0	3.0

- [1] M. Böge, in *Proceedings of 8th European Particle Accelerator Conference (EPAC-02)* (Paris, France, 2002), pp. 39–43.
- [2] A. Nadji, J. Besson, F. Bouvet, P. Brunelle, A. Buteau, L. Cassinari, M. Couprie, J. Denard, J. Filhol, C. Herbeaux, et al., in *Proceedings of PAC07* (Albuquerque NM, USA, 2007), pp. 932–934.
- [3] R. Bartolini, in *Proceedings of PAC07* (Albuquerque NM, USA, 2007), pp. 1109–1111.
- [4] *NLS-II Preliminary Design Report*, URL <http://www.bnl.gov/nsls2/project/PDR/>.
- [5] S. Krinsky, J. Bengtsson, and S. Kramer, in *Proceedings of 10th European Particle Accelerator Conference (EPAC'06)* (Edinburgh, Scotland, 2006), pp. 3487–3489.
- [6] *PETRA III Technical Design Report*, URL <http://petra3.desy.de/general/tdr/>.
- [7] *MAX IV Conceptual Design Report*, URL <http://www.maxlab.lu.se/maxlab/max4/index.html>.
- [8] S. Werin, S. Thorin, M. Eriksson, and J. Larsson, *Nucl. Instr. and Meth. A* **601**, 98 (2009).
- [9] M. Sjöström, H. Tarawneh, E. Wallén, and M. Eriksson, *Nucl. Instr. and Meth. A* **577**, 425 (2007).
- [10] M. Sjöström, E. Wallén, M. Eriksson, and L. J. Lindgren, *Nucl. Instr. and Meth. A* **601**, 229 (2009).
- [11] M. Eriksson, L. J. Lindgren, M. Sjöström, E. Wallén, L. Rivkin, and A. Streun, *Nucl. Instr. and Meth. A* **587**, 221 (2008).
- [12] M. Eriksson, Å. Andersson, S. Biedron, M. Demirkan, G. Leblanc, L. Lindgren, L. Malmgren, H. Tarawneh, E. Wallén, and S. Werin, in *Proceedings of 8th European Particle Accelerator Conference (EPAC-02)* (Paris, France, 2002), pp. 686–687.
- [13] H. Tarawneh, M. Eriksson, L. J. Lindgren, and B. Anderberg, *Nucl. Instr. and Meth. A* **508**, 480 (2003).
- [14] M. Eriksson, M. Berglund, M. Brandin, D. Kumbaro, P. Lilja, L.-J. Lindgren, L. Malmgren, M. Sjöström, S. Thorin, E. Wallén, et al., in *Proceedings of PAC07* (Albuquerque NM, USA, 2007), pp. 74–76.
- [15] M. Eriksson, A. Hansson, S. C. Leemann, L.-J. Lindgren, M. Sjöström, E. Wallén, L. Rivkin, and A. Streun, in *Proceedings of 11th European Particle Accelerator Conference (EPAC-08)* (Genova, Italy, 2008), pp. 2007–2009.
- [16] *MAX IV Detailed Design Report*, in preparation, URL <http://www.maxlab.lu.se/maxlab/max4/index.html>.
- [17] S. Lee and L. Teng, in *Proceedings of PAC 1991* (San Francisco CA, USA, 1991), pp. 2679–2681.
- [18] C. Steier, D. Robin, A. Wolski, G. Portmann, and J. Safranek, in *Proceedings of PAC03* (Portland OR, USA, 2003), pp. 3213–3215.
- [19] *OPA Lattice Design Code*, URL <http://slsbd.psi.ch/~streun/opa/>.
- [20] J. Bengtsson, *The Sextupole Scheme for the Swiss Light Source (SLS): An Analytic Approach*, SLS Internal Note 9/97, URL <http://slsbd.psi.ch/pub/slsnotes/sls0997.pdf>.
- [21] J. Bengtsson, W. Joho, P. Marchand, G. Muelhaupt, L. Rivkin, and A. Streun, *Nucl. Instr. and Meth. A* **404**, 237 (1998).
- [22] J. Bengtsson, *Tracy-2 User's Manual*, unpublished.
- [23] M. Cornacchia and Y. Chin, *Part. Accel.* **17**, 191 (1985).
- [24] S. C. Leemann and A. Streun, *Unusual Magnets in Storage Ring-based Synchrotron Light Sources*, in preparation.
- [25] M. Sjöström, E. Wallén, M. Eriksson, and L.-J. Lindgren, *Nucl. Instr. and Meth. A* **597**, 170 (2008).
- [26] R. Kersevan, M. Hahn, and I. Parat, in *Proceedings of 10th European Particle Accelerator Conference (EPAC'06)* (Edinburgh, Scotland, 2006), pp. 1420–1422.
- [27] E. Wallén, M. Berglund, H. Svensson, and M. Eriksson, in *Proceedings of 17th International Vacuum Congress (IVC-17)* (Stockholm, Sweden, 2007).
- [28] A. Hansson, M. Berglund, and E. Wallén, in *Proceedings of 11th European Particle Accelerator Conference (EPAC-08)* (Genova, Italy, 2008), pp. 3693–3695.
- [29] E. Al-Dmour, in *Proceedings of 11th European Particle Accelerator Conference (EPAC-08)* (Genova, Italy, 2008), pp. 31–35.
- [30] Å. Andersson, M. Bergqvist, M. Eriksson, L. Malmgren, and L. Thånell, in *Proceedings of 8th European Particle Accelerator Conference (EPAC-02)* (Paris, France, 2002), pp. 2118–2120.
- [31] P. Elleaume, in *Proceedings of 3rd European Particle Accelerator Conference (EPAC-92)* (Berlin, Germany, 1992), pp. 661–663.
- [32] L. Nadolski and J. Laskar, *Phys. Rev. ST Accel. Beams* **6**, 114801 (2003).
- [33] D. Robin, J. Safranek, and W. Decking, *Phys. Rev. ST Accel. Beams* **2**, 044001 (1999).
- [34] C. Steier, D. Robin, L. Nadolski, W. Decking, Y. Wu, and J. Laskar, *Phys. Rev. E* **65**, 056506 (2002).
- [35] J. Safranek, *Nucl. Instr. and Meth. A* **388**, 27 (1997).
- [36] R. Bartolini, I. P. S. Martin, J. H. Rowland, P. Kuske, and F. Schmidt, *Phys. Rev. ST Accel. Beams* **11**, 104002 (2008).
- [37] Å. Andersson, M. Böge, A. Lüdeke, V. Schlott, and A. Streun, *Nucl. Instr. and Meth. A* **591**, 437 (2008).

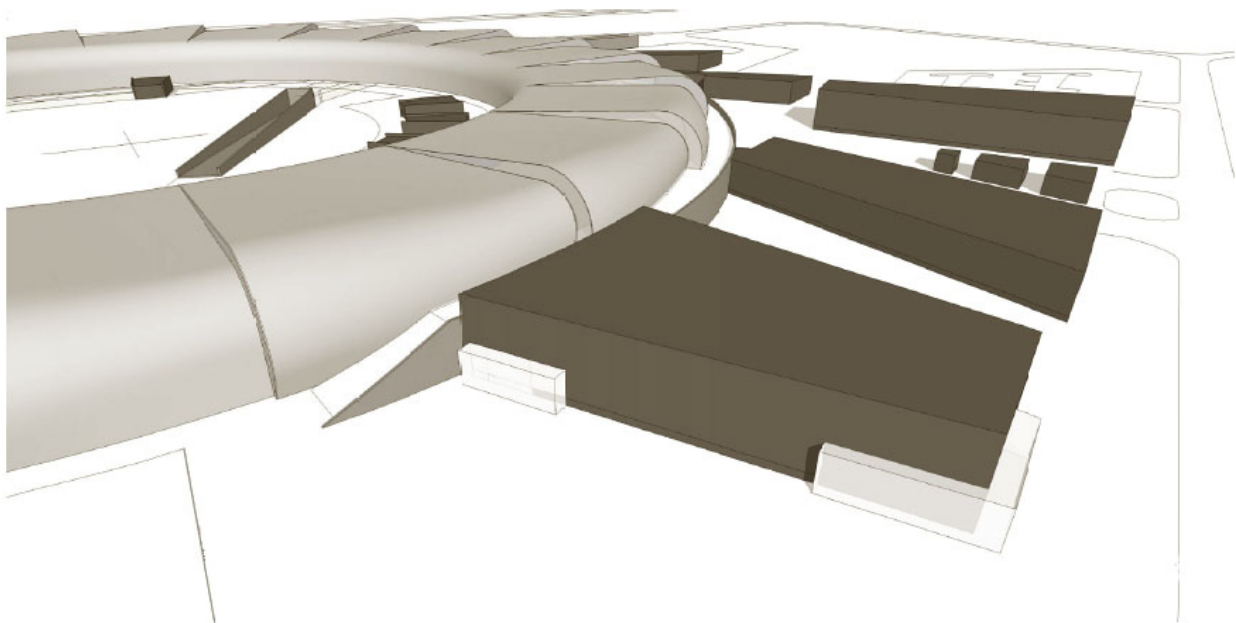
- [38] Å. Andersson, M. Böge, A. Lüdeke, and A. Streun, in *Proceedings of 11th European Particle Accelerator Conference (EPAC-08)* (Genova, Italy, 2008), pp. 1983–1985.
- [39] M. Böge, A. Lüdeke, and A. Streun, in *Proceedings of PAC09* (Vancouver, Canada, 2009).
- [40] M. S. Zisman, S. Chattopadhyay, and J. J. Bisognano, *ZAP User's Guide*, LBL 21270 (December 1986).
- [41] J. Le Duff, *Single and Multiple Touschek Effects*, CERN 89-01.
- [42] V. Litvinenko, private communication.
- [43] A. Streun, *Momentum acceptance and Touschek lifetime*, SLS Internal Note 18/97, URL <http://slsbd.psi.ch/pub/slsnotes/sls1897a.pdf>.
- [44] J. Chavanne, M. Hahn, R. Kersevan, C. Kitegi, C. Penel, and F. Revol, in *Proceedings of 11th European Particle Accelerator Conference (EPAC-08)* (Genova, Italy, 2008), pp. 2243–2245.
- [45] T. Hara, T. Tanaka, H. Kitamura, T. Bizen, X. Maréchal, T. Seike, T. Kohda, and Y. Matsuura, *Phys. Rev. ST Accel. Beams* **7**, 050702 (2004).
- [46] T. Tanaka and H. Kitamura, *J. Synchrotron Rad.* **8**, 1221 (2001).
- [47] Dispersion in the short straights is very low so that installing the RF cavities here will prevent emittance dilution from synchro-betatron oscillations.
- [48] The focusing quadrupoles between the dipoles have actually been split up and separated to make room for a short focusing sextupole in between, see Section II B.
- [49] This is a requirement in order to make installation of in-vacuum superconducting IDs feasible.
- [50] Although this appears to be a very low setting for the corrected chromaticity, it is considered feasible here because of the low accelerating radio frequency (see Section III C).
- [51] An option to use eight such cavities if the ring is fully loaded with IDs is being investigated. The total gap voltage of 2 MV would still give a maximum RF momentum acceptance of 5.3% for the fully loaded machine.
- [52] For reasons of clarity, the plots displayed here show a slightly modified diffusion defined as $D = \min \left(-2, \log \sqrt{(\Delta\nu_x)^2 + (\Delta\nu_y)^2} \right)$.



Appendix 2

Revised design of the MAX IV facility

Background material for the VR evaluation September 2009



Experiences from nonevaporable getter-coated vacuum chambers at the MAX II synchrotron light source

A. Hansson^a, E. Wallén, M. Berglund
 MAX-lab, Box 118, SE-221 00 Lund, Sweden

R. Kersevan, M. Hahn
 ESRF, BP 220, FR-38043 Grenoble Cedex, France

Vacuum chambers coated with nonevaporable getter (NEG) materials have been used in straight sections of synchrotron light sources for the last ten years. The MAX II storage ring, where four NEG-coated insertion device vacuum chambers and three NEG-coated dipole vacuum chambers have been installed, is the first synchrotron light source to also use NEG-coated dipole vacuum chambers. In connection with the installation of the latest two NEG-coated dipole chambers in April 2009 the evolution of the pressure and lifetime-limiting effects in MAX II has been determined from measurements with movable scrapers. The results have been compared with results from scraper measurements done in 2003, before any NEG-coated vacuum chambers were installed in the storage ring. Less than three months after the installation of the latest dipole chambers the vacuum system in MAX II was performing well with a pressure already lower than the pressure measured in 2003.

I. INTRODUCTION

Throughout the last ten years, the use of vacuum chambers coated with thin films of nonevaporable getter (NEG) materials in particle accelerators and storage rings has steadily increased. To a large extent the NEG material used for these ultra-high vacuum (UHV) applications has been a ternary alloy of titanium, zirconium and vanadium. An overview of the properties of thin films of the Ti-Zr-V NEG alloy is given by P. Chiggiato and P. Costa Pinto¹. In short, NEG improves the vacuum in the chambers both by direct pumping of the residual gas and by reducing the electron and photon-induced desorption. Active gases such as CO, CO₂, H₂O, N₂ and O₂ are chemisorbed on the NEG surface whereas H₂ diffuses into the getter bulk. Noble gases and CH₄ are not pumped by NEG materials. To activate the NEG it is heated to a temperature where the native oxide layer on the surface is dissolved into the bulk.

Up until the 1970's the vacuum levels in accelerator and storage ring vacuum systems was achieved by pumps connected to the vacuum chambers by means of flanges. As the vacuum chamber apertures got smaller and the machines got longer new linear pumping technologies, such as distributed sputter-ion pumps and NEG strips, were developed. For the LEP collider at CERN NEG strips made from St101, a commercial NEG alloy from SAES Getters, was used for about 22 km of the 27 km long LEP². St101 is a Zr-Al alloy with a composition of 84 % Zr and 16 % Al by weight (Zr 61 Al 39 at %) activated by heating to 740°C for 45-60 minutes³⁻⁴. Another SAES Getters NEG alloy, St707, was also found to be suitable for UHV conditions. The Zr-V-Fe alloy (Zr 70 V 24.6 Fe 5.4 wt %, Zr 57 V 36 Fe 7 at %) had the advantage of being activated at temperatures of 350-400°C, allowing passive activation during bakout⁵⁻⁶. NEG strips from St707 have been used at synchrotron light sources, e.g. at SPring-8⁷ and TLS⁸. By covering most of a test vacuum chamber with NEG strips pressures in the 10⁻¹⁴ Torr range was obtained⁶. To lower the

degassing from the chamber walls and further decrease the obtainable pressures a method to sputter-coat the inner vacuum chamber walls with NEG material was developed⁹. A suitable NEG alloy, Ti-Zr-V, with an activation temperature of 200°C and properties suitable for particle accelerators and storage rings was developed¹⁰⁻¹¹. The low activation temperature made it possible to use vacuum chambers made of aluminium and copper alloys.

The first storage ring to install a NEG-coated vacuum chamber was ESRF, where a narrow-gap aluminium insertion device (ID) vacuum chamber was installed in 1999¹². Today, a majority of the ID vacuum chambers in ESRF are NEG-coated¹³ and NEG-coated vacuum chambers are used at several light sources, e.g. at ELETTRA¹⁴, Diamond¹⁵, SOLEIL¹⁶ and MAX III¹⁷. At SOLEIL 56 % of the ring circumference is NEG-coated, including the quadrupole and sextupole straight sections. For the upgrade of the heavy ion synchrotron SIS 18 at GSI, NEG-coated dipole vacuum chambers will be used¹⁸. For synchrotron light sources however, NEG-coated dipole vacuum chambers have so far not been tested. This article reports on the first experience with NEG-coated dipole vacuum chambers in a synchrotron light source.

II. NEG AT MAX II

The MAX II synchrotron light source¹⁹ was commissioned in 1996. It is a 1.5 GeV third generation storage ring with a circumference of 90 m. It has a 10-fold periodicity with two dipole magnets in each cell. The original vacuum system in MAX II was made of stainless steel. To allow smaller gaps for the insertion devices, NEG-coated aluminium ID vacuum chambers were installed in the straight section between cell 4 and cell 5 and in the straight section between cell 9 and cell 10. The experience with the NEG-coated ID vacuum chambers was positive and together with reports from other synchrotron radiation facilities this fueled an interest in extended use of NEG-coated vacuum chambers. For the future synchrotron light source MAX IV, currently being designed at MAX-lab²⁰, the vacuum system is proposed to be almost entirely made up of NEG-coated vacuum chambers. To examine the feasibility

^aAuthor to whom correspondence should be addressed; electronic mail: anders.hansson@maxlab.lu.se

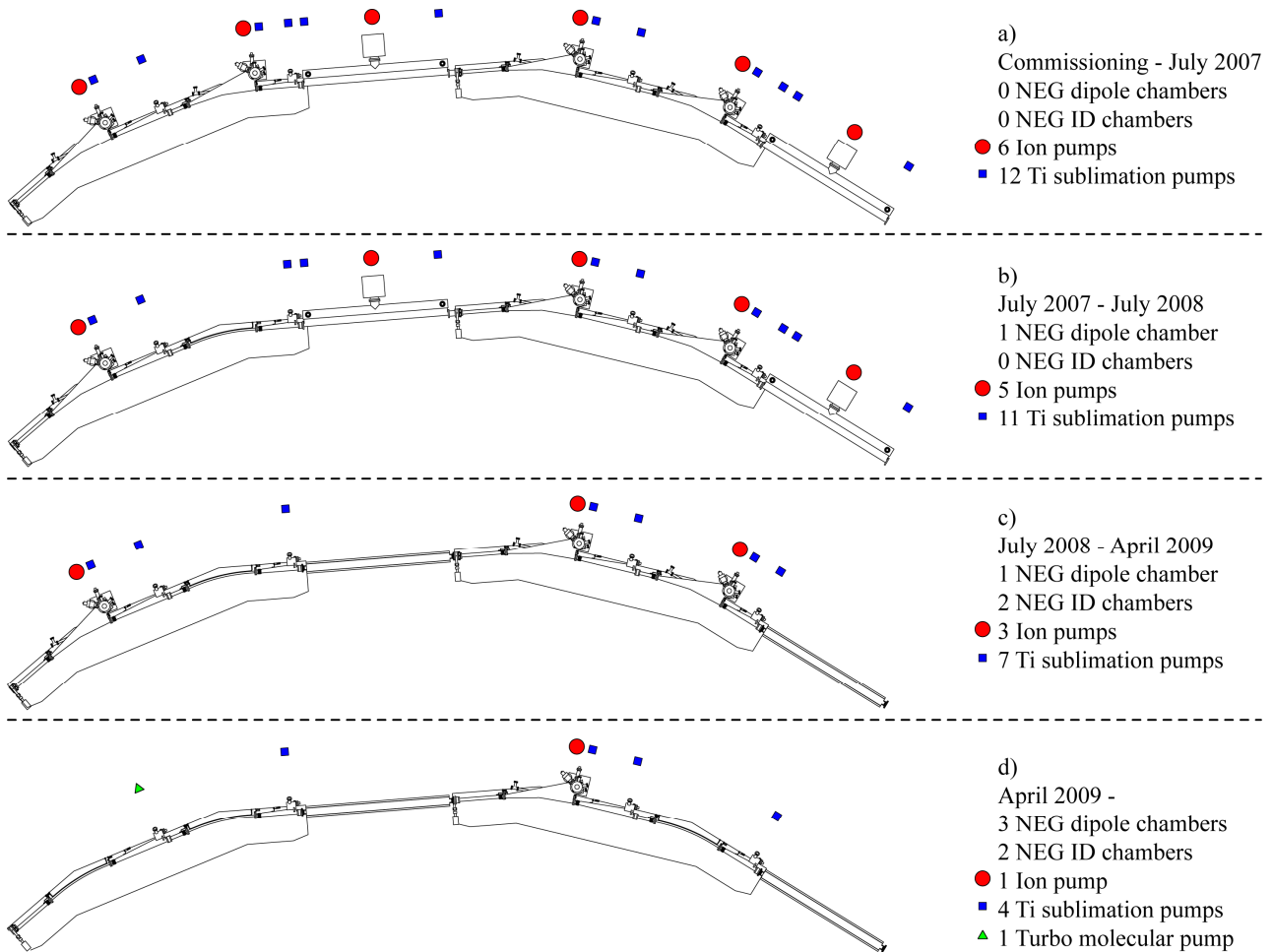


Fig. 1. (Color online) The vacuum system of cell 2 and cell 3 in the MAX II storage ring from a) commissioning to July 2007, b) July 2007 to July 2008, c) July 2008 to April 2009 and d) from April 2009 onwards.

of this design, NEG-coated dipole vacuum chambers were manufactured for installation into MAX II with the goal to evaluate how NEG-coated dipole chambers influence the operation of the storage ring.

Besides the two NEG-coated ID chambers mentioned above, five more NEG-coated chambers have been installed in MAX II. All of them have been installed in cell 2 and 3 of the storage ring. Figure 1 depicts the vacuum system of cell 2 and cell 3 in MAX II from commissioning to its current arrangement. Added to the figure are circles (corresponding to ion pumps), squares (corresponding to titanium sublimation pumps) and triangles (corresponding to turbo molecular pumps) showing how the distribution of pumps has changed during the years. In July 2007 a NEG-coated copper dipole vacuum chamber was installed in the second dipole of cell 2. In July 2008 the straight sections between cell 2 and 3 and between cell 3 and 4 were exchanged with NEG-coated aluminium ID vacuum chambers. Finally, in April 2009 two NEG-coated copper dipole vacuum chambers were installed in the first dipole in cell 2 and in the second dipole of cell 3. During this time the total amount of pumps in cell 2 and 3 (including the ID vacuum chambers) decreased from six ion pumps and twelve titanium sublimation pumps to only one ion pump, four titanium sublimation pumps and a turbo molecular pump. The turbo molecular pump was connected to the vacuum

system for the initial pumping from atmospheric pressure but has been kept running for most of the time since April 2009.

III. NEG-COATED COPPER DIPOLE VACUUM CHAMBERS

The standard dipole vacuum chambers of the MAX II storage ring are made of stainless steel. They are connected to two pumps each, one ion pump and one titanium sublimation pump. The new NEG-coated copper dipole vacuum chambers on the other hand have no additional pumps. They are made of 1 mm thick oxygen-free high thermal conductivity (OFHC) copper tubes with an inner diameter of 31 mm. An additional 1 mm thick copper tube, with an inner diameter of 10 mm, is spot welded and soldered to the outside of the larger tube and it is used for the cooling water supplying the necessary cooling of the vacuum chamber. The top part of Fig. 2 shows a drawing of the standard stainless steel dipole vacuum chamber. The bottom part of Fig. 2 shows a drawing of the new NEG-coated copper dipole vacuum chamber.

The NEG coating of the copper chambers was done at ESRF NEG coating facility's tower no. 2, using a one meter long solenoid producing a maximum field on axis of about 500 G, and with a flat-out field length of around 80 cm. The 1.3 m long copper chamber and sections of transition chambers made

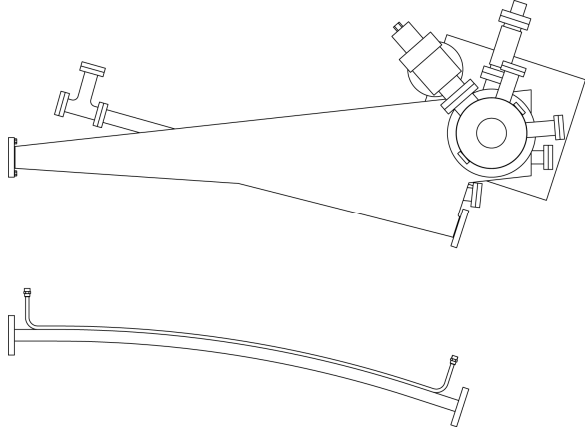


Fig. 2. Drawings of the standard stainless steel dipole vacuum chamber (top) and the new NEG-coated copper dipole vacuum chamber (bottom).

Table 1. Relative proportions of the residual gases in MAX II during operation.

Gas	Relative proportion (%)
H ₂	94.6
H ₂ O	2.2
CO	2.6
CO ₂	0.6

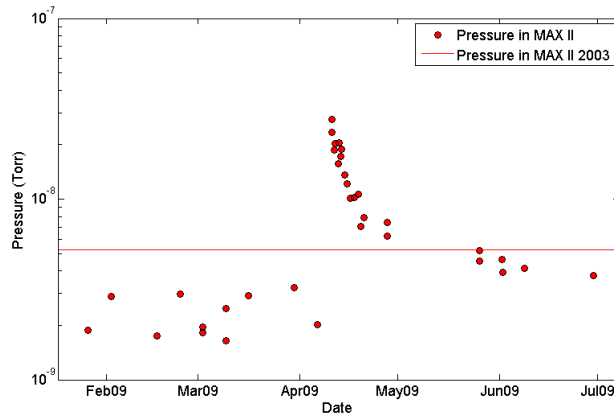


Fig. 3. (Color online) The pressure in the MAX II storage ring from February 2009 to July 2009. The solid line corresponds to the pressure in MAX II in 2003²¹.

for the purpose were therefore coated in two passes. The NEG material was sputtered onto the copper using a single Ti-Zr-V intertwined cathode made up of 0.5 mm wires. Due to the curvature of the chamber, and in order to keep the cathode close to the chamber's axis, four ceramic spacers were evenly spaced along the chamber, plus two adaptors at either end. The process gas and pressure were krypton at around 0.1 mbar, and the chamber temperature was around 110 °C. The composition of the NEG material has not been measured for the dipole chambers, but in July 2009 measurements were done at ESRF on the composition of the NEG material in an aluminum chamber sample coated using the same coating procedure as for the dipole chambers. The sample composition was 27.6 %

Ti, 41.8 % V and 30.6 % Zr by weight (33.2 % Ti, 48.4 % V and 19.4 % Zr by atomic composition)

Before installation into the MAX II storage ring the copper dipole vacuum chambers were prebaked and activated. The temperature was ramped from room temperature to 200°C in 8 hours. The chambers were kept at 200°C for at least 12 hours after which the temperature was ramped down to room temperature again in 8 hours. For the installation the chambers were vented with dry nitrogen gas. After installation, the chambers were activated again at 200°C following the same procedure as during the prebake.

Currently there are three NEG-coated copper dipole vacuum chambers installed in the MAX II storage ring. To evaluate the influence of the NEG-coated dipole chambers on the pressure and lifetime in the storage ring, measurements were performed with movable aperture restriction (scrapers) and with scintillation detectors registering the bremsstrahlung radiation emanating from the dipole vacuum chambers.

A. Scraper measurements

In 2003, before any NEG-coated vacuum chambers had been installed, scraper measurements were performed at MAX II to determine the acceptances and lifetimes of the storage ring²¹. Following the same procedure as in 2003, new scraper measurements were performed in connection with the installation of the last two NEG-coated dipole chambers in April 2009 in order to determine the evolution of the pressure and the lifetime before and after the installation and to compare this with the results from 2003.

The total lifetime, τ_{tot} , in MAX II is given by²¹

$$\frac{1}{\tau_{\text{tot}}} = \frac{1}{\tau_{\text{elastic}}} + \frac{1}{\tau_{\text{inelastic}}} + \frac{1}{\tau_{\text{touschek}}} \quad (1)$$

where τ_{elastic} and $\tau_{\text{inelastic}}$ are the lifetimes due to the elastic and inelastic scattering, respectively, of the beam electrons on the atoms of the residual gas and τ_{touschek} is the lifetime due to the Touschek effect. Assuming a rectangular acceptance, the elastic scattering lifetime is given by²²

$$\frac{1}{\tau_{\text{elastic}}} = cn_g \frac{2\pi r_e^2 Z^2 \langle \beta_V \rangle}{\gamma^2 \varepsilon_{AV} \pi} \frac{1}{\pi} \times \left[\pi + (R^2 + 1)\sin(2\arctan R) + 2(R^2 - 1)\arctan R \right] \quad (2)$$

where c is the speed of light, n_g is the residual gas density, r_e is the classical electron radius, Z is the atomic number of the residual gas, γ is the relativistic factor of the electrons in the stored beam and

$$R = \sqrt{\frac{\langle \beta_H \rangle \varepsilon_{AV}}{\langle \beta_V \rangle \varepsilon_{AH}}} \quad (3)$$

where ε_{AV} and ε_{AH} are the vertical and horizontal acceptance and $\langle \beta_V \rangle$ and $\langle \beta_H \rangle$ are the average vertical and horizontal beta functions in the storage ring. Eq. (2) is valid when the vertical acceptance is smaller than the horizontal acceptance. If the horizontal acceptance is smaller than the vertical acceptance Eqs. (2)-(3) can be used with H and V exchanged.

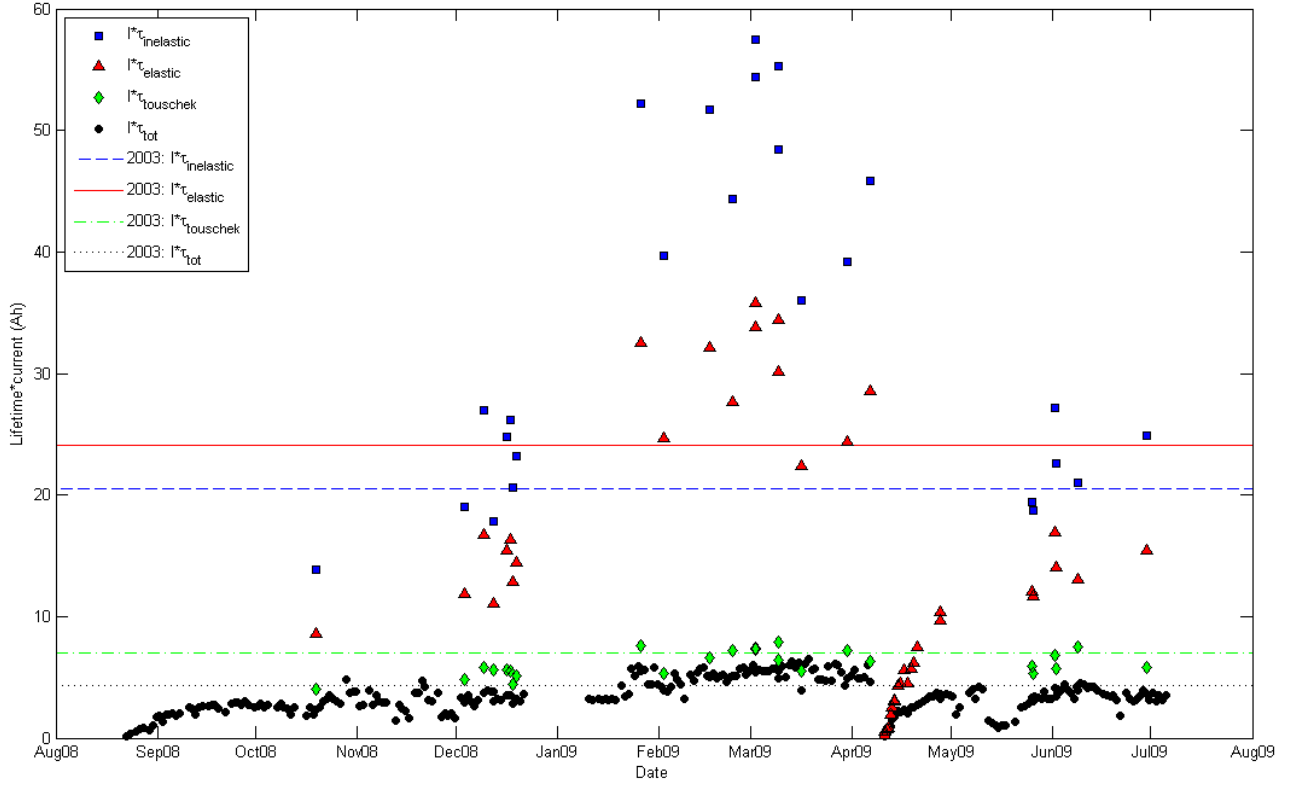


Fig. 4. (Color online) The product of stored beam current and total lifetime in MAX II from August 2008 to July 2009. Where available, the products of current and lifetime limitations due to inelastic scattering, elastic scattering and the Touschek effect are given. The lines correspond to the products of current and lifetime in MAX II in 2003²¹.

For MAX II in normal operating mode at full energy, γ is 2915, ε_{AH} is $5.6 \cdot 10^{-6}$ m, $\langle \beta_{\text{V}} \rangle$ is 6.3 m and $\langle \beta_{\text{H}} \rangle$ is 7.4 m. The relative proportions of the residual gases were determined with a residual gas analyzer (RGA), Balzers Quadstar 421, using tabulated values for the relative probabilities of ionization and relative ion currents of fragment ions²³. The result is given in Table 1. Comparing this with the result from 2003²¹, when the residual gas consisted of 96.5% H₂, 1.1% H₂O, 1.8% CO and 0.6% CO₂, it can be seen that the residual gas is still dominated by H₂ and that it has largely the same content as six years ago. No signs of methane or other gases not pumped by NEG could be found from the RGA measurement. The RGA is situated in the straight section between cell 5 and cell 6.

By combining Eqs. (1)-(2) and measuring the total lifetime at different positions of the vertical scraper (and thus different vertical acceptances) a fit can be made on the data to determine τ_{elastic} . With knowledge of the relative proportions of the residual gases the residual gas density n_{g} and from that the pressure in the storage ring can be determined. Figure 3 shows the pressure in MAX II in normal operation mode at full energy from February 2009 to July 2009. The solid line depicts the pressure measured in 2003²¹. The stored current in the storage ring varied between different scraper measurements, but was mainly in the region 140-180 mA. The installation of the two new NEG-coated copper dipole vacuum chambers in April 2009 can clearly be seen in Fig. 3. Although the pressure is not yet down to the levels it was before the April venting of cell 2 and 3, it is already lower than it was in 2003. Cell 2 and 3 were also vented during July 2008, when two NEG-coated ID chambers were installed. It took five months before the

pressure had reduced to the low levels shown in the left half of Fig 3, whereas the last scraper measurement in Fig 3 was done less than three months after the April 2009 venting.

The relative proportions of the residual gas, as measured by the RGA, were not affected by the April 2009 venting. However, since the RGA is situated in the straight section between cell 5 and cell 6, far from the vented section, it is possible that the initial content of the residual gas after the venting contained N₂ that did not show up on the RGA. The pressure measurements for the first days after the venting could thus be somewhat imprecise compared to the other results.

Using the results from the scraper measurements $\tau_{\text{inelastic}}$ can also be determined. Since the residual gas in MAX II is dominated by hydrogen the contribution from inelastic scattering on the electrons in the residual gas cannot be omitted when calculating $\tau_{\text{inelastic}}$ ²¹. Taking into account the inelastic scattering on both the residual gas nucleus and electrons the lifetime due to inelastic scattering is given by²⁴

$$\frac{1}{\tau_{\text{inelastic}}} = cn_{\text{g}} 4\alpha r_{\text{e}}^2 \left\{ \left[Z^2 \ln\left(\frac{183}{Z^{1/2}}\right) + Z \ln\left(\frac{1194}{Z^{1/2}}\right) \right] \times \frac{4}{3} \left[\ln\left(\frac{1}{\varepsilon_{\text{acc}}}\right) - \frac{5}{8} \right] + \frac{Z(Z+1)}{9} \left[\ln\left(\frac{1}{\varepsilon_{\text{acc}}}\right) - 1 \right] \right\} \quad (4)$$

where α is the fine structure constant $1/137$ and ε_{acc} is the momentum acceptance of the storage ring (2% in MAX II²⁵).

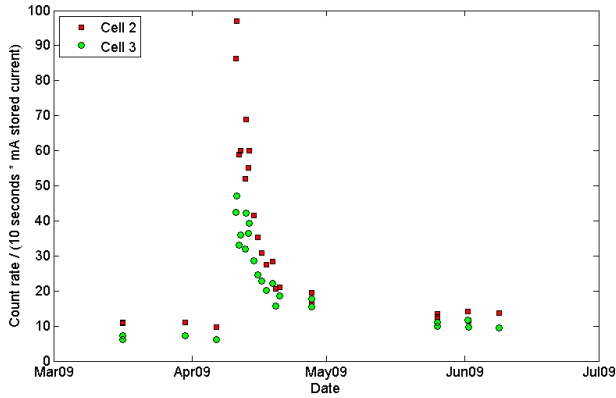


Fig. 5. (Color online) Count rate in the NaI detectors per 10 seconds and mA stored current in MAX II from March 2009 to June 2009.

Finally, τ_{touschek} is indirectly determined from results of the other lifetimes using Eq. (1).

Figure 4 show the product of the stored current and the lifetimes determined by the scraper measurements from August 2008 to July 2009. Added to the figure are the products of current and total lifetime for the days when MAX II was operating but no scraper measurement was done. The lines depict the products of current and lifetime in 2003²¹. The measurements of τ_{tot} and τ_{elastic} are not dependent on knowledge of the relative proportions of the residual gases, whereas $\tau_{\text{inelastic}}$ and thus τ_{touschek} are. Due to the uncertainty of the content of the residual gas during the first days after the venting $I \cdot \tau_{\text{inelastic}}$ and $I \cdot \tau_{\text{touschek}}$ are not shown in Fig. 4 for these days.

The beam lifetime in MAX II is limited by the Touschek effect rather than by the vacuum situation in the storage ring. This was the case in 2003 and is still valid six years later. In the beginning of May 2009 there were some problems with one of the standard dipole vacuum chambers in cell 1 and in June 2009 problems with the RF cavities prevented operation with full stored beam. Even with these problems the lifetime situation in MAX II is currently, less than three months after the installation of the two new NEG-coated dipole chambers, already similar to the situation in 2003. The main difference compared to 2003 is that $I \cdot \tau_{\text{elastic}}$ has decreased. This is explained by the fact that both the horizontal and vertical acceptance in MAX II has decreased since 2003. The horizontal acceptance has decreased from $9.6 \cdot 10^{-6}$ m to $5.6 \cdot 10^{-6}$ m, whereas the vertical acceptance has decreased from $7.4 \cdot 10^{-6}$ m to $5.4 \cdot 10^{-6}$ m. This is most likely due to horizontal absorbers installed upstream of the superconducting wigglers to shield the wigglers from dipole magnet synchrotron radiation, and the small vertical aperture of the NEG-coated ID vacuum chambers.

The average $I \cdot \tau_{\text{tot}}$ during June 2009 was 3.7 Ah which is close to the average $I \cdot \tau_{\text{tot}}$ during the last seven years of MAX II operation at about 4 Ah. In the first quarter of 2009, before the April 2009 venting the performance of MAX II was among the best since the startup of the storage ring. During a 30-day period the average stored current in MAX II was over 200 mA, the highest average current recorded.

B. Bremsstrahlung measurements

The pressure in MAX II as seen by the stored electron beam has been determined by scraper measurements in the section above. To evaluate the performance of the NEG-coated dipole vacuum chambers it would be of interest to determine the local pressure inside or close to the dipole chambers. Unfortunately, there are no calibrated vacuum gauges connected to the MAX II vacuum system. In an attempt to study the relative change of the pressure before and after the April 2009 dipole chamber installation two $2'' \times 2''$ sodium iodide (NaI) scintillation detectors were placed downstream the second dipole in cell 2 and 3 respectively. The bremsstrahlung radiation emanating from inelastic scattering on the residual gas is proportional to the pressure of the residual gas in that area. The NaI detectors were placed 3.2 m downstream of the end of the second dipole chambers in cell 2 and 3 looking at the bremsstrahlung from a 5 cm region 30-35 cm into the dipole chamber.

The count rate in the detectors per 10 seconds and mA stored current in MAX II from March 2009 to June 2009 is shown in Fig. 5. In April 2009 the second dipole chamber in cell 2 was changed from a standard stainless steel vacuum chamber to a new NEG-coated copper chamber. The second dipole chamber in cell 3 was vented during the installation but it had the same NEG-coated copper dipole vacuum chamber both before and after the April venting. The count rates in both detectors increased after the venting. The largest difference was for the detector downstream cell 2, where the new chamber had been installed. Two months after the venting the count rates in the detector downstream cell 2 were about 20 % higher than before the venting, whereas for cell 3 they were about 60 % higher. If the detectors only detected the bremsstrahlung from the dipole chambers the count rate would be proportional to the pressure. However, the detectors were also sensitive to particle losses from the Touschek effect and to the settings of the insertion devices in the ring. To minimize the influence of this the settings in MAX II were kept as identical as possible during the measurements shown in Fig. 5. But due to these uncertainties the count rates can only be seen as a very rough estimate of the relative pressure levels in the dipole vacuum chambers.

IV. CONCLUSIONS

Since 2003 four NEG-coated aluminium ID vacuum chambers and three NEG-coated copper dipole vacuum chambers have been installed in the MAX II synchrotron light source. For each standard ID vacuum chamber replaced by a new NEG-coated ID vacuum chamber one ion pump and two titanium sublimation pumps have been disconnected from the vacuum system. For each NEG-coated dipole vacuum chamber one ion pump and one titanium sublimation pump have been disconnected. Even though the cross-sections of the new vacuum chambers are significantly smaller than for the old chambers and even though there are no extra pumps connected to the new chambers, the pressure and lifetime in MAX II are still similar to the values from 2003. In cell 2 of MAX II only a titanium sublimation pump and a turbo molecular pump are connected to the vacuum system and even though the NEG-coated dipole vacuum chambers are mixed with stainless steel vacuum chambers exposed to synchrotron radiation, the

lifetime in MAX II, three months after the latest venting, is close to the average lifetime during the last seven years. During a month in early 2009, when the vacuum system of MAX II included one NEG-coated dipole chamber and four NEG-coated ID chambers, the average stored current in MAX II was over 200 mA, the highest average current recorded for a 30-day period. Judging by the experiences from MAX II, NEG-coated vacuum chambers, including dipole vacuum chambers, do not appear to have any negative impact on the performance and operation of a synchrotron light source.

V. ACKNOWLEDGEMENTS

The authors would like to thank F. Bodart, J.-L. Bersier and H. Colou for their work on the coating bench at ESRF and J. Thånell and M. Nilsson for the installation of the NEG-coated vacuum chambers at MAX-lab. The authors also would like to thank Prof. M. Eriksson for the possibility to carry out this study.

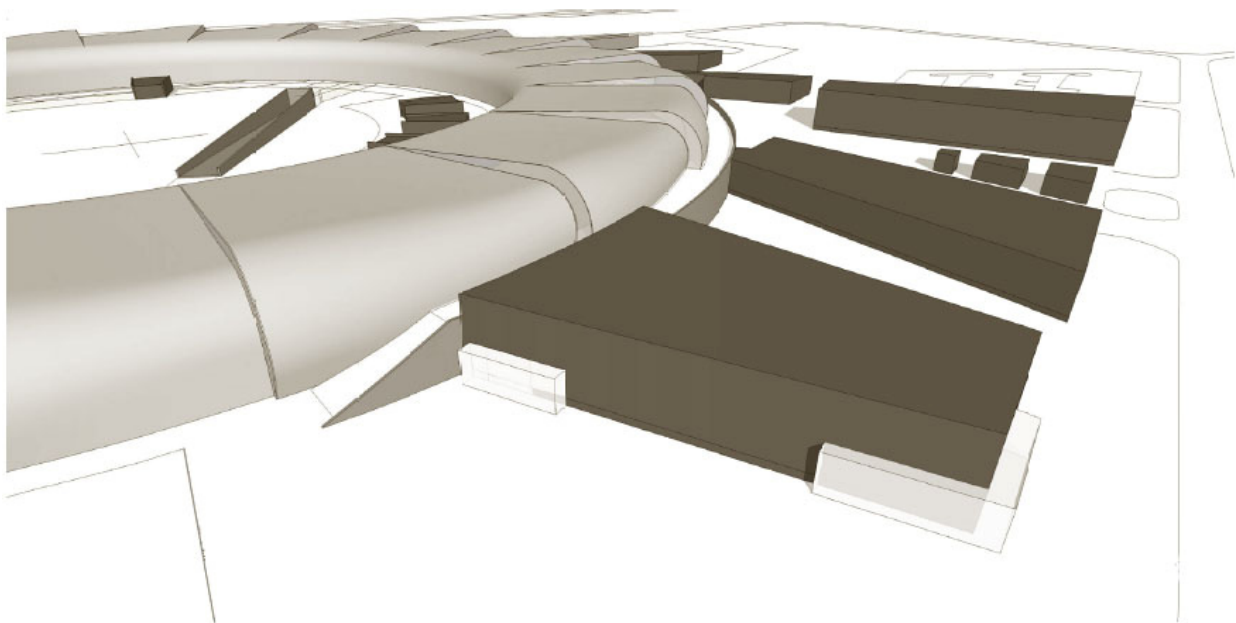
- ¹P. Chiggiato and P. Costa Pinto, *Thin Solid Films* **515**, 382 (2006).
²LEP Vacuum Group, *Vacuum* **41**, 1882 (1990).
³C. Benvenuti and F. Francia, *J. Vac. Sci. Technol. A* **6**, 2528 (1988).
⁴C. Benvenuti and F. Francia, *J. Vac. Sci. Technol. A* **8**, 3864 (1990).
⁵H. J. Halama and Y. Guo, *J. Vac. Sci. Technol. A* **9**, 2070 (1991).
⁶C. Benvenuti and P. Chiggiato, *Vacuum* **44**, 511 (1993).
⁷H. A. Sakaue, Y. Hirano, S. R. In, S. Yokouchi, K. Watanabe, and S. H. Be, *Vacuum* **44**, 523 (1993).
⁸D.J. Wang, J.R. Chen, G.Y. Hsiung, J.G. Shyy, J.R. Huang, S.N. Hsu, K.M. Hsiao, and Y.C. Liu, *J. Vac. Sci. Technol. A* **14** 2624 (1996).
⁹C. Benvenuti, P. Chiggiato, F. Cicoira, and Y. L'Aminot, *J. Vac. Sci. Technol. A* **16**, 148 (1998).
¹⁰C. Benvenuti, J. M. Cazeneuve, P. Chiggiato, F. Cicoira, A. Escudeiro Santana, V. Johanek, V. Ruzinov, and J. Fraxedas, *Vacuum* **53**, 219 (1999).
¹¹P. Chiggiato and R. Kersevan, *Vacuum* **60**, 67 (2001).
¹²R. Kersevan, *Proceedings of EPAC, Vienna, Austria, 2000*, p. 2291 (<http://accelconf.web.cern.ch/AccelConf/e00/papers/thp5b11.pdf>).
¹³M. Hahn, for the ESRF Vacuum Group, *Vacuum* **81**, 759 (2007).
¹⁴F. Mazzolini, J. Miertusova, F. Pradal, and L. Rumiz, *Proceedings of EPAC, Paris, France, 2002*, p. 2577 (<http://accelconf.web.cern.ch/AccelConf/e02/PAPERS/WEPDO026.pdf>).
¹⁵J. D. Herbert, O. B. Malyshev, K. J. Middleman, and R. J. Reid, *Vacuum* **73**, 219 (2004).
¹⁶C. Herbeaux, N. Béchu, and J.-M. Filhol, *Proceedings of EPAC, Genoa, Italy, 2008*, p. 3696 (<http://accelconf.web.cern.ch/AccelConf/e08/papers/thpp142.pdf>).
¹⁷M. Sjöström, E. Wallén, M. Eriksson, and L.-J. Lindgren, *Nucl. Instr. and Meth. A* **601**, 229 (2009).
¹⁸M.C. Bellachioma, J. Kurdal, M. Bender, H. Kollmus, A. Krämer, and H. Reich-Sprenger, *Vacuum* **82**, 435 (2007).
¹⁹Å. Andersson, M. Eriksson, L.-J. Lindgren, P. Röjssel, and S. Werin, *Nucl. Instr. and Meth. A* **343**, 644 (1994).
²⁰<http://www.maxlab.lu.se/maxlab/max4/>
²¹E. Wallén, *Nucl. Instr. and Meth. A* **508**, 487 (2003).
²²H. Wiedemann in *Particle Accelerator Physics* (Springer, Berlin, 2007), p. 325.
²³Balzers Instruments, *Partial Pressure Measurement in Vacuum Technology* (Balzers Instruments, Liechtenstein, 1996), p. 26.
²⁴C.J. Bocchetta in *Proceedings to the CERN Accelerator School, CAS 98-04* (CERN, Geneva, 1998), p.243.
²⁵Å. Andersson, private communications.



Appendix 3

Revised design of the MAX IV facility

Background material for the VR evaluation September 2009



Some considerations on proposed
rings and beamlines

RS

Version 2, August 27, 2009

Introduction

This report is a collection of smaller studies related to performance of the soft-X-ray beamlines at 3.0 GeV and 1.5 GeV rings with revised design.

First chapter describes shortly the space requirements and the role of coupling for soft-X-ray beamlines based on collimated plane grating monochromator (cPGM) design.

Chapter 2 illustrates the benefits if, instead of moving and updating existing MAX II, a 1.5 GeV ring with revised design was built.

In the meeting related to the soft-X-ray beamlines (June 10th, 2009) the parameters of the revised 1.5 GeV ring were discussed in general together with the option of locating some soft-X-ray beamlines to the revised 3.0 GeV ring. Also the relocation of the low photon energy beamlines (I3 and I4 at MAX III) to the revised 1.5 GeV ring was considered. Finally, the electron energy of the revised 1.5 GeV ring was discussed extensively. Chapters 3-5 deals with these points. However, the heat load issues related to soft-X-ray beamlines at revised 3.0 GeV ring are not dealt yet at all.

Chapter 6 shows what is to be expected from bending magnets if they are to be used as sources of synchrotron radiation at revised 1.5 GeV ring.

Chapter 1

Performance of the cPGMs at 1.5 GeV ring

According to Conceptual Design Report (CDR) [1] and the later update [2], all soft X-ray monochromators planned for 3.0 GeV and 1.5 GeV rings are based on cPGM design. Practically all of these beamlines are designed for very high spectral resolution and the distances between optical components become an important issue; a simplified explanation is as follows: If the first mirror (M1), which collimates the photon beam, is further away from the source, the beam becomes higher (and wider) in the beamline - this will yield to aberration related performance limit. On the other hand, the longer the distance is from the source to the collimating mirror, the better the ratio of the focusing distance (focusing mirror (FM) - exit slit (ES)) to the collimation distance (source - M1). These two contributions have different importance for different sources: for a small, low divergence source the beam size in the beamline becomes an issue later than for bigger and more divergent source. The aim of this study is to estimate these effects in detail.

1.1 Simulations

The starting point for simulation is following: a cPGM beamline is placed either on 3.0 GeV or 1.5 GeV ring with revised design. The electron beam parameters are calculated with SPECTRA [3] based on the machine file built by Erik Wallén [4]. The coupling constant between vertical and horizontal emittance in the file is quite high, 10%, and at revised 1.5 GeV ring it can be smaller - that would benefit these high resolution cPGM beamlines considerably. The relevant parameters are shown in Table 1.1.

The last column of Table 1.1 shows the parameters for original 1.5 GeV ring as that was the starting point for the beamline design during the CDR process and it is possible that there are some detailed beamline plans with such source characteristics. The source for revised 1.5 GeV ring beamline is an EPU41 undulator with 41 mm period; it will cover energy range of about 90-1500eV. The source for the beamline at revised 3.0 GeV ring is an EPU52 that covers energies from 150 to 1500eV. The field strengths were obtained from CDR (EPU52) and from Ref. [5]. The beamline performance was estimated by

Table 1.1: Horizontal and vertical emittances, sizes and divergences of the electron beam in different storage rings.

	3.0 GeV	1.5 GeV	1.5 GeV
	revised design	revised design	original design
ϵ_x (nm rad)	0.24	5.6	0.34
ϵ_y (nm rad)	0.009	0.56	0.034
σ_x (μm)	49	201	52
σ_y (μm)	7	40	8
$\sigma_{x'}$ (μrad)	5.4	28	6.5
$\sigma_{y'}$ (μrad)	1.3	14	4.4

RAY-ray tracing package [6] at lowest energies (90 and 150eV) and at 1000eV - the source characteristics at these energies were taken from SPECTRA or, if the source size at higher harmonics was needed, calculated directly with equations presented in Ref. [7].

The first optical element was set directly after the radiation shield; in case of revised 1.5 GeV ring, the safe distance between the source and the middle of the first mirror is set to 12 m whereas at revised 3.0 GeV ring the corresponding distance is 22 m. Existing cPGMs indicate that the exit arm for the focusing mirror should be between 10-15 m for high resolution beamlines, this parameter was fixed to 12 m based on earlier simulations. The monochromator and the focusing mirror require typically about 3.5 m space. With these parameters, the source to exit slit distance is 27.5 m and 37.5 m for revised 1.5 GeV and revised 3.0 GeV ring beamlines, respectively. First simulations were done with a first mirror collimating both vertically and horizontally. At low energy limit, the high illumination of the focusing mirror was limiting the resolution at both cases. If the first optical element was moved to 12 m from the source at revised 3.0 GeV ring, the limitation at low energy vanished. At 1000 eV, the source divergence is much smaller and the simulated performance was very close to the calculated values (which do not account for aberrations) even if the first mirror was at 22 m. At this revised 3.0 GeV ring, the high energy performance was dictated by the distance ratio of source-M1 and FM-ES. As the high energy side favored long source-M1 distance, the aberration was studied a bit more: It turns out that it is mostly the illuminated length (not so much the height) that limits the resolution. This illumination can be reduced by focusing the beam horizontally with M1. In this case the horizontal focusing of M1 was set to the exit slit - this also provides convenient common (vert. & hor.) focus for re-focusing optics. With this kind of arrangement, the resolution achieved higher values at revised design 3.0 GeV ring with 22 m source-M1 distance than with 12 m. The horizontal focusing improves also the resolution at revised 1.5 GeV ring, but due to high divergences, it is quite likely that there is no gain by moving the M1 further from the source. Maximum resolutions are given in Table 1.2¹. It should be noted that it is crucial to use high quality gratings to take full advantage of new sources.

¹Slope errors of 1" (sag.) and 0.1" (tang.) was used for mirrors whereas 0.04" (sag. & tang.) was used for the grating (1221lines/mm). These values should be achievable with present technology. Maximum resolution was obtained with $\text{cff} = 12$, $\text{slit} = 1\mu\text{m}$.

Table 1.2: Ultimate resolution with standard grating (1221 l/mm). *The high energy results are obtained with M1 which collimates both vertically and horizontally as the divergences and thus the aberration limits are smaller.

	source - M1 = 12 m	source - M1 = 22 m
$h\nu$	1.5 GeV, rev. design	3.0 GeV, rev. design
90	70 000	-
150	-	78 000
1000	24 000*	29 000*

1.2 Comments on beamline geometry

To achieve the resolution requirements set by the CDR, a source to exit slit distances of 27.5 m and 37.5 m are foreseen for revised 1.5 GeV and 3.0 GeV rings, respectively. According to the simulations, the radiation shield is not limiting the performance if one focuses the beam horizontally before the focusing mirror. The space for refocusing and experimental stations varies with beamline and applications. The beamline length of a typical beamline at 3.0 GeV with revised design is planned to be 50 m, this provides 12.5 m for refocusing/experiments. If the same space is reserved (and in many application it is certainly needed) for the refocusing stage of the beamlines at revised 1.5 GeV ring, the total length would be 40 m. If micro-focusing is needed, the space requirements might get even higher - this has to be studied further when there is more detailed information on focusing needs.

1.3 cPGM beamlines at 1.5 GeV storage ring with revised design: the role of coupling

Electron beam size and the emittance at revised 1.5 GeV ring corresponding to different coupling strengths are presented in Table 1.3 All the values are obtained from SPECTRA. With these parameters, the source size for EPU41 undulator at 90, 500, and 1000 eV are presented in Table 1.4

Assuming that the monochromator would be in normal mode (high transmission - good high order suppression), the resolution would behave as depicted in Fig. 1.1.

The benefit of small source size is obvious: the flux at experiment corre-

Table 1.3: Horizontal and vertical emittances, sizes and divergences of the electron beam in revised 1.5 GeV ring with different coupling strengths.

	10%	1%	0.1%
ϵ_x (nm rad)	5.6	5.6	5.6
ϵ_y (nm rad)	0.56	0.056	0.0056
σ_x (μm)	200.8	200.8	200.8
σ_y (μm)	39.6	12.52	4.2
$\sigma_{x'}$ (μrad)	27.89	27.89	27.89
$\sigma_{y'}$ (μrad)	14.14	4.47	1.41

Table 1.4: Source size and divergences used in the simulations and calculations.

$h\nu$ (eV)		10%	1%	0.1%
90	σ_x/σ_y (μm)	202.1/45.7	202.1/26.1	202.1/23.2
	$\sigma_{x'}/\sigma_{y'}$ (μrad)	55.5/50.0	55.5/48.2	55.5/48.0
500	σ_x/σ_y (μm)	201.0/40.8	201.0/15.8	201.0/10.5
	$\sigma_{x'}/\sigma_{y'}$ (μrad)	34.5/24.7	34.5/20.8	34.5/20.4
1000	σ_x/σ_y (μm)	200.9/40.2	200.9/14.3	200.9/7.9
	$\sigma_{x'}/\sigma_{y'}$ (μrad)	31.4/20.2	31.4/15.1	31.4/14.5

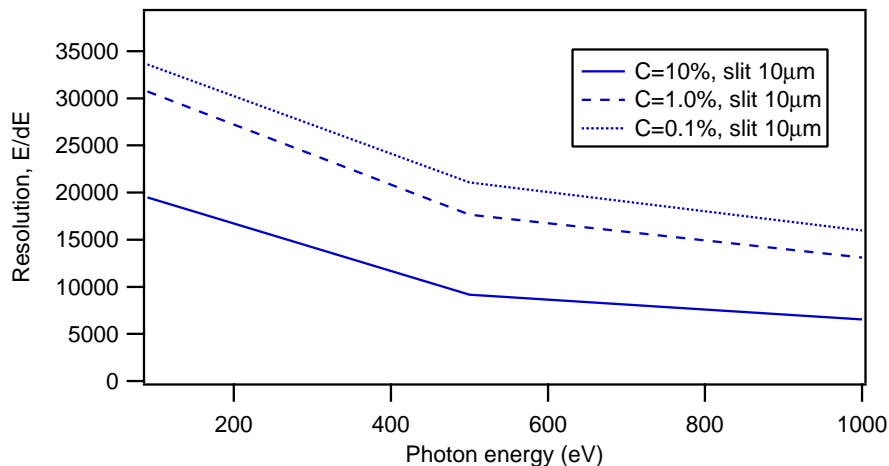


Figure 1.1: Relative energy resolution at 90, 500 and 1000 eV with different coupling in the revised 1.5 GeV ring. In the simulations, 1221 1/mm grating was used, the slope errors of the optics are as described in Page 3, exit slit was set to $10\mu\text{m}$.

sponding to different coupling is about the same but resolution is much better. In other way, for same energy resolution, small-source-case delivers much more flux than the big-source-case. It is possible to estimate the energy resolution and the various contributions into it (source size, slit size, slope errors of mirrors and gratings) by using approximate analytical expressions [9]. If all contributions are regarded as Gaussian parameters, they can simply be summed up. Such plots are attached for three above mentioned energies and couplings. To test the validity of these calculations, real sources were generated with URGENT code [10] and those source files were used in RAY for ray tracing simulations at 90 eV with 10% and 0.1% coupling. The results are collected in Table 1.5, the c_{ff} value is so-called fix focus constant - the high c_{ff} -value will yield to demagnified source but the transmission with high c_{ff} values is very low.

The attached figures show clearly that the source contribution is the main resolution limiting factor up to c_{ff} -value of about 10 if machine coupling is at 10%. This will change so that with 0.1% coupling, the source-size contribution can be decreased below other factors with c_{ff} -values below 5.5. This is an important point regarding the transmission. According to these results, it is desired to have a coupling at least down to 1%, if the coupling is as low as 0.1%, the

Table 1.5:

	$c_{ff}=2.25$		$c_{ff}=4.5$		$c_{ff}=12$	
Coupling	10%	0.1%	10%	0.1%	10%	0.1%
ΔE (simulation)	4.44	2.80	2.26	1.69	1.595	1.414
ΔE (calculation)	4.62	2.68	2.39	1.65	1.44	1.30
Flux (ph./sec)	3.5e12	3.2e12	1.7e12	1.6e12	5.1e11	4.8e11

source is diffraction limited up to 2.7 keV^2 ; that is far above soft-X-ray region. On the other hand, meeting this limit does not mean that electron beam has zero effect on source size; it is just smaller than the photon size contribution. According to discussion with Mikael Eriksson [8], 1% coupling is certainly possible, even 0.1% should be within reach - Touschek lifetime would nevertheless go down with smaller coupling factor (this will be calculated). Required length of the beamlines (40m) was also mentioned - together with the fact that there would be four beamlines of this design.

²In the sense that electron beam size is equal to photon spot size

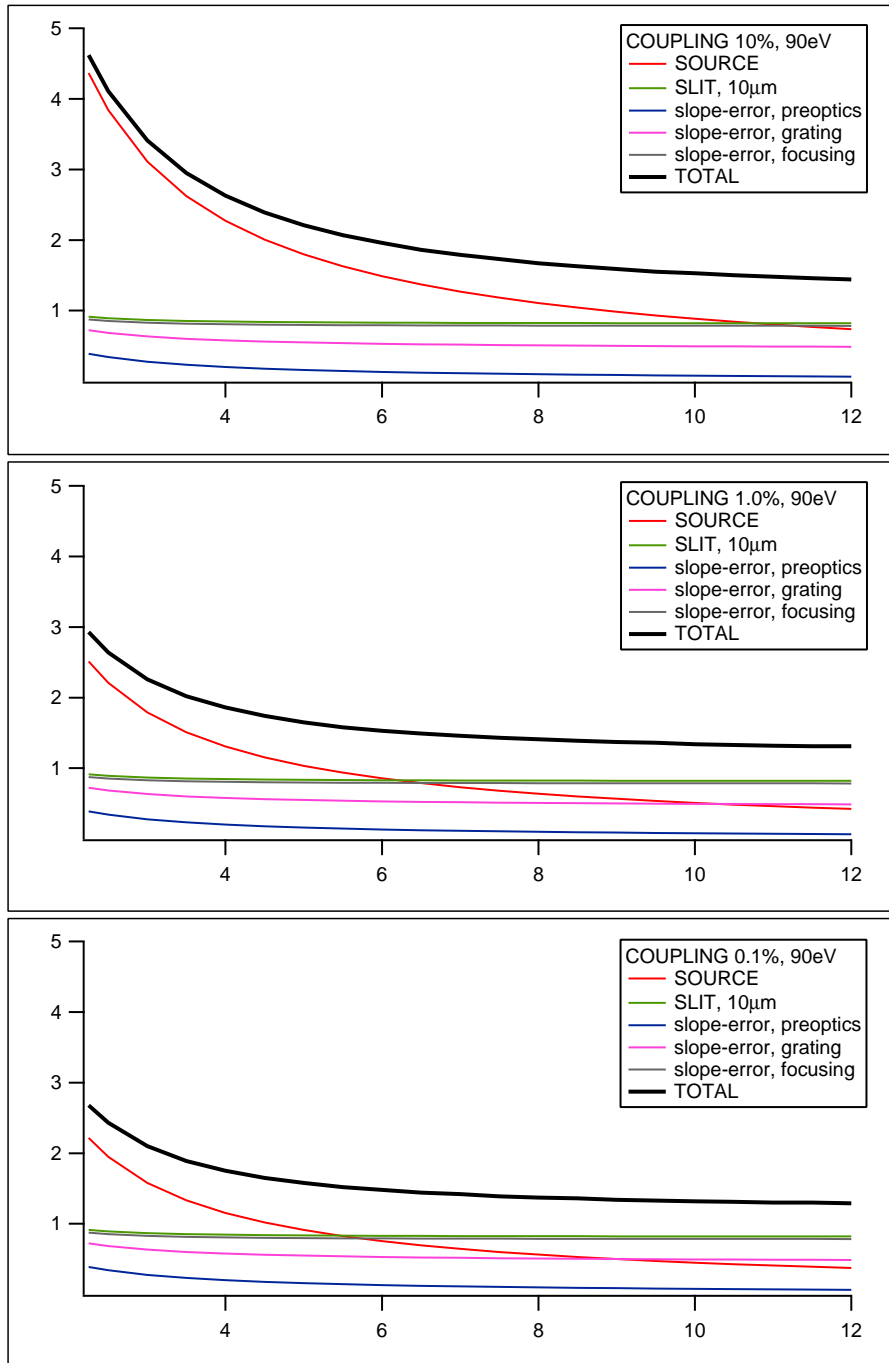


Figure 1.2: Various contribution to the total resolution (meVs) with different coupling at 90 eV.

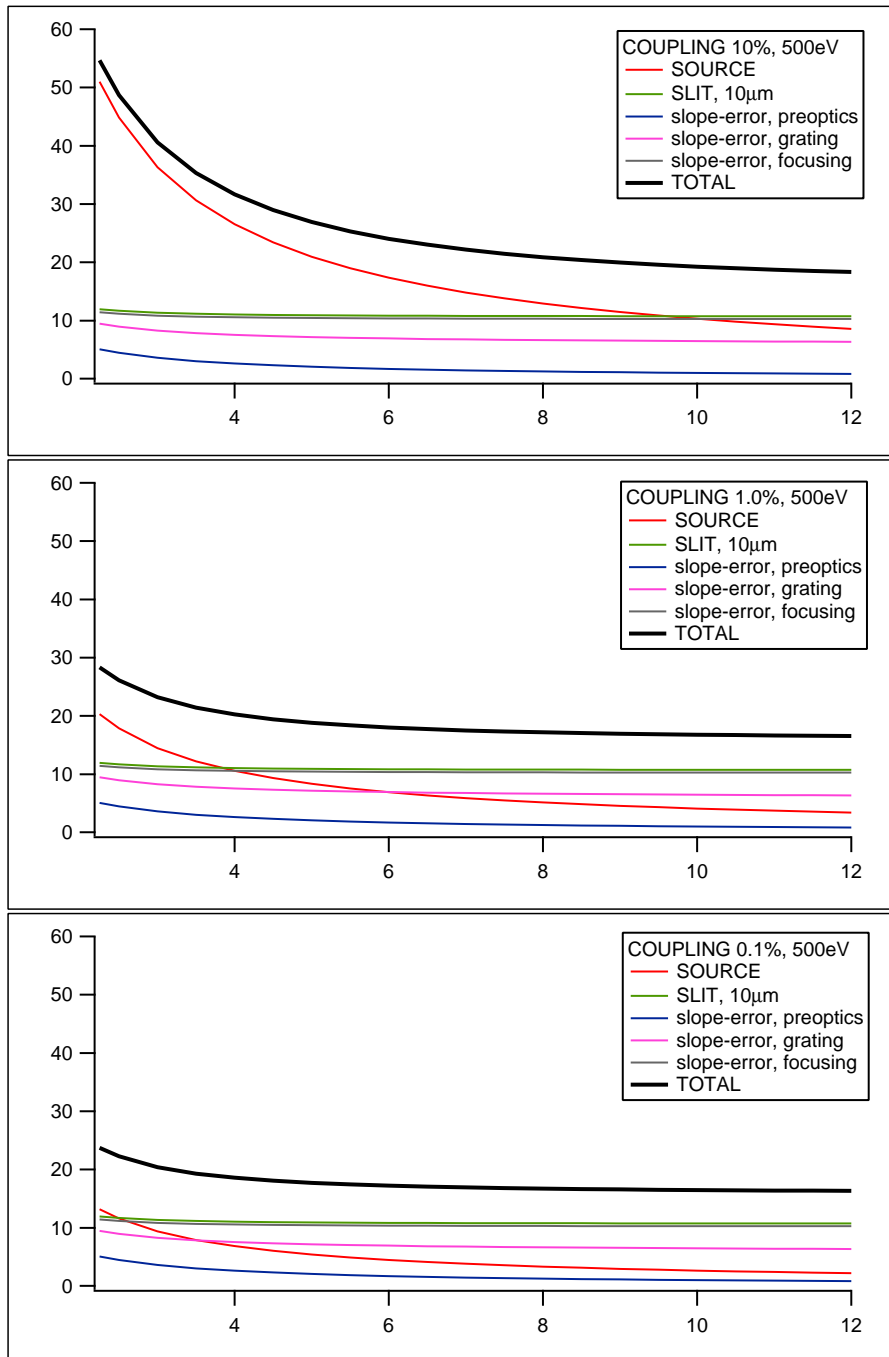


Figure 1.3: Various contribution to the total resolution (meVs) with different coupling at 500 eV.

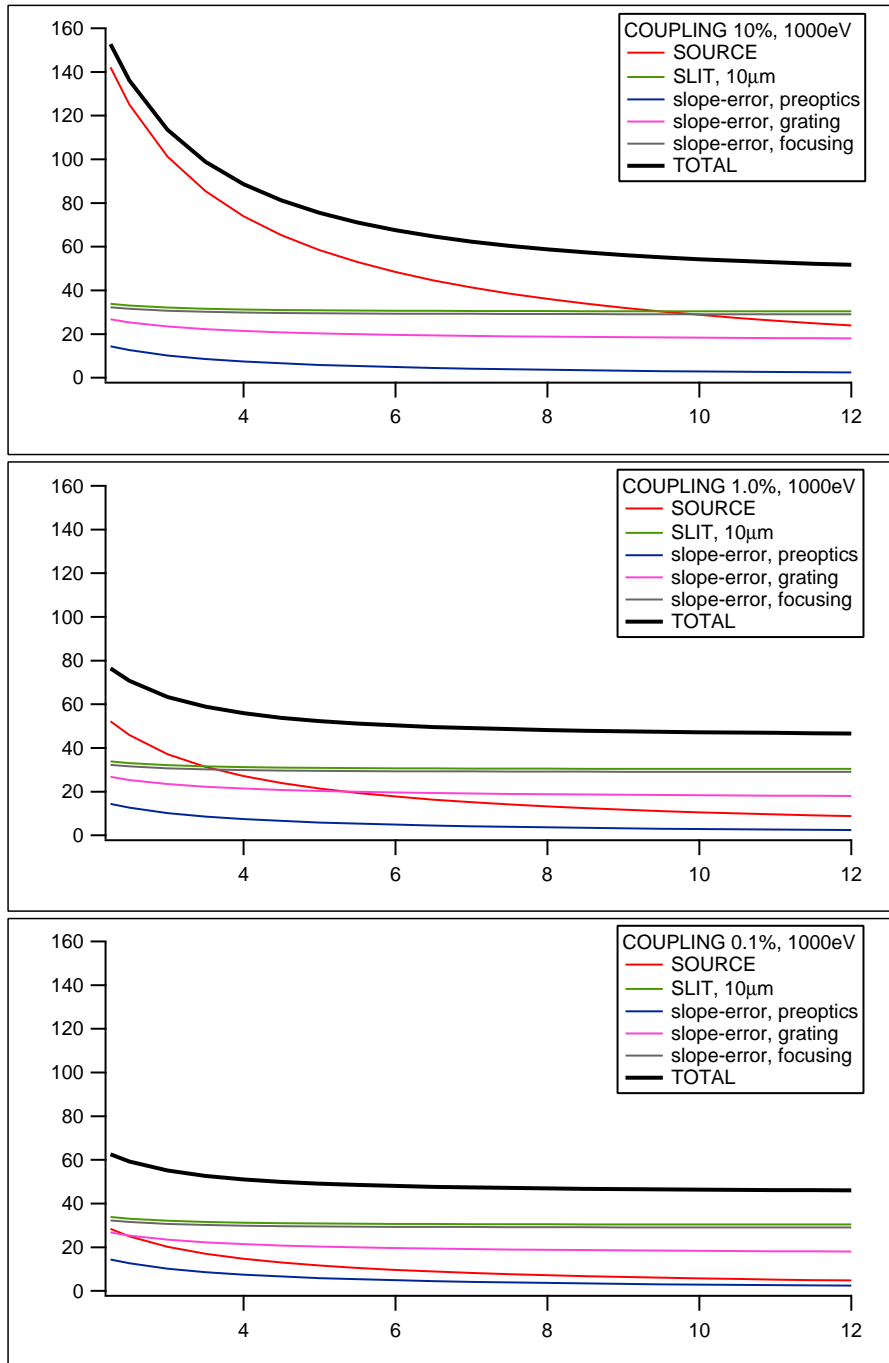


Figure 1.4: Various contribution to the total resolution (meVs) with different coupling at 1000 eV.

Chapter 2

Comparison of upgraded MAX II vs. a 1.5 GeV ring with revised design

The machine parameters for updated MAX II and the new 1.5 GeV storage ring with revised design are presented in Table 2.1. The new, revised ring has all the benefits: it can be run at higher current, the straight section are slightly longer and the minimum gap is lower than in updated MAX II ring.

Table 2.1: The source characteristics of updated MAX II and revised 1.5 GeV ring as estimated by SPECTRA. The emittance for MAX II UPD is taken from Ref. [2].

	MAX II UPD	revised 1.5 GeV ring
Maximum current (mA)	300	500
Circumference (m)	90	96
Number of straight sect.	10	12
Straight section length (m)	3.14	ca. 3.4
ϵ_x (nm rad)	10.0	5.6
Coupling	0.01	0.01
Beam size ($\sigma_{h/v}$, μm)	374/16	200.8/12.5
Beam divergences ($\sigma'_{h/v}$, μrad)	27.8/6.3	27.9/4.5

At present, the average current of MAX II is about 200 mA (with two injection per day). If existing MAX II beamlines together with their present insertion devices are relocated to a updated MAX II, the flux will increase by a factor of 1.5 by increased (and constant) ring current. If these beamlines were relocated to the new ring, the flux would increase by a factor of 2.5.

The lower emittance of the revised 1.5 GeV ring means that the source size, both horizontally and vertically, is smaller than in the updated MAX II, together with higher flux, the new source provide substantial improvement.

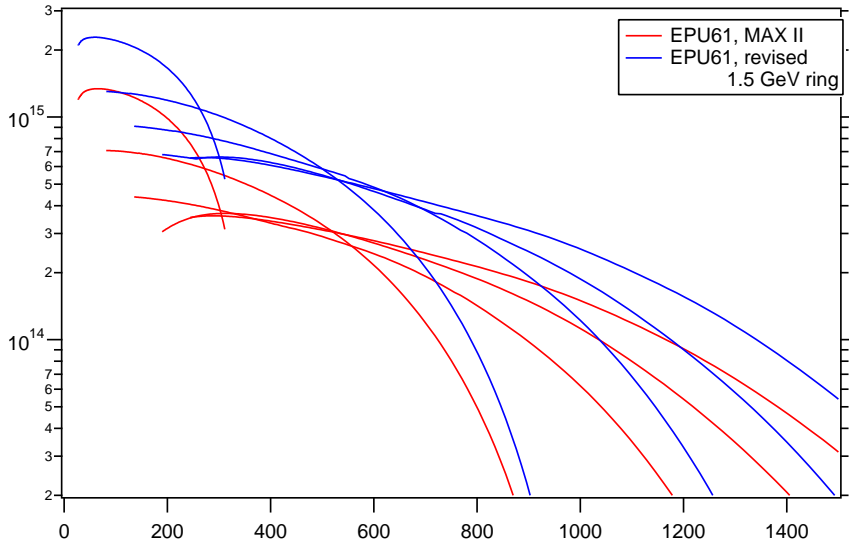


Figure 2.1: Flux of EPU61 undulator on $400\mu\text{rad} \times 400\mu\text{rad}$ aperture both at updated MAX II and at new 1.5 GeV ring with revised design.

2.1 An example: updated beamline I511

Beamline I511 at MAX II will be updated together with its insertion device. The proposed EPU has a period length of 61 mm and it has a total magnetic length of 2458 mm. The effective field at minimum gap (16 mm) is 0.8567 T ($K=4.88$) which gives the minimum energy of 27.1 eV. Undulator flux at both rings is shown in Fig. 2.1.

The beamline is modeled and simulated in detail but the source was assumed to be existing MAX II ring. This particular beamline is used for RIXS experiments and there it is crucial to have as high flux as possible to a very small spot. The small horizontal source size is directly reflected into the spot size at sample position. The following Table 2.2 shows the results based on ray-tracing in case of these two sources. The design goal for cI511 was to produce a spot smaller

Table 2.2: The energy resolution, flux and spot size at sample plane for cI511 at updated MAX II and at revised 1.5 GeV ring. The photon energy is 100 eV.

	MAX II update	revised 1.5 GeV ring
Flux at sample (ph./sec)	9.2×10^{12}	2.3×10^{13}
Energy resolution (meV)	6.8	6.6
Spot size at sample (h/v, μm)	22.1/3.6	23.4/3.8

than $25 \mu\text{m} \times 5 \mu\text{m}$; at MAX II, horizontal baffling has to be used to meet this requirement, this cuts down flux a little bit but the result is smaller spot - at revised 1.5 GeV ring this can be avoided and this gives additional increase in flux at sample. The energy resolution improves slightly but the effect is almost negligible.

Chapter 3

A comparison between the present MAX III sources for low energies vs. the same energy ranges at a revised 1.5 GeV ring

3.1 Undulator parameters

So far, the undulators used in the simulations result from complete magnetic simulations. For the following cases (including Chapters 4 and 6), the parameters of the undulators had to be defined. For most accurate description, extensive magnetic simulations should be carried out. However, the properties of undulators are studied quite widely and there exists empirical equation to estimate the maximum magnetic field of the undulators at various gaps [11]. Achievable maximum magnetic field together with the period length dictate the lowest achievable photon energy; in other way, if the lowest photon energy is known the shortest allowed period length can be defined. The study of Elleaume *et al* [11] gives description for three cases: pure permanent magnet undulator producing vertical, horizontal, or circular field. The EPU structure at 0-dephasing corresponds to the vertical field case so that was chosen as the model case here - this setting also corresponds to the highest heat load for the optics.

The minimum gap for such out-of-vacuum devices at revised 1.5 GeV ring would be 14 mm. The insertion devices for low energies are ideal in the sense that the period length is the shortest possible. First task was to find out how does the undulator at revised 1.5 GeV ring compare with the existing undulator at MAX III ring. Later on, another simulation was performed for the revised 1.5 GeV ring which was set to run at 1.0 GeV electron energy. In case of new ring, the undulators were supposed to be 3.0 m long, clearly longer than at MAX III, where the magnetic structure of EPU69 is 1.98 m long. The parameters used

in the simulations are presented in Table 3.1

Table 3.1: Period length (λ), maximum magnetic field (B_{max}), deflection parameter (K) and the lowest achievable photon energy for MAX III and corresponding undulators at 1.0/1.5 GeV rings based on revised design. The 150 mm period undulator is closed down to only 61 mm.

	$\lambda(\text{mm})$	B(T)	K	$h\nu(\text{eV})$	P(kW)
EPU,MAX III	69.1	0.9088	5.86	3.7	0.15
PMU, revised 1.5 GeV ring	87.5	1.236	10.1	4.7	3.23
PMU, revised 1.0 GeV ring	71.7	1.102	7.38	4.7	1.13
PMU, revised 1.5 GeV ring	150	0.544	7.62	4.7	0.63

It is interesting to note that for the low energy undulator, the gain in going from 1.5 GeV electron beam energy to 1.0 GeV is at maximum only about 22%. Both new options provide clearly higher flux (about 2 times) all over the 5-50 eV range. In addition, the higher ring energy means that relative gain is higher at high energy side of the photon energy range compensating nicely the weaker transmission of the beamline at those energies. The results for these undulators together with the flux from present undulator are presented in Fig. 3.1. In all these calculations the acceptance was set to $1 \text{ mrad} \times 1 \text{ mrad}$.

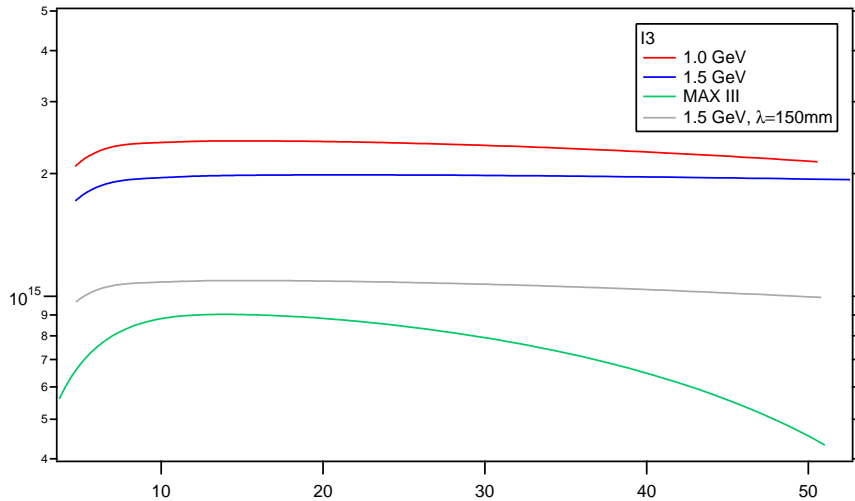


Figure 3.1: Flux of low energy undulator at 1.0 GeV and 1.5 GeV rings based on revised design ($I_R=500\text{mA}$) compared with the present MAX III undulator ($I_R=300\text{mA}$). The gray line depicts the flux of a low-heat-load-undulator providing the same energy range. It should be noted that maximum design current of MAX III is 1A but that can not be realized at present.

Chapter 4

A comparison of flux for some specific beamlines if the ring with revised design is ran at 1.0 GeV instead of 1.5 GeV.

Although lower ring energy means that one can use shorter periods and thus house more of them into the 3 m space, it might be that the performance of the soft-X-ray beamlines would suffer from low ring energy. This was studied by modeling three different undulators, each providing the photon energy required for specific applications. The period length of the four different undulators at revised 1.0 GeV and 1.5 GeV rings are defined as described in Chapter 3; they are presented in Table 4.1.

Table 4.1: Period length (λ), maximum magnetic field (B_{max}), deflection parameter (K) and the lowest achievable photon energy presented for both revised 1.0 GeV and 1.5 GeV rings. All the undulators are 3.0 m long.

	$\lambda(\text{mm})$	$B_{max}(\text{T})$	K	$h\nu_{min}(\text{eV})$	P(kW)
PEEM, 1.5 GeV, rev.	46.5	0.782	3.40	68	1.3
XPS, 1.5 GeV, rev.	53.1	0.883	4.38	38	1.7
RIXS, 1.5 GeV, rev.	57.4	0.942	5.06	27	1.9
PEEM, 1.0 GeV, rev.	38.5	0.638	2.29	68	0.38
XPS, 1.0 GeV, rev.	44.1	0.742	3.06	38	0.52
RIXS, 1.0 GeV, rev.	47.7	0.802	3.57	27	0.60

The source parameters for the revised 1.5 GeV ring were provided by Wallén [4], the corresponding parameters for the 1.0 GeV ring were obtained from the ones of the 1.5 GeV ring just by scaling down the horizontal emittance according to the electron energies. The parameters are collected below in Table 4.2.

Table 4.2: The source characteristics of the rings base on revised design with two electron beam energies as estimated by SPECTRA [3].

	1.5 GeV, rev.	1.0 GeV, rev.
ϵ_x (nm rad)	5.6	2.5
coupling	0.01	0.01
beam size ($\sigma_{h/v}$, μm)	200.8/12.5	134.2/8.4
beam divergences ($\sigma'_{h/v}$, μrad)	27.9/4.5	18.6/3.0

The flux curves of three different soft-X-ray undulators are presented in Fig. 4.1. For all these calculations, an acceptance angle of $400 \mu\text{rad} \times 400\mu\text{rad}$ was used; ring current was set to 500 mA.

The results show clearly that for soft-X-ray region, the undulator at 1.5 GeV ring provide higher flux except for photon energies below 100 eV - there the difference is about 20% at maximum. On the other hand, at 750 eV, the undulator at 1.5 GeV ring provides an order of magnitude higher flux compared to the undulator at 1.0 GeV ring. In the upper limit of soft-X-ray regime, at 1500 V, the difference is more than three orders of magnitude reflecting the completely different nature of 1.0 GeV and 1.5 GeV rings.

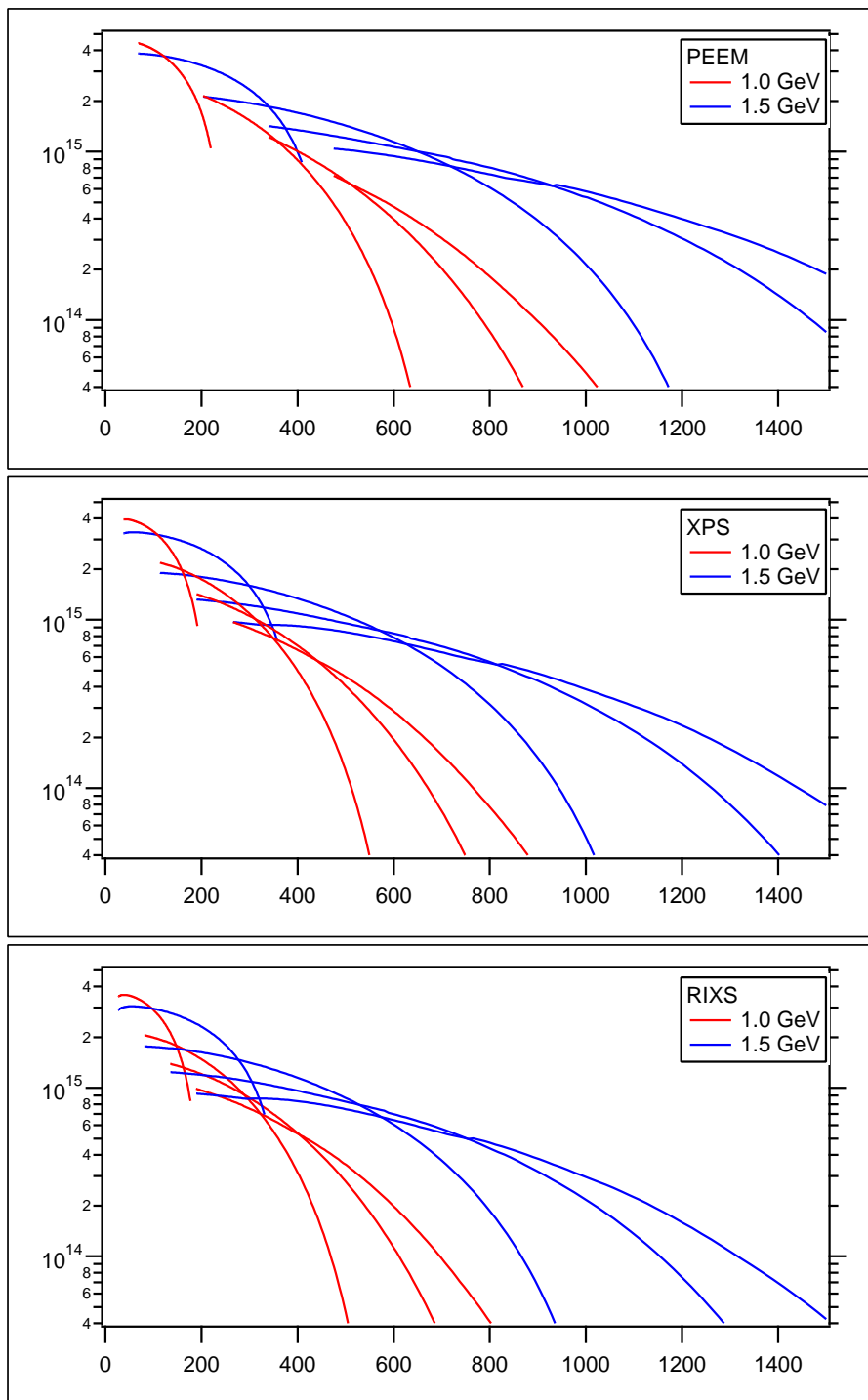


Figure 4.1: Flux curves of various undulators at revised 1.0 GeV and 1.5 GeV rings.

Chapter 5

Comparison between 1.5 GeV and 3 GeV rings with revised design for producing soft x-rays

In the ring design presented in the CDR, the 1.5 GeV ring was physically similar to the 3.0 GeV ring. Because of the lower electron energy, the emittance of the original 1.5 GeV ring was much lower. As also the ID length and the minimum gap were similar, it turned out that for most soft-X-ray beamlines, original 1.5 GeV ring provided optimal condition in terms of both brightness and absolute flux up to about 300 eV. The proposed 1.5 GeV ring based on revised design is physically smaller and the emittance is more than an order of magnitude higher than in the original ring described in CDR. Comparing the rings with revised design, the 3.0 GeV ring has smaller emittance and it provides possibility for very high brightness. In addition, the straight section are longer than in the revised 1.5 GeV ring, allowing for at least 4 m long insertion devices. The relevant ring parameters of revised 3.0 GeV are collected below in Table 5.1

Table 5.1: The source characteristics of the revised 3.0 GeV ring as estimated by SPECTRA [3] after setting the emittance as described in Ref [2].

ϵ_x (nm rad)	0.24
coupling	0.03
beam size ($\sigma_{h/v}$, μm)	46.5/6.6
beam divergences ($\sigma'_{h/v}$, μrad)	5.2/1.4

To find out the performance, the XPS undulator designed for revised 1.5 GeV ring was selected as a reference. The parameters of the corresponding undulators at revised 3.0 GeV ring used in the calculations are collected in Table 5.2. In this case, undulators for revised 3.0 GeV ring were designed as follows: First undulator was defined in a way to meet the low energy requirement for XPS

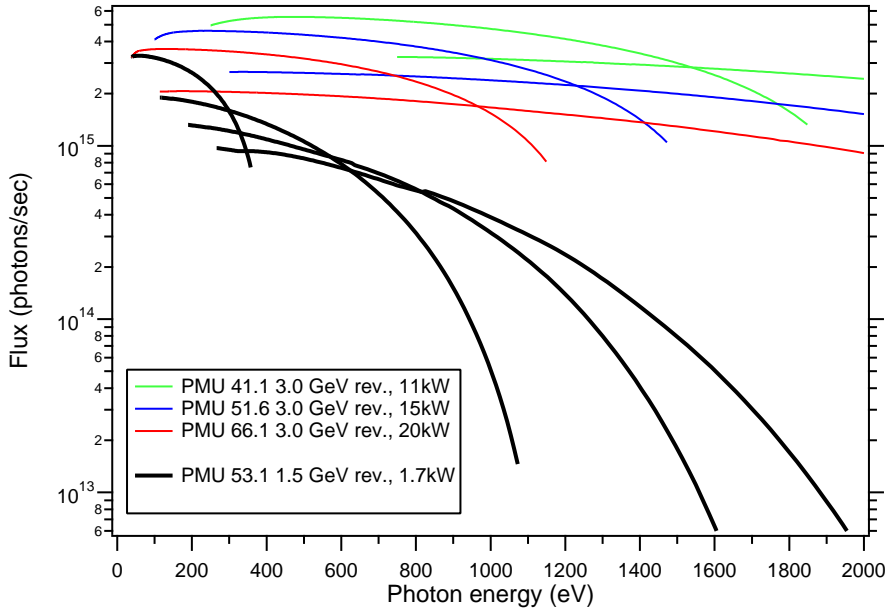


Figure 5.1: Three undulators at revised 3.0 GeV ring compared with the undulator covering the 38-1500 eV energies at revised 1.5 GeV ring.

undulator at revised 1.5 GeV ring. Second was defined to meet the more relaxed lower energy limit (100eV) for the same beamline where as the third one shows an undulator starting from about 250 eV.

Table 5.2: Period length (λ), maximum magnetic field (B_{max}), deflection parameter (K) and the lowest achievable photon energy for undulators at revised 3.0 GeV ring. All the undulators are 4.0 m long.

	λ (mm)	B_{max} (T)	K	$h\nu_{min}$ (eV)	P(kW)
PMU 66.1	66.1	1.317	8.13	38	20
PMU 51.6	51.6	1.158	5.58	100	15
PMU 41.1	41.1	0.997	3.82	250	11

Following graph (Fig 5.1) provides some information about the performance of the undulator designed for soft-X-ray beamline. For comparison, 53.1mm XPS-PMU produces about 1.7 kW power at 1.5 GeV soft-X-ray ring. The flux is calculated to a rectangular acceptance window of size $4\sigma'$ at the lowest photon energy, and they are 260 μ rad, 160 μ rad and 100 μ rad wide, respectively so that they collect relatively same amount of available light.

The figure clearly shows that with higher ring energy the relative flux increases at high energy side of the energy spectrum. However, the difference at 1.5 keV is in the present case about one order of magnitude (PMU 53.1 at revised 1.5 GeV ring and PMU 66.1 at revised 3.0 GeV ring covering the same energy range), clearly less than between revised 1.5 GeV ring ran at 1.5 or 1.0 GeV.

The heat loads related to undulators providing soft-X-rays at revised 3.0 GeV

ring are very, very high; at Spring-8, for example, exotic insertion devices are used to avoid such high heat loads at the central cone but the polarization properties of the generated light can not be controlled completely without extreme complexity in the insertion device.

Another option is to use higher period undulator with bigger gap. For example, if 68 eV is set as minimum energy, PMU66.1 at revised 3.0 GeV ring will produce about 10.7 kW with 15.5 mm gap; the flux at energies above 68 eV (for the 1st harmonic, the minimum energy for 3rd harmonic will be 204 eV) is identical to the one presented in Fig. 5.1.

Chapter 6

Relocation of BL's to bending magnet sources at revised 1.5 GeV ring

Beamline D1011 is using bending magnet radiation from MAX II, that beamline can be relocated quite easily to new soft-X-ray ring. The bending radius of new ring would be 3.82 m, slightly larger than at MAX II, 3.33 m but the beam current would be twice as high and thus the flux will also increase (see Fig. 6.1).

If there is strong need for straight sections, I311 could also be relocated to a bending magnet; even the first mirror is directly capable of catching reasonable amount of bending magnet radiation by having an acceptance of about 3 mrad. The flux will certainly be lower than at current I311 but still high enough for solid state experiments at moderate energies.

The relocation of existing I411 to a bending magnet is possible. For successful gas phase experiments, a flux of more than 10^{10} photons/sec is required. If the beamline transmission is higher than 0.1% that level can be reached. If relocated I411 is the main gas phase facility in the 50-250 eV region its relocation on straight section would still be better option.

According to Spectra file, the vertical source size at bending magnet section of the revised 1.5 GeV ring with 1% coupling would be about $31 \mu\text{m}$, lower than at present MAX II (10% coupling) straight section so the achievable resolution would remain about the same as now.

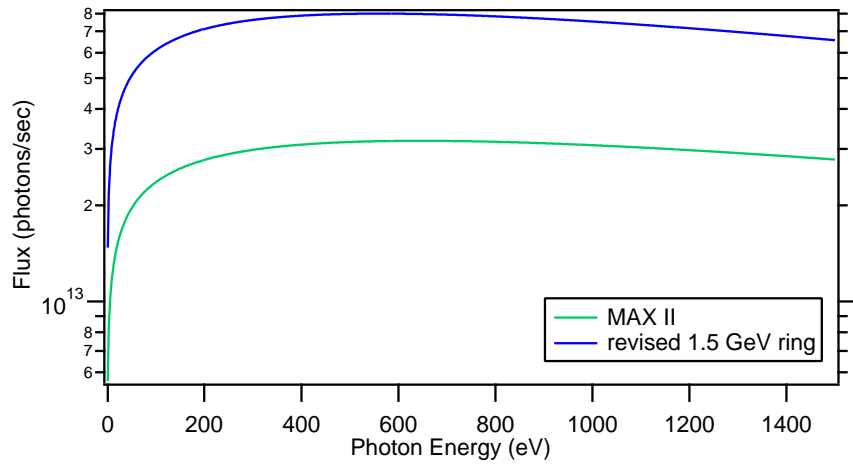


Figure 6.1: The bending magnet spectrum of MAX II ($I_R=200$ mA) and revised 1.5 GeV ring ($I_R=500$ mA). For both cases, the acceptance is 4.7 mrad horizontally.

Conclusions

The change from original 1.5 GeV MAX IV ring to a one with much shorter circumference has effects on beamlines but it should be possible to meet the resolution and spot size requirements set by the CDR. According to simulations and calculations, the beamline length of 40 m at maximum is foreseen for revised 1.5 GeV ring. The 50 m defined for the beamlines at revised 3.0 GeV ring should be adequate even for high resolution micro focusing beamlines in the soft-X-ray regime - that might change if the end stations extend several meters from the final focus.

Even for relocated beamlines and undulators, revised 1.5 GeV will provide higher performance compared to updated MAX II ring. Future insertion devices can be built to take full advantage of longer straight sections and smaller minimum gap. In addition, the new ring can house more insertion devices. Therefore, the revised 1.5 GeV ring looks very attractive option.

The only beamlines gaining from lower ring energy at revised 1.5 GeV ring would be I3 and to some extent I4 if they are to be located at that ring - even in the case of I3, the flux will increase only about 20%. On the other hand, the performance of the soft-X-ray beamlines operating from 50-100 eV to about 1 keV will be compromised if the electron energy of that ring is lowered to 1.0 GeV. Based on this analysis, the smaller ring based on revised design should be operated at 1.5 GeV rather than at 1.0 GeV.

For the soft-X-ray beamlines, undulators at revised 3.0 GeV ring will provide much higher flux at 1 keV and above but the price is very strong increase in the heat load. Preferably the lowest achievable energy should be some hundreds of eVs instead of some tens of eVs. A survey on heat loads at other facilities is under way.

Relocation of existing bending magnet and undulator beamlines to revised 1.5 GeV ring should be possible with very small modifications and the performance will increase compared to the existing ones at MAX II. Even if I411 is relocated on a bending magnet source, gas phase experiments should be possible with some limitations on high resolution work.

Bibliography

- [1] *MAX IV Conceptual Design Report*, www.maxlab.lu.se.
- [2] *MAX IV, A World Leading Synchrotron Radiation laboratory*, brochure, www.maxlab.lu.se.
- [3] T. Tanaka and H. Kitamura, *J. Synchrotron Radiation* **8**, 1221 (2001).
- [4] E. Wallén, SPECTRA parameter file.
- [5] E. Wallén and I. Blomqvist, *MAX IV Insertion Devices*, presentation for MAX IV Evaluation, Lund, 2005.
- [6] F. Schäfers, Technical Report, BESSY TB 202/96, 1-50, 1996.
- [7] P. Elleaume, *Rev. Sci. Instrum.* **63**, 321 (1992).
- [8] Private communication with Mikael Eriksson.
- [9] R. Follath, F. Senf, *Nucl. Instr. and Meth. in Phys. Res A* **390**, 388 (1997).
- [10] R.P. Walker and B. Diviacco, *Rev. Sci. Instrum.* **63**, 392 (1992).
- [11] P. Elleaume, J. Chavenne, B. Faartz, *NIM A* **455**, 503 (2000).